Fast-wave averaging with phase changes: Asymptotics and application to moist atmospheric dynamics

By

Yeyu Zhang

A dissertation submitted in partial fulfillment

of the requirements for the degree of

Doctor of Philosophy

(Mathematics)

at the

UNIVERSITY OF WISCONSIN – MADISON

2020

Date of final oral examination: Dec 7, 2020

The dissertation is approved by the following members of the Final Oral Committee:

Professor Leslie M Smith, Professor, Mathematics

Professor Samuel N Stechmann, Professor, Mathematics

Professor Nan Chen, Assistant Professor, Mathematics

Professor Jonathan E Martin, Professor, Atmospheric and Oceanic Sciences

Abstract

Many systems involve the coupled nonlinear evolution of slow and fast components, where, for example, the fast waves might be acoustic (sound) waves with a small Mach number or inertio-gravity waves with small Froude and Rossby numbers. In the past, for some such systems, an interesting property has been shown: the slow component actually evolves independently of the fast waves, in a singular limit of fast wave oscillations. Here, a fast-wave averaging framework is developed for a moist Boussinesq system with additional complexity beyond past cases, now including phase changes between water vapor and liquid water. The main question is: Do phase changes induce coupling between the slow component and fast waves? Or does the slow component evolve independently, according to moist quasi-geostrophic equations? Compared to the dry dynamics, a substantial challenge is that the method needs to be adapted to a piecewise operator with variable coefficients, due to phase changes. A formal asymptotic analysis is presented here.

For purely saturated flow without phase changes, it is shown that precipitation does not induce coupling, and the slow modes evolve independently. With phase changes present, the limiting equations show that phase boundaries could possibly induce coupling between the slow modes and fast waves. However, these possibilities were not clearly settled from theoretical considerations alone. Here, to investigate further, a suite of numerical simulations is conducted, using a sequence of small values including Fr=Ro=0.1, 0.01, and 0.001. For Fr=Ro=0.1, the influence of waves on the slow component is small, and its magnitude is roughly 0.1 to 0.4. For smaller values of Fr and Ro, the influence of waves is still somewhat small, but it does not decrease proportionally to Fr and Ro as Fr and Ro are decreased to 0.01 and 0.001. As an explanation and physical interpretation, it is shown that, while linear waves have a time average of zero, the piecewise-linear waves that arise due to phase changes actually have a nonzero time-averaged component.

Acknowledgements

My deep gratitude goes first to Professor Leslie Smith, who expertly guided me through my graduated education and who shared the excitement of five years of discovery. Her unwavering enthusiasm for physics kept me constantly engaged with my research, and her personal generosity helped make my time at UW-Madison enjoyable. It is a great privilege and honor to work and study under her guidance.

I would like to express my deep and sincere gratitude to Professor Samuel Stechmann for providing invaluable guidance throughout the research. His dynamism, vision, sincerity, and motivation have deeply inspired me. I am extending my heartfelt thanks to his wife Professor Qin Li for her recommendation and support for my future employment.

In addition, a thank you to Assistant Professor Nan Chen, who introduces me to the data science field and whose talent and knowledge for data assimilation and machine learning techniques make my future path full of bright and promising. I appreciate the helpful comments from the reviewers of the papers. The members of the committee for oral examination manifested their distinguished skills and talents in their own fields as seen in their way of correction and ideas shared. In particular, Professor Jonathan Martin, co-authored the paper [59] which contributed a lot to my dissertation. I also gratefully acknowledge funding from NSF-DMS-1907667 and NSF-AGS-1443325.

I acknowledge the great group put together by Professor Smith consisting of Dr.Wetzel, Parvathi madathil kooloth, and myself. Our meetings were valuable.

Last but not the least, I would like to thank my family: my parents for giving birth to me in the first place and supporting me spiritually throughout my life.

List of Figures

6.1 Random large-scale initial conditions: velocity u (left) and stream function ψ (right). 2D slices are shown with $x = \pi$ held fixed. 48

7.1 Behavior of the fast–slow term $\langle \vec{u}_{(W')} \cdot \nabla PV_e \rangle$ as ε tends toward zero, for the case of a randomly selected initial condition. The duration for the time averaging is $T = 0.6$, and for the phase-change cases the cloud fraction is $||H_s(q_t - q_{vs,0})||_1 = 22\%$. The L^2 norm of $\langle \vec{u}_{(W')} \cdot \nabla PV_e \rangle$ is plotted and is normalized by dividing by the initial L^2 norm of $\vec{u}_{(W')} \cdot \nabla PV_e$. 53

7.2 Same as Figure 7.1, except for the slow-slow term $\langle \vec{u}_{(M,PV_e)} \cdot \nabla PV_e \rangle$. 54

7.3 Initial conditions for a sensitivity study, with initial turbulent velocity u (left) and a moist bubble in total water q_t (right). 2D slices are shown with $x = \pi$ held fixed. The bubble of q_t has initial moisture perturbation centred at $\vec{x}_0 = (\pi, \pi, 0.625\pi)$. 57

7.4 Same as figure 7.1, except for initial conditions of a turbulent velocity field and a moist bubble, and for only a resolution of 128^3. 58

7.5 Same as figure 7.2, except for initial conditions of a turbulent velocity field and a moist bubble, and for only a resolution of 128^3. 58

7.6 Behavior of the fast–slow term $\langle \vec{u}_{(W')} \cdot \nabla PV_e \rangle$ for the case of a randomly selected initial condition, for different values of the cloud fraction, $||H_s(q_t - q_{vs,0})||_1$. The duration for the time averaging is $T = 0.6$, and $\varepsilon = O(0.01)$. The L^2 norm of $\langle \vec{u}_{(W')} \cdot \nabla PV_e \rangle$ is plotted and is normalized by dividing by the initial L^2 norm of $\vec{u}_{(W')} \cdot \nabla PV_e$. 60

8.1 From left to right are initial H_s at $t = 0$, $\langle H_s \rangle$ and $|\langle \vec{u}_{(W')} \cdot \nabla M \rangle|$. 2D slices are shown for $x = \pi$ held fixed. Red areas in the first panel represents clouds (liquid water). Yellow patterns in second panel indicate the regions where phase changes happen frequently. Hot spots (yellow to red) in the third panel indicate high values of the fast-slow coupling term. 62

8.2 (Top) $H_s(t, x_0, y_0, z_0)$ vs. time t for $t \in [0, 0.67]$, with H_s measured from a red-spot position (x_0, y_0, z_0) in figure 8.1. There are 45 total alternating time windows: 23 for the saturated state, and 22 for the unsaturated state. Quantitatively, 58% of the time is spent in the saturated state, compared to 42% time in the unsaturated state. (Bottom) The green triangles represent the time ratio spent in unsaturated windows, while the red squares correspond to time spent in saturated windows (time ratio = time in each window/T, where $T = 0.67$). 63

8.3 The purple curve is the time evolution of water $q_t(t, x_0, y_0, z_0)$, for fixed (x_0, y_0, z_0) chosen from a red spot position in figure 8.1. The green line is the saturation threshold $q_{vs,0} = 0.5$. 64

8.4 Piecewise solution of (8.11) for $M = 0$ such that the phase interface is at $y = 0$. 67

List of Tables

7.1 Behavior of terms in the PV_e evolution equation from (6.7)–(6.14) in the moist Boussinesq simulations with phase changes, for the case of a randomly selected initial condition. The duration for the time averaging is $T = 0.6$, the resolution is 128^3, and the cloud fraction is $||H_s(q_t - q_{vs,0})||_1 = 22\%$. The L^2 norm of $\langle f \rangle$ is normalized by dividing by the initial L^2 norm of f, where f represents the various terms displayed. 55

7.2 Same as table 7.1, except for the purely saturated case, which has a cloud fraction of 100%. 56

Contents

Abstract **i**

Acknowledgements **ii**

List of Figures **iv**

List of Tables **v**

1 Introduction **1**

2 Model setup **5**

2.1 Abstract formulation 5

2.2 Moist atmospheric dynamics 6

2.3 Treatment of the Heaviside functions 10

2.4 Slow and fast variables 11

2.5 Connection between moist atmospheric dynamics and abstract formulation . . 17

3 Fast-wave averaging for the dry dynamics **20**

4 Fast-wave averaging with phase changes **23**

4.1 Abstract framework 23

4.2 Slow modes and fast waves: decomposition and interactions 26

4.3 Evolution of M 28

4.4 Evolution of PV_e 32

4.5 The effects of phase changes 36

5 Effects of rainfall, and reduced M and PV_e limiting dynamics **38**

5.1 A purely saturated environment with $V_r = 1$ 38

5.1.1 Evolution of M. 38

5.1.2 Evolution of PV_e. 40
5.1.3 Summary of the slow dynamics in a saturated domain with $V_r = 1$. . . . 41
5.2 A purely saturated environment with $V_r = O(\varepsilon^{-1})$ 42
5.3 The PQG equations with phase changes for balanced initial conditions 43

6 Methodology **45**
6.1 Numerical method 45
6.2 Discussion of time scales and values of the parameter ε 46
6.3 Cloud fraction 46
6.4 Large-scale, random initial conditions 48
6.5 Evaluation of nonlinear terms in PV_e evolution equation 49
6.6 (M, PV_e)-inversion for finite ε 50

7 Results of numerical simulations **52**
7.1 A first assessment: fast-wave averaging with phase changes 52
7.2 Sensitivity studies and robustness tests 56

8 Explanation and physical interpretation **61**
8.1 A closer look at simulated data 61
8.2 ODE system 64
8.2.1 General Solution for ODE System in Different Phases 65
8.2.2 A simple solution example with $M = 0$ 66

9 Conclusions and Discussion **68**
9.1 Asympotic analysis 68
9.2 Numerical assessment 69

A Non-dimensional equations and distinguished limit **72**

B Change of Variables in Different Environments **75**

C Inverse change of variables to recover (u, v, w, θ_e, q_t) **82**

D Fourier decomposition of $\mathscr{L}_*$ **87**

E Analysis of Resonant Interaction for Slow Dynamics **94**

Bibliography **98**

Chapter 1

Introduction

The dry Boussinesq equations describe an idealization of atmospheric and oceanic fluid systems, in which the dynamics include the effects of the earth's rotation together with density and/or temperature stratification. The effects of rotation and stratification are mathematically represented by skew-symmetric linear operators, leading to the presence of neutrally stable wave oscillations. These waves act to modify the fluid evolution characterized by the bilinear operator. Furthermore, the linearized equations also admit non-propagating solutions, often referred to as 'slow modes' or 'vortical modes', based on their structure. There is a long history of study aimed at mathematical and physical understanding of wave and vortical interactions in the context of the dry Boussineq and related equations to describe geophysical flows, e.g. [1, 2, 3, 4, 5, 16, 17, 22, 33, 38, 40, 43, 45, 51, 52, 60].

In the limit of asymptotically large rotation and stable stratification, rigorous proofs show, remarkably, that the nonlinear dynamics associated with the slow modes decouple from waves altogether [16, 17, 38, 40]. In a sense, then, in considering the evolution of the slow component, the effects of the fast waves are averaged out; hence the name *fast-wave averaging* refers to the proofs. In earlier work, a similar type of fast-wave averaging property was also shown for compressible fluid dynamics, in the limit of small Mach number, where the fast waves correspond to acoustic (sound) waves [30, 31, 37]. These examples fall under the category of fast singular limits of hyperbolic partial differential equations (PDEs), with unbalanced initial conditions, which have been the topic of numerous other studies as well [11, 12, 13, 48, 49].

The quasi-geostrophic (QG) equations describe the evolution of the slow, vortical mode

in the limit of small Rossby and Froude numbers (large rotation and stratification, respectively). Two cases should be distinguished, according to the initial conditions [30, 31, 37, 38]. On the one hand, if the initial conditions contain no waves (or if the waves are sufficiently small in amplitude or norm), it is said that the initial data are balanced or well-prepared. In this case, the solutions of the Boussinesq equations will converge to solutions of the QG equations. On the other hand, if the initial conditions are general and can contain wave contributions, it is said that the initial data are unbalanced or ill-prepared. This latter case is where fast-wave averaging is relevant. Remarkably, even for unbalanced initial conditions, the QG equations describe the limiting dynamics of the slow modes, and the fast waves are also present in the limit but do not influence the QG evolution.

For dry dynamics without moisture, much is known about evolution from both balanced and unbalanced initial conditions. For moist dynamics with phase changes, on the other hand, much less is known. In the case of balanced initial conditions, a formal asymptotic derivation of precipitating QG (PQG) equations has been presented [50], and some properties of the PQG equations have been investigated [14, 15, 56, 57], but no rigorous proofs have been shown. The other case, with unbalanced initial conditions, is the topic of the present dissertation . Some main questions are: Do the PQG equations describe the evolution of the slow modes, in the limit of small Froude and Rossby numbers, even if the initial conditions are unbalanced? Is the slow-mode evolution influenced by waves, or not?

Moving beyond the dry Boussinesq equations, we investigate moist Boussinesq equations with changes of water between different phases (vapor, liquid, etc.). The real atmosphere involves these additional effects in the form of clouds, rainfall, etc., and by including them into the equations of motion, more realistic settings can be investigated. The topic of moist dynamics has received increasing attention in recent years, including both rigorous results [6, 7, 27, 28, 34, 41, 61, 62, 63] and asymptotic analysis [8, 9, 26, 29, 32, 39, 47, 50]. The present dissertation provides a bridge between previous asymptotic analysis and rigorous results, by consideration of fast-wave averaging with moisture and phase changes.

From the point of view of fast-wave averaging, the main question is: Does the slow component still evolve essentially independently of the fast wave component? Or do phase changes enhance the coupling between the slow and fast components? If moisture and/or phase changes are included, several new challenges arise, and we propose techniques for overcoming them. Three examples are as follows. First, to include moisture, additional variables must be added to the system, and they give rise to additional eigenmodes. Are the new, moist eigenmodes to be considered slow eigenmodes or fast eigenmodes? The new moist eigenmodes have been shown to be slow, unless precipitation is rapid enough to render them as fast [25]. Second, and more significant, a key aspect of fast-wave averaging is the *identification* of the fast and slow components of the system, based on an eigenvalue/eigenvector problem. In the past, for dry dynamics without moisture, Fourier-based methods have allowed identification of the different eigenmodes and their frequencies, e.g. [38]. If phase changes are present, then Fourier methods cannot be used, since the constant-coefficient linear operator of the dry case becomes a variable-coefficient and nonlinear operator in the case with phase changes. To overcome this challenge, a type of potential vorticity (PV) inversion can be used, although it must be a new type of inversion called PV-and-M inversion to account for the phase changes and the slow, moist variable M [50]. Third, and perhaps most significant, the operator is actually nonlinear in the case with phase changes, as mentioned above. As a result, it is not clear a priori whether a system with phase changes can even be *decomposed* in a meaningful way into a superposition of slow and fast components. Here, we propose a treatment of the nonlinear operator as a linear operator, for the purposes of mode decomposition, and to use a linear version of PV-and-M inversion for the mode decomposition [58, 59], while still retaining the fully nonlinear behavior of the dynamics. With these techniques, a theoretical framework is proposed here for performing fast-wave averaging with phase changes.

In the present dissertation, a formal asymptotic analysis is presented, and it lays the foundation for possible rigorous analysis in the future. After carrying out the asymptotic procedure, the analysis of the possible resonances and/or time averaging is not brought to closure, due to remaining questions about the behavior of waves in the presence of phase changes. Nevertheless, while closure is not obtained completely, many terms can be eliminated from

consideration based on available information about the eigenmodes (e.g., the zero-frequency eigenmodes have no vertical velocity, etc.), so partial simplification can be obtained. Also, the final result here provides a framework for investigation by numerical simulation [64]. In some of wave–vortical-interactions studies [1,2,3,4,5,16,17,22,33,38,40,43,45,51,52,60], it is statistical properties of forced turbulence or turbulent decay that are the main topic of interest. Note that in the present dissertation the main focus is instead on initial value problems. It would be interesting to investigate statistical properties of turbulence in the future. The present study provides a view of the wave–vortical interactions in initial value problems, as such a setup is most directly in line with the fast-wave averaging framework.

In Chapter 2, we describe several important aspects of the fast-wave-averaging setup that are proposed for handling phase changes, along with a description of the main application of interest: the moist version of the Boussinesq equations. Chapter 3 reviews fast-wave averaging for the dry equations, followed by results for the case of phase changes in Chapter 4. In Chapter 5, we discuss reductions of the equations derived in Chapter 4, by considering a single-phase, purely saturated environment, and the PQG equations with phase changes, but with waves filtered out. A notable feature of Chapter 5 is the addition of rainfall, which is excluded from Chapter 4 for simplicity. A description of the setup of numerical simulations and data analysis methods is presented in Chapter 6. The numerical investigation of fast-wave averaging is then presented in Chapter 7 and is aimed at the main questions of the dissertation, such as: Do the slow modes still evolve independently of the fast waves, even in the presence of phase changes? Following the numerical experiments, an explanation and physical interpretation are described in Chapter 8. Conclusions are discussed in Chapter 9 separately for asymptotic analysis (Section 9.1) and numerical assessment (Section 9.2).

Chapter 2

Model setup

In this chapter, the model equations are described from two perspectives: first, from an abstract perspective involving generic linear operator $\mathscr{L}$ and (nonlinear) bilinear operator $\mathscr{B}$, and second, in terms of the specific physical variables of interest for atmospheric dynamics (velocity, temperature, etc.).

Also, two of the challenges that arise from phase changes are discussed. First, Heaviside functions arise from phase changes, and their treatment in fast-wave averaging is discussed. Second, a decomposition into slow vs. fast variables is needed, and it is complicated by phase changes, which introduce (spatially and temporally) variable coefficients in the linear operator, in contrast to the constant-coefficient linear operators that typically appear in one-phase dynamics. A decomposition method is described based on a new type of potential vorticity inversion, called PV-and-M inversion, and it is valid even with the variable-coefficient linear operator due to phase changes.

2.1 Abstract formulation

For fast-wave averaging, many systems can be written in abstract form as

$$\frac{\partial \vec{v}}{\partial t} + \mathscr{L}(\vec{v}) + \mathscr{B}(\vec{v}, \vec{v}) = 0, \tag{2.1}$$

where $\vec{v}$ is the state vector and the operators $\mathscr{L}$, $\mathscr{B}$ are respectively linear and bi-linear [38].

Fast waves arise when the linear operator $\mathscr{L}$ has a large component that is $O(\varepsilon^{-1})$,

where ε is a small parameter. In this case, the linear operator $\mathscr{L}$ may be decomposed as $\mathscr{L} = \varepsilon^{-1}\mathscr{L}_* + \mathscr{L}_0$, so that (2.1) may be re-written as

$$\frac{\partial \vec{v}}{\partial t} + \varepsilon^{-1}\mathscr{L}_*(\vec{v}) + \mathscr{L}_0(\vec{v}) + \mathscr{B}(\vec{v}, \vec{v}) = 0, \tag{2.2}$$

where the dominant terms are identified by the prefactor $O(\varepsilon^{-1})$. Concrete expressions for $\vec{v}$, $\mathscr{L}$, and $\mathscr{B}$ will be provided later in this section. This abstract formulation is helpful because it indicates the basic structure of the system, and it allows the principles of fast-wave averaging to be described transparently (see Sections 3 and 4).

2.2 Moist atmospheric dynamics

Atmospheric dynamics are modeled here by the moist Boussinesq equations with phase changes:

$$\frac{D\vec{u}}{Dt} + \varepsilon^{-1}\hat{z} \times \vec{u} + \varepsilon^{-1}\nabla\phi = \varepsilon_1^{-1} b\, \hat{z} \tag{2.3}$$

$$\nabla \cdot \vec{u} = 0 \tag{2.4}$$

$$\frac{D\theta_e}{Dt} + \varepsilon_1^{-1} w = 0 \tag{2.5}$$

$$\frac{Dq_t}{Dt} - \varepsilon_2^{-1} w - V_r \frac{\partial q_r}{\partial z} = 0 \tag{2.6}$$

where $D/Dt = \partial_t + \vec{u}\cdot\nabla$ is the material derivative, $\vec{u} = (\vec{u}_h, w)$ is the three-dimensional velocity with horizontal components $\vec{u}_h = (u, v)$ and vertical component w, and $\hat{z}$ is a unit vector in the vertical direction. The $\hat{z} \times \vec{u}$ term is $(-v, u, 0)^\intercal$, and it arises in the Coriolis term. The anomalous thermodynamical variables are pressure ϕ, equivalent potential temperature $\theta_e = \theta + q_v$, potential temperature θ, buoyancy b, and the mixing ratios q_v (water vapor), q_r (rain water) and $q_t = q_v + q_r$ (total water). The model in (2.3)-(2.6) has been non-dimensionalized based on characteristic mid-latitude synoptic scales, as described in the Appendix A (A.12 - A.16).

The parameter V_r represents the (nondimensional) terminal velocity of rain drops. The

terminal velocity V_r in nature will depend on the rain drop radius, but it is common for models to not explicitly represent the radii of droplets, so V_r is often parameterized as a function of the mixing ratio q_r [21]; here, a further simplification is made, and V_r is assumed to be a constant [23, 25]. The constant V_r will be used to include, or not include, the effects of precipitation in a simple way. At one extreme, setting $V_r = 0$ removes the effects of rainfall; it would then be appropriate for the rain water q_r to be relabeled as cloud water q_c, and the equations describe non-precipitating cloud dynamics [19, 20, 54]. Instead, with $V_r > 0$, the model in (2.3)-(2.6) represents a simplified version of precipitating cloud microphysics called fast autoconversion and rain evaporation (FARE) microphysics [23, 25]. While FARE microphysics lacks some of the detailed processes of clouds and precipitation in nature [21, 32], it has several advantageous features. For instance, FARE microphysics includes the essential aspect of precipitation (V_r); it provides the foundation upon which more complex microphysics schemes can be built [42, 50]; and it provides a setup that is simple enough for mathematical analysis (e.g., see also the energy principles in section 4 of [42] and section 2.6 of [23]).

With the exception of buoyancy $b(\vec{x}, t)$, each thermodynamical variable $f^{total}(\vec{x}, t)$ has been decomposed into a (given, linear) background function of altitude z and an anomaly, such that $f^{total}(\vec{x}, t) = \tilde{f}(z) + f(\vec{x}, t)$. Vertical derivatives of the background functions $\tilde{\theta}_e$, and $\tilde{q}_t$ are absorbed into the parameters ε_1 and ε_2 [50]. Although not fundamental to our approach, we make the choices $\tilde{q}_r = 0$, $\tilde{q}_t = \tilde{q}_v = q_{vs}(z)$. In our setup, the linear function $q_{vs}(z) = B_{vs} z$ (with constant B_{vs}) is a crude approximation to the saturation water vapor profile $q_{vs}(\phi, \theta)$ [23, 46]. Our choices for $\tilde{q}_t$, $\tilde{q}_v$ and $\tilde{q}_r$ imply that the background environment is at saturation, such that phase changes will occur for initial conditions with regions that are close to saturation. As an added benefit, simpler algebraic manipulations result from the background state $\tilde{q}_r = 0, \tilde{q}_t = \tilde{q}_v = q_{vs}(z)$.

Phase changes enter the model through the buoyancy. The buoyancy b is by definition an anomalous quantity, with multiple equivalent expressions depending on the choice of thermodynamical variables—for example, $b = b(\theta, q_v, q_r)$, or equivalently $b = b(\theta_e, q_t)$. No matter the choice, the most important feature is that the buoyancy changes its functional form across

phase boundaries, adding a new nonlinearity to the system, due to phase changes. The phase boundaries are defined as locations where the anomalous total water q_t is zero. In the simplified dynamics under consideration here, the total water is solely water vapor in unsaturated regions such that $q_t = q_v$; in saturated regions, excess water above the saturation level is entirely liquid water such that $q_t = q_r$. Hence, we may conveniently use Heaviside functions H_u, H_s to write

$$b = H_u b_u + H_s b_s, \tag{2.7}$$

where H_u, H_s are defined as

$$H_u = \begin{cases} 1 \text{ for } q_t < 0 \\ \\ 0 \text{ for } q_t \geq 0 \end{cases} \qquad \text{and } H_s = 1 - H_u, \tag{2.8}$$

and where expressions for the unsaturated buoyancy b_u and the saturated buoyancy b_s are given by

$$b_u = [\theta_e + (\varepsilon - 1)q_t], \qquad b_s = [\theta_e - \varepsilon q_t]. \tag{2.9}$$

The different water constituents can be described as

$$q_v = q_t,\ q_r = 0 \quad \text{if} \quad q_t < 0, \quad \text{and} \quad q_v = 0,\ q_r = q_t \quad \text{if} \quad q_t > 0, \tag{2.10}$$

which define the anomalous vapor q_v and the anomalous rain q_r from anomalous total water q_t. See [23,42] for additional description of the thermodynamic variables and their co-relationships.

The three parameters $\varepsilon, \varepsilon_1, \varepsilon_2$ incorporate the important physical constraints of rapid rotation and strong stable stratification, typical of the mid-latitude atmosphere at synoptic scales. These parameters are the Rossby Ro and Froude Fr numbers:

$$Ro = \frac{U}{fL} = \varepsilon \qquad Fr_1 = \frac{U}{N_1 H} = \varepsilon_1 \qquad Fr_2 = \frac{U}{N_2 H} = \varepsilon_2, \tag{2.11}$$

where U is a characteristic wind speed (≈ 10 m/s), H (L) is a characteristic height (length) in the vertical (horizontal) directions, and we assume that height-to-length ratio $H/L = O(1)$ for simplicity. The (dimensional) frequencies N_1 and N_2 are given by

$$
\begin{aligned}
{N_1}^2 &= \frac{g}{\theta_0}\frac{d\tilde{\theta}_e}{dz} = \frac{g}{\theta_0}\frac{d}{dz}(\tilde{\theta} + \frac{L_v}{c_p}\tilde{q}_v) = \frac{g}{\theta_0}\left(B + \frac{L_v}{c_p}B_{vs}\right) \\
{N_2}^2 &= -\frac{g}{\theta_0}\frac{L_v}{c_p}\frac{d\tilde{q}_t}{dz} = -\frac{g}{\theta_0}(\frac{L_v}{c_p}B_{vs})
\end{aligned}
\tag{2.12}
$$

where $g \approx 10$ m/s^2 is the acceleration of gravity, $\theta_0 \approx 300$ K is a reference temperature, $c_p = 10^3$ J kg^{-1} K^{-1} is the specific heat and $L_v = 2.5 \times 10^6$ J kg^{-1} is the latent heat factor. For stable stratification, $N_1, N_2, B = d\tilde{\theta}/dz$ are positive and $B_{vs} = d\tilde{q}_t/dz$ is negative. Note that the notation Fr_2 and N_2 is used in analogy to Froude number and buoyancy frequency, respectively, although Fr_2 and N_2 are defined in terms of total water instead of buoyancy. The buoyancy frequencies that are associated with unsaturated regions (N_u) and saturated regions (N_s) are given by the following expressions:

$$
{N_u}^2 = \frac{g}{\theta_0}\frac{d\tilde{\theta}}{dz} = \frac{g}{\theta_0}B, \quad {N_s}^2 = \frac{g}{\theta_0}\frac{d\tilde{\theta}_e}{dz} = \frac{g}{\theta_0}\left(B + \frac{L_v}{c_p}B_{vs},\right) \tag{2.13}
$$

with the relationships

$$
{N_u}^2 = {N_1}^2 + {N_2}^2 \qquad N_s = N_1. \tag{2.14}
$$

Therefore the unsaturated and saturated Froude numbers are, respectively

$$
Fr_u = \frac{U}{({N_1}^2 + {N_2}^2)^{1/2}H} \qquad Fr_s = \frac{U}{N_1 H} \tag{2.15}
$$

and we have the identities $Fr_u^{-2} = Fr_1^{-2} + Fr_2^{-2}$ and $Fr_s^{-1} = Fr_1^{-1}$.

For ease of calculations, we consider the special (but physically reasonable) case $-L_v B_{vs}/c_p = B/2$ such that $N_1 = N_2$ and $Fr_1 = Fr_2$ (so $\varepsilon_1 = \varepsilon_2$). Furthermore, in the asymptotic relation $\varepsilon \sim \varepsilon_1$, we set the $O(1)$ constant equal to unity such that there is one distinguished parameter ε appearing in (2.3) – (2.6), as described in Appendix A (A.17-A.21).

2.3 Treatment of the Heaviside functions

Special consideration is required for the Heaviside functions, H_u and H_s. To see their role, recall the abstract formulation from (2.1), and notice that now, due to phase changes, it must be rewritten as

$$\frac{\partial \vec{v}}{\partial t} + H_u(\vec{v})\mathscr{L}_u(\vec{v}) + H_s(\vec{v})\mathscr{L}_s(\vec{v}) + \mathscr{B}(\vec{v},\vec{v}) = 0. \tag{2.16}$$

This is the abstract form of the model in (2.3)–(2.6), where the linear term $\mathscr{L}(\vec{v})$ has been replaced by $H_u(\vec{v})\mathscr{L}_u(\vec{v}) + H_s(\vec{v})\mathscr{L}_s(\vec{v})$ to account for the effect of phase changes on the buoyancy, as described in (2.7)–(2.9). Each of the linear operators, $\mathscr{L}_u$ and $\mathscr{L}_s$, is by itself a constant-coefficient operator. However, in the dynamical equations of motion in (2.16), each of the linear operators, $\mathscr{L}_u$ and $\mathscr{L}_s$, is accompanied by a prefactor, $H_u(\vec{v})$ and $H_s(\vec{v})$, respectively, so that $H_u(\vec{v})\mathscr{L}_u(\vec{v}) + H_s(\vec{v})\mathscr{L}_s(\vec{v})$ is a *nonlinear* operator.

How can fast-wave averaging be carried out if the linear operator $\mathscr{L}$ has been replaced by a nonlinear operator, $H_u(\vec{v})\mathscr{L}_u(\vec{v}) + H_s(\vec{v})\mathscr{L}_s(\vec{v})$, due to phase changes? This nonlinearity introduces complications. For instance, fast-wave averaging involves a decomposition and superposition of the fast and slow components of the system, traditionally based on the linear operator $\mathscr{L}$ (e.g., see [38] or Chapter 3 below). In the case of the nonlinear operator, $H_u(\vec{v})\mathscr{L}_u(\vec{v}) + H_s(\vec{v})\mathscr{L}_s(\vec{v})$, it is unclear how to formulate a superposition of fast and slow components, since linear superposition ideas are likely incompatible with this nonlinear operator.

Here, we propose that the Heaviside functions, H_u and H_s, be treated as given functions, at the stages of the fast-wave-averaging analysis. The perspective and setup are then as follows. The solution $\vec{v}^{\,\varepsilon}(\vec{x},t)$ is assumed to be known for each value of ε. It is the solution for the moist atmospheric dynamics with phase changes in (2.3)–(2.6), or the abstract form of a system with phase changes in (2.16). The goal of fast-wave averaging is then to discover whether the solution $\vec{v}^{\,\varepsilon}(\vec{x},t)$ can be decomposed into fast and slow components, and to discover how the fast and slow components evolve in time. From this perspective, the solution $\vec{v}^{\,\varepsilon}(\vec{x},t)$ is already known, and so the Heavisides $H_u(\vec{v}^{\,\varepsilon})$ and $H_s(\vec{v}^{\,\varepsilon})$ are also already known. The known

Heavisides could then be written as given functions, $H_u(\vec{x},t)$ and $H_s(\vec{x},t)$, for the purposes of the fast-wave-averaging analysis, and the abstract formulation of the system could be regarded as

$$\frac{\partial \vec{v}}{\partial t} + H_u(\vec{x},t)\mathscr{L}_u(\vec{v}) + H_s(\vec{x},t)\mathscr{L}_s(\vec{v}) + \mathscr{B}(\vec{v},\vec{v}) = 0. \tag{2.17}$$

Here, a posteriori, the abstract formulation has been restored to its traditional form of (2.1), in terms of a linear operator $\mathscr{L} = H_u(\vec{x},t)\mathscr{L}_u + H_s(\vec{x},t)\mathscr{L}_s$. As a result of the linearity of $\mathscr{L}$, many of the techniques from prior fast-wave-averaging studies can be applied here to the case with phase changes; and this is one of the main advantages of treating H_u and H_s as given functions during the fast-wave averaging analysis. The treatment of Heaviside functions will be re-visited in the discussion and conclusion Section 9.1.

Note, to be clear, that the solution $\vec{v}^{\,\varepsilon}(\vec{x},t)$ is generated from the fully nonlinear dynamics in (2.3)–(2.6) or (2.16), where the Heavisides $H_u(\vec{v})$ and $H_s(\vec{v})$ are functions of the state variable vector $\vec{v}$. It is only *a posteriori*, during the fast-wave-averaging analysis, that the Heavisides are known and therefore written as given functions, $H_u(\vec{x},t)$ and $H_s(\vec{x},t)$, for the purposes of the fast-wave-averaging analysis.

2.4 Slow and fast variables

An important part of fast-wave averaging is the definition of the slow and fast components of the system. In past studies, the slow and fast components have typically been defined based on the eigenvalues and eigenvectors of the linear operator $\mathscr{L}$; if $\mathscr{L}$ is a constant-coefficient operator, then Fourier-based methods can be used to find the eigenvectors and eigenvalues, e.g. [5,16,38,52]. Here, however, $\mathscr{L}$ is a variable-coefficient operator, due to phase changes and associated Heaviside functions, as described in (2.17). Consequently, Fourier-based methods are ineffective for finding the eigenvectors and eigenvalues of $\mathscr{L}$ with phase changes, and it is unclear a priori how to decompose the system into its slow and fast components.

One past example of a variable-coefficient case of fast-wave averaging is equatorial waves [11, 12, 13]. In that case, the variable-coefficient terms are the Coriolis terms, which,

near the equator, are of the form yu and yv, where $\vec{u}_h = (u, v)$ is the horizontal velocity and y is the spatial coordinate in the north–south direction (similar to latitude). Because of the special structure of the variable-coefficient Coriolis terms, the eigenvectors and eigenvalues can be found analytically, using Hermite polynomials and analogy with the quantum harmonic oscillator [38]. Consequently, while the variable-coefficient Coriolis terms present other substantial challenges [11, 12, 13], they maintain the desirable property of analytical formulas for eigenvectors and eigenvalues. In comparison, in the present case, analytical formulas for all eigenvectors and eigenvalues will not be possible, due to phase changes.

The difficulties of a variable–coefficient operator $\mathscr{L}(\vec{x}, t)$ can be overcome by the following observation: In order to achieve a slow–fast decomposition, it suffices to identify the *null space* of $\mathscr{L}(\vec{x}, t)$. In other words, it is not necessary to find all eigenvectors $\vec{v}$ and eigenvalues λ that satisfy

$$\mathscr{L}\vec{v} = [H_u(\vec{x}, t)\mathscr{L}_u + H_s(\vec{x}, t)\mathscr{L}_s]\vec{v} = \lambda\vec{v}, \tag{2.18}$$

the eigenvalue–eigenvector equation for the variable-coefficient operator $\mathscr{L}(\vec{x}, t)$. Instead, it suffices to find the vectors $\vec{v}$ that are in the null space and satisfy

$$\mathscr{L}\vec{v} = [H_u(\vec{x}, t)\mathscr{L}_u + H_s(\vec{x}, t)\mathscr{L}_s]\vec{v} = 0. \tag{2.19}$$

The nullspace provides sufficient information for accomplishing the slow–fast decomposition; this is because the decomposition takes the form [16, 17, 38, 40]

$$\begin{aligned}
\vec{v}^{\,\varepsilon}(\vec{x}, t) &= \vec{v}^{\,0}(\vec{x}, t, \tau)|_{\tau=t/\varepsilon} + o(1) \\
&= e^{-\frac{t}{\varepsilon}\mathscr{L}}\bar{v}(\vec{x}, t) + o(1) \\
&= e^{-\frac{t}{\varepsilon}\mathscr{L}}[\bar{v}_{slow}(\vec{x}, t) + \bar{v}_{fast}(\vec{x}, t)] + o(1) \\
&= \bar{v}_{slow}(\vec{x}, t) + e^{-\frac{t}{\varepsilon}\mathscr{L}}\bar{v}_{fast}(\vec{x}, t) + o(1) \quad \text{for} \quad \varepsilon \to 0,
\end{aligned} \tag{2.20}$$

where the slow component $\bar{v}_{slow}(t, \vec{x})$ has no oscillations, and $\bar{v}_{fast}$ contains rapidly oscillating waves. (Note that we describe in (2.20) the decomposition for the case of a constant-coefficient

operator $\mathscr{L}$, for simplicity, for the purposes of the present paragraph; the decomposition takes a slightly modified form in the case of a variable-coefficient operator, as described in subsequent sections.) The key aspect is that, in order to write (2.20), detailed information of each eigenvalue λ is actually not needed. If the nullspace of $\mathscr{L}$ can be identified, then it defines the slow component $\bar{v}_{slow}$, and the fast component can be defined as the residual $\bar{v}_{fast} = \bar{v} - \bar{v}_{slow}$. The precise values of all non-zero eigenvalues λ are not needed to write a slow–fast decomposition as in (2.20).

To identify components of the nullspace of $\mathscr{L}(\vec{x}, t)$, we rely on insights from past literature about the zero-frequency eigenmodes. First, it is well-known that a zero-frequency eigenmode is the vortical mode, which can be described by a variable called potential vorticity (PV) [24, 38]. Physically, this eigenmode is related to the familiar balance conditions of geostrophic and hydrostatic balance. Second, for a moist system, another zero-frequency eigenmode arises, and it can be described by a variable called M [50, 58, 59].

For simplicity of the algebraic manipulations when phase changes are included, we focus on the case of zero rainfall speed $V_r = 0$ (the remainder of Chapter 2, Chapter 4, Chapter 6, and Chapter 7). The results for $V_r = 0$ are qualitatively the same for $V_r = O(1)$, as presented for a purely saturated environment in Section 5.1. In Section 5.2, we also briefly describe the case $V_r = O(\varepsilon^{-1})$ in a purely saturated domain, but this case corresponds to a different asymptotical regime, since then M is not a slow variable.

To find components of the nullspace of $\mathscr{L}(\vec{x}, t)$, we make a change of variables to utilize the two quantities PV_e and M that characterize two zero-frequency eigenmodes. To define the PV_e and M as slow variables, the basic idea is that vertical velocity w is related to fast waves, and we therefore wish to define quantities that are not influenced by w in the linear operator [50]. By inspection of (2.5) and (2.6), it is straightforward to eliminate the terms $\varepsilon_i^{-1} w$ from the θ_e and q_t equations using the linear combination

$$M = q_t + G_m \theta_e, \qquad G_m = \frac{\varepsilon_2}{\varepsilon_1}, \tag{2.21}$$

resulting in the dynamical equation (for $V_r = 0$)

$$\frac{DM}{Dt} = 0. \tag{2.22}$$

Perhaps less obvious, we next demonstrate that an appropriate slow, potential vorticity variable is defined as

$$PV_e = \xi + F\frac{\partial \theta_e}{\partial z}, \qquad F = \frac{\varepsilon}{\varepsilon_1}, \tag{2.23}$$

where ξ is the vertical component of the total vorticity $\nabla \times \vec{u}$. To find the equation for PV_e, take the curl of the horizontal momentum equation from (2.3), and then connect the result with the θ_e-equation (2.5), to arrive at

$$\frac{\partial PV_e}{\partial t} + F\frac{\partial \left(\vec{u} \cdot \nabla \theta_e\right)}{\partial z} + NL_\xi = 0, \tag{2.24}$$

$$NL_\xi = \nabla_h \times \left(\vec{u}_h \cdot \nabla_h \vec{u}_h + w\frac{\partial \vec{u}_h}{\partial z}\right) = \vec{u} \cdot \nabla \xi + \xi(u_x + v_y) + (w_x v_z - w_y u_z).$$

Then the material derivative of PV_e is given by

$$\frac{DPV_e}{Dt} = -F(\vec{u}_z \cdot \nabla \theta_e) - \xi(u_x + v_y) - (w_x v_z - w_y u_z). \tag{2.25}$$

Notice that, upon linearizing (2.22) and (2.24) about a resting base state, one can see that M and PV_e do not change with time—i.e., they represent zero-frequency eigenmodes. Thus, after the complete change of variables described below, both M and PV_e will be in the nullspace of the operator $\mathscr{L}_*$ introduced in the abstract formulation (2.2).

While PV_e and M represent slow components of the system, additional variables are needed to represent the fast components of the system, and thereby to completely specify the entire system. Indeed, by adding the q_t-equation (2.6) to the dry Boussinesq system, one can see that the phase space of divergence-free solutions has an extra degree of freedom as compared to the dry case [24,25]. In past dry studies, a Fourier-based approach has been used to decompose systems into their fast eigenmodes and slow eigenmodes (see, e.g. [5, 16, 33, 38, 45, 52]). Here,

however, a Fourier-based approach cannot be used for the Boussinesq system (2.3)-(2.6) with phase changes of water because of the potential for discontinuities introduced by the Heaviside operators in the expression for the buoyancy (2.7). On the other hand, we may formally divide the phase space into the (PV_e, M) variables and wave variables.

Formally speaking, we define wave variables W_1 and W_2 by

$$W_1 = \nabla^2 w, \quad W_2 = \xi_z - F\nabla_h^2 \left(H_u b_u + H_s b_s\right), \tag{2.26}$$

motivated by their relation to dry inertia-gravity waves, which involve vertical velocity w (used for the definition of W_1) and geostrophic/hydrostatic imbalance (W_2) [18,24,44,45]. From these definitions, one finds their evolution equations to be (see Appendix B)

$$\frac{\partial W_1}{\partial t} + \varepsilon^{-1} W_2 + \nabla_h^2 \left(\vec{u} \cdot \nabla w\right) - \partial_z \nabla_h \cdot \left(\vec{u}_h \cdot \nabla_h \vec{u}_h + w \frac{\partial \vec{u}_h}{\partial z}\right) = 0 \tag{2.27}$$

$$\begin{aligned} \frac{\partial W_2}{\partial t} - \varepsilon^{-1} \partial_z^2 \left(\nabla^{-2} W_1\right) - F\nabla_h^2 \left(C_{(H)} \nabla^{-2} W_1\right) + \partial_z \left(N L_\xi\right) \\ - F\nabla_h^2 \left(H_u \vec{u} \cdot \nabla b_u + H_s \vec{u} \cdot \nabla b_s\right) = 0, \end{aligned} \tag{2.28}$$

where the operator

$$\begin{aligned} C_{(H)} &= H_u(\varepsilon_1^{-1} + \varepsilon_2^{-1} - \frac{\varepsilon}{\varepsilon_2}) + H_s(\varepsilon_1^{-1} + \frac{\varepsilon}{\varepsilon_2}) \\ &= \varepsilon^{-1}\left(H_u(\frac{\varepsilon}{\varepsilon_1} + \frac{\varepsilon}{\varepsilon_2} - \frac{\varepsilon^2}{\varepsilon_2}) + H_s(\frac{\varepsilon}{\varepsilon_1} + \frac{\varepsilon^2}{\varepsilon_2})\right). \end{aligned} \tag{2.29}$$

Notice that the equations (2.27) and (2.28) have the structure

$$\frac{\partial W_1}{\partial t} + \varepsilon^{-1} W_2 + (\text{nonlinear terms}) = 0$$

$$\frac{\partial W_2}{\partial t} - \varepsilon^{-1} \partial_z^2 \left(\nabla^{-2} W_1\right) - \varepsilon^{-1}(\text{linear terms with } C_{(H)}) + (\text{nonlinear terms}) = 0,$$

both with large linear terms. They are independent quantities with rapid varyiations in time,

since W_1 depends on the vertical velocity w, while W_2 contains information about the fast component of all other primary variables: the horizontal velocities u, v (through vertical vorticity ξ, the equivalent potential temperatures θ_e and the total water q_t (through the buoyancy b_u, b_s), as well as phase interfaces through the Heaviside functions H_u, H_s.

For a complete description, it is necessary to also include inertial waves with frequency ε^{-1}, which are not represented by W_1, W_2 and their equations (2.27) and (2.28). The inertial waves correspond to the evolution of mean velocities u_m and v_m, given by

$$\frac{\partial u_m(z)}{\partial t} - \varepsilon^{-1} v_m(z) + \overline{\partial_z(uw)} = 0, \tag{2.30}$$

$$\frac{\partial v_m(z)}{\partial t} + \varepsilon^{-1} u_m(z) + \overline{\partial_z(vw)} = 0, \tag{2.31}$$

where the overline denotes the horizontal average. Together, equations (2.27), (2.28), (2.30) and (2.31) describe the evolution of the wave components (W_1,W_2,u_m,v_m).

The six-dimensional vector $\vec{v}^{\,\intercal} = (M, PV_e, W_1, W_2, u_m, v_m)$ spans divergence-free solutions of (2.3)-(2.6), and the operators in the abstract equation (2.2) – $\mathscr{L}_*$, $\mathscr{L}_0$ and $\mathscr{B}$ – are 6×6 matrices. For compactness in what follows, we will use the notation

$$\mathscr{L}_* \vec{v}_{(M,PV_e)} = 0, \qquad \vec{v}^{\,\intercal}_{(M,PV_e)} = (M, PV_e, 0, 0, 0, 0), \tag{2.32}$$

$$\mathscr{L}_* \vec{v}_{(W)} \neq 0, \qquad \vec{v}^{\,\intercal}_{(W)} = (0, 0, W_1, W_2, u_m, v_m), \tag{2.33}$$

where $\vec{v}_{(M,PV_e)}$ denotes the slow component of the state vector, and $\vec{v}_{(W)}$ is the fast component. For analysis of the slow variables, it is not necessary to specify the fast variables (W), but we found it helpful to do so, in order to be more explicit with regard to the calculations and results that follow in Chapter 4. Notice that W_1 and W_2 and their evolution equations involve many derivatives of Heaviside functions, which complicate their use and interpretations. Nevertheless, W_1 and W_2 serve the purpose of facilitating a concrete, though formal, presentation.

2.5 Connection between moist atmospheric dynamics and abstract formulation

With $\vec{v}^{\,\intercal} = (M, PV_e, W_1, W_2, u_m, v_m)$ and equations (2.22), (2.24), (2.27), (2.28), (2.30), (2.31), we can now define the operators appearing in the abstract equation (2.2). The fast-linear $\mathscr{L}_*$ and slow-linear $\mathscr{L}_0$ operators have the form

$$\mathscr{L}_* = \begin{pmatrix} 0 & 0 & 0 & 0 & 0 & 0 \\ 0 & 0 & 0 & 0 & 0 & 0 \\ 0 & 0 & 0 & 1 & 0 & 0 \\ 0 & 0 & -c & 0 & 0 & 0 \\ 0 & 0 & 0 & 0 & 0 & -1 \\ 0 & 0 & 0 & 0 & 1 & 0 \end{pmatrix} \qquad \mathscr{L}_0 = \begin{pmatrix} 0 & 0 & 0 & 0 & 0 & 0 \\ 0 & 0 & 0 & 0 & 0 & 0 \\ 0 & 0 & 0 & 0 & 0 & 0 \\ 0 & 0 & -d & 0 & 0 & 0 \\ 0 & 0 & 0 & 0 & 0 & 0 \\ 0 & 0 & 0 & 0 & 0 & 0 \end{pmatrix} \tag{2.34}$$

where the operators c and d are given by

$$c = \left(\partial_z^2 + F\nabla_h^2((\frac{\varepsilon}{\varepsilon_1} + \frac{\varepsilon}{\varepsilon_2})H_u + \frac{\varepsilon}{\varepsilon_1}H_s)\right)\left(\nabla^{-2}\right) \tag{2.35}$$

$$d = F\nabla_h^2(\frac{\varepsilon}{\varepsilon_2}(H_s - H_u))\left(\nabla^{-2}\right) \tag{2.36}$$

and $\varepsilon^{-1}c + d = \varepsilon^{-1}\partial_z^2\nabla^{-2} + F\nabla_h^2(C_{(H)}\nabla^{-2})$, where $C_{(H)}$ is in (2.29). Thus c and d separately represent the $O(\varepsilon^{-1})$ and $O(1)$ contributions, respectively, inside the operator $C_{(H)}$ (see Appendix B for more details.) The operator $\mathscr{L}_*$ plays an important role in the fast-wave averaging procedure, and because only the first and second rows contain all zero entries, we note that $\mathscr{L}_*\vec{v}_{(M,PV_e)} = 0$ while $\mathscr{L}_*\vec{v}_{(W)} \neq 0$.

The bi-linear operator $\mathscr{B}$ is given by

$$\mathscr{B} = \begin{pmatrix} \vec{u}\cdot\nabla M \\ \vec{u}\cdot\nabla PV_e + F\dfrac{\partial \vec{u}}{\partial z}\cdot\nabla\theta_e + \xi(u_x+v_y) + (w_x v_z - w_y u_z) \\ \nabla_h^2\left(\vec{u}\cdot\nabla w\right) - \partial_z\nabla_h\cdot\left(\vec{u}_h\cdot\nabla_h\vec{u}_h + w\dfrac{\partial\vec{u}_h}{\partial z}\right) \\ -F\nabla_h^2\left(H_u\vec{u}\cdot\nabla b_u + H_s\vec{u}\cdot\nabla b_s\right) + \partial_z\left(NL_\xi\right) \\ \overline{\partial_z(uw)} \\ \overline{\partial_z(vw)} \end{pmatrix} \tag{2.37}$$

such that

$$\mathscr{B}(\vec{v}^{\,a},\vec{v}^{\,b}) = \begin{pmatrix} \vec{u}^{\,a}\cdot\nabla M^b \\ \vec{u}^{\,a}\cdot\nabla PV_e^b + F\dfrac{\partial\vec{u}^{\,a}}{\partial z}\cdot\nabla\theta_e^b + \xi^a(u_x^b+v_y^b) + (w_x^a v_z^b - w_y^a u_z^b) \\ \nabla_h^2\left(\vec{u}^{\,a}\cdot\nabla w^b\right) - \partial_z\nabla_h\cdot\left(\vec{u}_h^{\,a}\cdot\nabla_h\vec{u}_h^{\,b} + w^a\dfrac{\partial\vec{u}_h^{\,b}}{\partial z}\right) \\ -F\nabla_h^2\left(H_u\vec{u}^{\,a}\cdot\nabla b_u^b + H_s\vec{u}^{\,a}\cdot\nabla b_s^b\right) + \partial_z\left(NL_\xi\right) \\ \overline{\partial_z(u^a w^b)} \\ \overline{\partial_z(v^a w^b)} \end{pmatrix}, \tag{2.38}$$

where $F = \varepsilon/\varepsilon_1$, and the products in NL_ξ are analogously decomposed in terms of $()^a\cdot()^b$; see (2.24) for the definition of NL_ξ. The velocity $\vec{u}$ and equivalent potential temperature θ_e are found from the inverse transformation in Appendix C.

During the process of inverting the 6-dimensional state vector $\vec{v}^{\,\intercal} = (M, PV_e, W_1, W_2, u_m, v_m)$ to 5-dimensional state vector $\vec{v}^{\,\intercal} = (u, v, w, \theta_e, q_t)$, we use the definitions of $M, PV_e, W_1, W_2, u_m, v_m$ displayed by (2.21), (2.23), (2.26), (2.30), (2.31). One of the key inversion relations gives the streamfunction ψ as

$$\nabla_h^2\psi + \frac{\partial}{\partial z}\Big\{\frac{1}{2}H_u[\partial_z\psi - \nabla_h^{-2}W_2 + M] + H_s[\partial_z\psi - \nabla_h^{-2}W_2]\Big\} = PV_e. \tag{2.39}$$

This elliptic PDE is a type of PV inversion, although it differs from conventional PV inversion in its inclusion of M (as in [58, 59]) and also wave variable W_2. After solving for $\psi = F(M, PV_e, W_1, W_2)$ and defining $\xi = \nabla_h^2 \psi$, one may find the equivalent potential temperature θ_e from (2.23). The velocity field $\vec{u}$ is found using (2.26), the definition $\xi = v_x - u_y$ and the incompressibility condition (see Appendix C: C.12, C.18, C.19).

Chapter 3

Fast-wave averaging for the dry dynamics

Before considering the more complicated case with phase changes (see Chapter 4), here we describe the dry version of fast-wave averaging [38]. To simplify the presentation, from now on we set all $O(1)$ non-dimensional quantities equal to unity, for example $F = 1$ and $G_m = 1$. We start by reviewing the main steps in the procedure, and then discuss the decoupling between fast and slow dynamics (see Chapter 5), with details given in D and E.

The multiple scales method is the main tool, and accordingly the solution $\vec{v}^{\,\varepsilon}(\vec{x}, t, \tau)$ is expanded as

$$\vec{v}^{\,\varepsilon}(\vec{x}, t, \tau) = \vec{v}^{\,0}(\vec{x}, t, \tau)|_{\tau=t/\varepsilon} + \varepsilon \vec{v}^{\,1}(\vec{x}, t, \tau)|_{\tau=t/\varepsilon} + ... \tag{3.1}$$

using two different time scales: t (slow) and $\tau = \frac{t}{\varepsilon}$ (fast). Note that $\tau = O(1)$ when $t = O(\varepsilon)$, and hence the nomenclature 'fast' when referring to the time scale τ. When (3.1) is inserted in to (2.2), the $O(\varepsilon^{-1})$ balance yields

$$\frac{\partial \vec{v}^{\,0}}{\partial \tau} + \mathscr{L}_*(\vec{v}^{\,0}) = 0 \quad \Rightarrow \quad \vec{v}^{\,0}(\vec{x}, t, \tau) = e^{-\tau \mathscr{L}_*} \bar{v}(\vec{x}, t), \tag{3.2}$$

where t and τ have been treated as independent variables, and $\bar{v}(\vec{x}, t)$ is the initial field with respect to the fast τ evolution. Then collecting $O(\varepsilon^0)$ terms gives

$$\frac{\partial \vec{v}^{\,1}}{\partial \tau} + \mathscr{L}_*(\vec{v}^{\,1}) = -\left(\frac{\partial \vec{v}^{\,0}}{\partial t} + \mathscr{L}_0(\vec{v}^{\,0}) + \mathscr{B}(\vec{v}^{\,0}, \vec{v}^{\,0}) \right) \tag{3.3}$$

with $\vec{v}^{\,0}$ given by (3.2). Next we may multiply both sides of (3.3) by the integrating factor $e^{\tau\mathscr{L}_*}$ and use Duhamel's formula to arrive at

$$\vec{v}^{\,1} = e^{-\tau\mathscr{L}_*}\vec{v}^{\,1}(\vec{x},t,\tau)|_{\tau=0} - \tau\bigg(e^{-\tau\mathscr{L}_*}\frac{\partial\bar{v}}{\partial t}(\vec{x},t) + e^{-\tau\mathscr{L}_*}R(\vec{x},t)\bigg), \tag{3.4}$$

where R is the averaging integral given by

$$R(\vec{x},t) = \frac{1}{\tau}\int_0^\tau e^{s\mathscr{L}_*}\left(\mathscr{L}_0(e^{-s\mathscr{L}_*}\bar{v}) + \mathscr{B}(e^{-s\mathscr{L}_*}\bar{v}, e^{-s\mathscr{L}_*}\bar{v})\right)ds. \tag{3.5}$$

The last step is to enforce the sub-linear growth condition to guarantee that $\vec{v}^{\,1}$ grows sub-linearly as a function of τ. If the sub-linear growth condition is not satisfied, then $\vec{v}^{\,1}$ could grow, say, linearly as a function of τ, and the $\varepsilon\vec{v}^{\,1}$ term in (3.1) could become as large as the $\vec{v}^{\,0}$ term (on the long time scale as $t = O(1)$ and $\tau = O(\varepsilon^{-1})$), thereby violating the assumed orders of magnitude in (3.1). Applying the sub-linear growth condition, we multiply (3.4) by τ^{-1} (and by $e^{\tau\mathscr{L}_*}$) and take the limit as $\tau\to\infty$; the result is

$$\frac{\partial\bar{v}(\vec{x},t)}{\partial t} = -\lim_{\tau\to\infty}\frac{1}{\tau}\int_0^\tau e^{s\mathscr{L}_*}\left(\mathscr{L}_0(e^{-s\mathscr{L}_*}\bar{v}) + \mathscr{B}(e^{-s\mathscr{L}_*}\bar{v}, e^{-s\mathscr{L}_*}\bar{v})\right)ds, \tag{3.6}$$

which is the fast-wave averaging equation.

For the dry dynamics with buoyancy $b = \theta$ and $q_t = 0$, the Fourier transform of (3.6) has been analyzed by several authors, and in particular for scrutinizing the resonant triad interactions arising from the bi-linear term, e.g. [5,17,33,40,43,45]. They showed that resonant interactions involving fast waves and slow modes cannot transfer energy into the slow modes, which result implies the decoupling between fast and slow modes in the limit $\varepsilon\to 0$. Then an inverse transform of the Fourier-space equation for the slow modes leads to conservation of potential vorticity given by

$$\frac{D}{Dt}PV = (\frac{\partial}{\partial t} + \vec{u}_{(PV)}\cdot\nabla)PV = 0, \tag{3.7}$$

where the potential vorticity PV is the dry counterpart of PV_e given by (2.23), namely

$$PV = \xi + \frac{\partial \theta}{\partial z}. \tag{3.8}$$

We remind the reader that ξ is the vertical component of the vorticity vector, and we have taken $F = 1, G_m = 1$, etc. In (3.7), notice that PV is advected by a slow component of the velocity denoted $\vec{u}_{(PV)}$. In the limit as $\varepsilon \to 0$, $\vec{u}_{(PV)}$ may be found by inverting a linear elliptic equation for the velocity streamfunction ψ:

$$\nabla^2 \psi = PV, \tag{3.9}$$

which is obtained from (3.8) using geostrophic and hydrostatic balance [38], such that

$$\xi = \nabla_h^2 \psi, \quad \theta = \frac{\partial \psi}{\partial z}, \quad \vec{u}_{(PV)} = \left(-\frac{\partial \psi}{\partial y}, \frac{\partial \psi}{\partial x}, 0 \right). \tag{3.10}$$

Thus the limiting dynamics for slow PV are completely decoupled from fast oscillations.

Moreover, Embid and Majda [17] rigorously proved the asymptotic solution

$$\bar{v}(t, \vec{x}) = \bar{v}_{slow}(t, \vec{x}) + e^{-\frac{t}{\varepsilon}\mathscr{L}_*} \bar{v}_{fast}(t, \vec{x}) + o(1), \quad \varepsilon \to 0, \tag{3.11}$$

for the state vector $\bar{v}(t, \vec{x})$, where the slow component $\bar{v}_{slow}(t, \vec{x})$ has no oscillations and $\bar{v}_{fast}$ contains only rapidly oscillating waves. For analogy with the calculations that will follow, we note that the operation $e^{-\frac{t}{\varepsilon}\mathscr{L}_*} \bar{v}_{slow}(t, \vec{x}) = I \bar{v}_{slow}(t, \vec{x})$ for $\bar{v}_{slow}$ in the nullspace of $\mathscr{L}_*$, where I is the identity matrix.

Chapter 4

Fast-wave averaging with phase changes

4.1 Abstract framework

Compared with previous dry analysis in Chapter 3, here we investigate fast-wave averaging for moist atmospheric dynamics with phase changes. When water is converted from vapor to liquid and vice versa, the buoyancy changes its functional form at phase boundaries, represented mathematically by the Heaviside operators $H_u(\vec{x},t), H_s(\vec{x},t)$ in (2.7) and (2.16). As discussed, we will treat $H_u(\vec{x},t), H_s(\vec{x},t)$ as known functions of $(\vec{x},t)$ for the fast-wave averaging analysis and proceed to analyse (2.17). Since the phase boundaries $H_u(\vec{x},t), H_s(\vec{x},t)$ are determined by the complete (thermo) dynamics, they have a fast component, and therefore, a main new element of the formulation is the τ-dependence in the linear operator $\mathscr{L}_*(t,\tau)$. For clarity, we repeat the steps of the multi-scale asymptotic analysis, arriving at a condition to eliminate sub-linear growth in the $O(1)$ equations, thus defining the fast-wave-averaging equations. Differences from (3.6) will arise from the τ-dependence in the linear operator $\mathscr{L}_*(t,\tau)$.

In this section, we set the rainfall parameter $V_r = 0$ for simplicity of the presentation and calculations. Later in Section 5, we include the effects of rainfall in the context of reduced systems (purely saturated without phase changes, and balanced initial conditions absent waves altogether). In those simpler systems, it is shown that $V_r \neq 0$ produces an extra term in the slow M-equation, but otherwise does not fundamentally alter conclusions regarding limiting slow dynamics.

Starting again from the beginning, the expansion

$$\vec{v}^{\,\varepsilon}(\vec{x},t,\tau) = \vec{v}^{\,0}(\vec{x},t,\tau)|_{\tau=t/\varepsilon} + \varepsilon\vec{v}^{\,1}(\vec{x},t,\tau)|_{\tau=t/\varepsilon} + \cdots \tag{4.1}$$

is inserted into the system

$$\frac{\partial\vec{v}}{\partial t} + \varepsilon^{-1}\mathscr{L}_*(t,\tau)(\vec{v}) + \mathscr{L}_0(t,\tau)(\vec{v}) + \mathscr{B}(\vec{v},\vec{v}) = 0. \tag{4.2}$$

Collecting $O(\varepsilon^{-1})$ terms leads to the balance

$$\frac{\partial\vec{v}^{\,0}}{\partial\tau} + \mathscr{L}_*(t,\tau)(\vec{v}^{\,0}) = 0, \tag{4.3}$$

with solutions

$$\vec{v}^{\,0}(\vec{x},t,\tau) = e^{-\int_0^\tau \mathscr{L}_*(t,\tau')d\tau'}\bar{v}(\vec{x},t), \tag{4.4}$$

and the initial condition $\bar{v}(\vec{x},t)$ depends only on $(\vec{x},t)$. Notice that the operator $e^{-\tau\mathscr{L}_*}$ in (3.2) has been replaced by $e^{-\int_0^\tau \mathscr{L}_*(t,\tau')d\tau'}$. The next order $O(\varepsilon^0)$ balance yields

$$\frac{\partial\vec{v}^{\,1}}{\partial\tau} + \mathscr{L}_*(t,\tau)(\vec{v}^{\,1}) = -\left(\frac{\partial\vec{v}^{\,0}}{\partial t} + \mathscr{L}_0(t,\tau)(\vec{v}^{\,0}) + \mathscr{B}(\vec{v}^{\,0},\vec{v}^{\,0})\right), \tag{4.5}$$

and one may integrate with respect to τ keeping t as $\varepsilon \to 0$. The calculus is straightforward, though slightly more complicated than for the dry case, and for illustration we provide details for the $\partial\vec{v}^{\,0}/\partial t$ term on the right hand side of (4.5). The standard integrating factor method gives

$$\begin{aligned}
\vec{v}^{\,1} &= -e^{-\int_0^\tau \mathscr{L}_*(t,\tau')d\tau'}\int_0^\tau e^{\int_0^s \mathscr{L}_*(t,s')ds'}\frac{\partial(e^{-\int_0^s \mathscr{L}_*(t,s')ds'}\bar{v})}{\partial t}ds + \cdots \\
&= -e^{-\int_0^\tau \mathscr{L}_*(t,\tau')d\tau'}\int_0^\tau e^{\int_0^s \mathscr{L}_*(t,s')ds'}[\frac{\partial(e^{-\int_0^s \mathscr{L}_*(t,s')ds'})}{\partial t}\bar{v} + \frac{\partial\bar{v}}{\partial t}e^{-\int_0^s \mathscr{L}_*(t,s')ds'}]ds + \cdots \\
&= -e^{-\int_0^\tau \mathscr{L}_*(t,\tau')d\tau'}\tau\frac{\partial\bar{v}}{\partial t} - e^{-\int_0^\tau \mathscr{L}_*(t,\tau')d\tau'}\int_0^\tau(-\int_0^s \frac{\partial\mathscr{L}_*(t,s')}{\partial t}ds')\bar{v}ds + \cdots
\end{aligned} \tag{4.6}$$

where $\vec{v}^{\,1} = \vec{v}^{\,1}(\vec{x}, t, \tau)$ and $\bar{v} = \bar{v}(\vec{x}, t)$. Note that the operator $(-\int_0^s \frac{\partial \mathscr{L}_*(t,s')}{\partial t} ds')$ applied to a vector with structure $(a, b, 0, 0, 0, 0)^\intercal$ yields zero because the first two columns of $\mathscr{L}_*$ are zero (see (2.34)) and the same idea for the operator $\mathscr{L}_0(t, s)$ (see (2.34)). It also follows that $e^{-\int_0^s \frac{\partial \mathscr{L}_*(t,s')}{\partial t} ds'}(a, b, 0, 0, 0, 0)^\intercal = I$, where I is the identity matrix and $\mathscr{L}_0(t, s)(a, b, 0, 0, 0, 0)^\intercal = \vec{0}$. The property of previous two linear operators will be widely used during the next sections where we derive the evolution equation for M and PV_e.

The full equation for $\bar{v}^{\,1}$ is given by

$$\vec{v}^{\,1} = e^{-\int_0^\tau \mathscr{L}_*(t,\tau')d\tau'} \vec{v}^{\,1}|_{\tau=0} - e^{-\int_0^\tau \mathscr{L}_*(t,\tau')d\tau'} \left\{ \tau \frac{\partial \bar{v}}{\partial t} - \int_0^\tau (\int_0^s \frac{\partial \mathscr{L}_*(t,s')}{\partial t} ds') \bar{v} ds \right.$$

$$\left. + \int_0^\tau e^{\int_0^s \mathscr{L}_*(t,s')ds'} [\mathscr{L}_0(t, s)(e^{-\int_0^s \mathscr{L}_*(t,s')ds'} \bar{v}) + \mathscr{B}(e^{-\int_0^s \mathscr{L}_*(t,s')ds'} \bar{v}, e^{-\int_0^s \mathscr{L}_*(t,s')ds'} \bar{v})] ds \right\}. \quad (4.7)$$

To control sublinear growth in (4.7), as before, we require $\vec{v}^{\,1} = o(\tau)$. In the limit $\varepsilon \to 0$, $\tau = t/\varepsilon \to \infty$ with $t = O(1)$, the fast-wave-averaging equation is thus given by

$$\frac{\partial \bar{v}(\vec{x}, t)}{\partial t} = \lim_{\tau \to \infty} \frac{1}{\tau} \int_0^\tau \left\{ (\int_0^s \frac{\partial \mathscr{L}_*(t,s')}{\partial t} ds') \bar{v} - e^{\int_0^s \mathscr{L}_*(t,s')ds'} [\mathscr{L}_0(t, s)(e^{-\int_0^s \mathscr{L}_*(t,s')ds'} \bar{v}) + \right.$$

$$\left. + \mathscr{B}(e^{-\int_0^s \mathscr{L}_*(t,s')ds'} \bar{v}, e^{-\int_0^s \mathscr{L}_*(t,s')ds'} \bar{v})] \right\} ds, \quad (4.8)$$

where the operators $\mathscr{L}_*$, $\mathscr{L}_0$ and $\mathscr{B}$ are defined in section (2.5).

The remaining sections are aimed at understanding the fast-wave-averaging system (4.8), and in particular, the evolution equations for the slow modes M and PV_e. Emphasis will be given to analysis of the bi-linear operator $\mathscr{B}$ corresponding to the nonlinear term, which has the potential to generate non-vanishing, resonant interactions between wave motions.

4.2 Slow modes and fast waves: decomposition and interactions

To focus on the evolution the slow variables M and PV_e, and possible decoupling of their evolution from fast oscillations, we may project (4.8) onto the first two components of $\bar{v} = (M, PV_e, W_1, W_2, u_m, v_m)|_{\tau=0}$ as defined in section 2.4. To this end, let us separate slow and fast components using the definitions:

$$\bar{v}(\vec{x},t) = \bar{v}_{(M,PV_e)}(\vec{x},t) + \bar{v}_{(W)}(\vec{x},t), \tag{4.9}$$

where

$$\bar{v}_{(M,PV_e)}(\vec{x},t) = \begin{pmatrix} M(\vec{x},t) \\ PV_e(\vec{x},t) \\ 0 \\ 0 \\ 0 \\ 0 \end{pmatrix}, \quad \bar{v}_{(W)}(\vec{x},t) = \begin{pmatrix} 0 \\ 0 \\ W_1(\vec{x},t,0) \\ W_2(\vec{x},t,0) \\ u_m(\vec{x},t,0) \\ v_m(\vec{x},t,0) \end{pmatrix}. \tag{4.10}$$

The nomenclature 'slow' and 'fast' follows naturally from $\mathscr{L}_*\bar{v}_{(M,PV_e)} = 0$ while $\mathscr{L}_*\bar{v}_{(W)} \neq 0$ (see section 2.4). It remains to be shown whether or not the time evolution of the slow modes $\bar{v}_{(M,PV_e)}$ is influenced by interactions with the fast modes $\bar{v}_{(W)}$ via interactions on the right hand side of the fast-wave-averaging equation (4.8).

Before presenting a detailed calculation of bi-linear terms in (4.8), we recall general features of the operator $\mathscr{B}(\vec{v}^{\,a}, \vec{v}^{\,b})$ from (2.38). Multiplication by $\vec{e}_1^{\,\mathsf{T}} = (1,0,0,0,0,0)$ and

$\vec{e}_2^{\,\intercal} = (0,1,0,0,0,0)$ yields, respectively:

$$\vec{e}_1^{\,\intercal} \cdot \mathscr{B}\Big(\begin{pmatrix} M^a \\ {PV_e}^a \\ {W_1}^a \\ {W_2}^a \\ u_m^a \\ v_m^a \end{pmatrix}, \begin{pmatrix} M^b \\ {PV_e}^b \\ {W_1}^b \\ {W_2}^b \\ u_m^b \\ v_m^b \end{pmatrix} \Big) = \vec{u}^{\,a} \cdot \nabla M^b, \tag{4.11}$$

and

$$\vec{e}_2^{\,\intercal} \cdot \mathscr{B}\Big(\begin{pmatrix} M^a \\ {PV_e}^a \\ {W_1}^a \\ {W_2}^a \\ u_m^a \\ v_m^a \end{pmatrix}, \begin{pmatrix} M^b \\ {PV_e}^b \\ {W_1}^b \\ {W_2}^b \\ u_m^a \\ v_m^a \end{pmatrix} \Big) = \vec{u}^{\,a} \cdot \nabla PV_e^b + \frac{\partial \vec{u}^{\,a}}{\partial z} \cdot \nabla \theta_e^b + \xi^a (u_x^b + v_y^b) + (w_x^a v_z^b - w_y^a u_z^b). \tag{4.12}$$

Also notice that, in terms of the initial field $\bar{v}(\vec{x},t) = \bar{v}_{(M,PV_e)}(\vec{x},t) + \bar{v}_{(W)}(\vec{x},t)$, the bilinear interactions on the right-hand-side of (4.8) may be separated into 'slow-slow', 'slow-fast', 'fast-slow' and 'fast-fast' as follows:

$$\mathscr{B}(\mathscr{A}\bar{v}, \mathscr{A}\bar{v}) = \mathscr{B}(\mathscr{A}\bar{v}_{(M,PV_e)}, \mathscr{A}\bar{v}_{(M,PV_e)})$$

$$+ \mathscr{B}(\mathscr{A}\bar{v}_{(M,PV_e)}, \mathscr{A}\bar{v}_{(W)}) + \mathscr{B}(\mathscr{A}\bar{v}_{(W)}, \mathscr{A}\bar{v}_{(M,PV_e)}) + \mathscr{B}(\mathscr{A}\bar{v}_{(W)}, \mathscr{A}\bar{v}_{(W)}), \tag{4.13}$$

where we have used $\mathscr{A} = e^{-\int_0^s \mathscr{L}_*(t,s')ds'}$ for compactness. Then using $\mathscr{A}(a,b,0,0,0,0)^\intercal = I(a,b,0,0,0,0)^\intercal = (a,b,0,0,0,0)^\intercal$, (4.13) simplifies to become

$$\mathscr{B}(\mathscr{A}\bar{v}, \mathscr{A}\bar{v}) = \mathscr{B}(\bar{v}_{(M,PV_e)}, \bar{v}_{(M,PV_e)})$$

$$+ \mathscr{B}(\bar{v}_{(M,PV_e)}, \mathscr{A}\bar{v}_{(W)}) + \mathscr{B}(\mathscr{A}\bar{v}_{(W)}, \bar{v}_{(M,PV_e)}) + \mathscr{B}(\mathscr{A}\bar{v}_{(W)}, \mathscr{A}\bar{v}_{(W)}). \tag{4.14}$$

To isolate the evolution of the slow modes $\bar{v}_{(M,PV_e)}$, the strategy is to project (4.8) onto its first two components using (4.11)-(4.12), and the decomposition of the bi-linear term given by (4.14). Different from the dry case, the 'slow-slow' nonlinear interactions depend on the fast time scale $\tau = t/\varepsilon$ through the Heaviside operators hidden inside of the PV-and-M inversion. Thus the language 'slow-slow' may be slightly misleading in this context, but is adopted nevertheless for analogy with the single-phase case. In fact, in the presence of phase boundaries, it is plausible that fast oscillations feedback onto the dynamics of M and PV_e through all of the blinear terms in (4.8). The likelihood of such feedback will be demonstrated using concrete calculations in the next two sections.

4.3 Evolution of M

By projections of the fast-wave-averaging system (4.8), one may separately analyze the evolution equations for M, PV_e, W_1, W_2, u_m, v_m, and study their coupling terms. It is worth noting that the complexity of the equations is significantly different, with M the simplest and W_2 the most complex. Here we analyze the M and PV_e equations because they are the most relevant for atmospheric modeling of large-scale weather, and fortunately the analysis is relatively simple. The equations for the fast components will be considered elsewhere.

A projection of (4.8) onto the M-mode may be written as:

$$\lim_{\tau\to\infty} -\tau\frac{\partial}{\partial t}\begin{pmatrix} M(\vec{x},t) \\ 0 \\ 0 \\ 0 \\ 0 \\ 0 \end{pmatrix} = \lim_{\tau\to\infty}\int_0^\tau \left[\vec{e}_1^{\,\intercal}\cdot\mathscr{B}(\bar{v}_{(M,PV_e)},\bar{v}_{(M,PV_e)})\right]\begin{pmatrix} 1 \\ 0 \\ 0 \\ 0 \\ 0 \\ 0 \end{pmatrix} ds +$$

$$+\lim_{\tau\to\infty}\int_0^\tau [\vec{e}_1^{\,\mathsf{T}}\cdot\mathscr{B}(e^{-\int_0^s \mathscr{L}_*(t,s')ds'}\bar{v}_{(W)},\bar{v}_{(M,PV_e)})]\begin{pmatrix}1\\0\\0\\0\\0\\0\end{pmatrix}ds+$$

$$+\lim_{\tau\to\infty}\int_0^\tau [\vec{e}_1^{\,\mathsf{T}}\cdot\mathscr{B}(\bar{v}_{(M,PV_e)},e^{-\int_0^s \mathscr{L}_*(t,s')ds'}\bar{v}_{(W)})]\begin{pmatrix}1\\0\\0\\0\\0\\0\end{pmatrix}ds+$$

$$+\lim_{\tau\to\infty}\int_0^\tau [\vec{e}_1^{\,\mathsf{T}}\cdot\mathscr{B}(e^{-\int_0^s \mathscr{L}_*(t,s')ds'}\bar{v}_{(W)},e^{-\int_0^s \mathscr{L}_*(t,s')ds'}\bar{v}_{(W)})]\begin{pmatrix}1\\0\\0\\0\\0\\0\end{pmatrix}ds, \tag{4.15}$$

where $\vec{e}_1^{\,\mathsf{T}}=(1,0,0,0,0,0)$. In (4.15), we have made the column vector $\vec{e}_1$ explicit to emphasize the projection, but henceforth we use the symbol $\vec{e}_1$ for compactness. The linear terms from

(4.8) vanish using the operator properties related with $\mathscr{L}_*(t,s)$

$$\left(\int_0^s \frac{\partial \mathscr{L}_*(t,s')}{\partial t} ds'\right) \begin{pmatrix} a \\ b \\ c \\ d \\ e \\ f \end{pmatrix} = \begin{pmatrix} 0 \\ 0 \\ \tilde{c} \\ \tilde{d} \\ \tilde{e} \\ \tilde{f} \end{pmatrix} \quad \text{and} \quad e^{\int_0^s \mathscr{L}_*(t,s')ds'} \begin{pmatrix} a \\ b \\ c \\ d \\ e \\ f \end{pmatrix} = \begin{pmatrix} a \\ b \\ c' \\ d' \\ e' \\ f' \end{pmatrix}, \tag{4.16}$$

for arbitrary $\vec{v} = (a,b,c,d,e,f)^{\intercal}$ and the operator property for $\mathscr{L}_0(t,s)$ is similar as mentioned in Section 4.1. Then, to analyze each of the four non-linear terms on the right-hand-side of (4.15), we use the concrete form of the bi-linear operator given by (4.11).

The first term on the right hand side of equation (4.15) (the 'slow-slow' impact on the evolution of M) becomes

$$\int_0^\tau \left[\vec{e}_1^{\intercal} \cdot \mathscr{B}(\bar{v}_{(M,PV_e)}, \bar{v}_{(M,PV_e)})\right] \vec{e}_1 ds \tag{4.17}$$

$$= \int_0^\tau [\vec{u}_{(M,PV_e)}(\vec{x},t,s) \cdot \nabla M(\vec{x},t)] \vec{e}_1 ds, \tag{4.18}$$

where the velocity $\vec{u}_{(M,PV_e)}$ can be found from an inversion formula (see Appendix C). Even though M and PV_e themselves do not depend on the fast time scale τ, the velocity $\vec{u}_{(M,PV_e)}$ derived from M and PV_e inversion *does* have a fast component due to the presence of Heaviside functions in the inversion formula. Applying the same ideas, the second term on the right-hand-side of (4.15) (the 'fast-slow' impact on the evolution of M) becomes,

$$\int_0^\tau \left[\vec{e}_1^{\intercal} \cdot \mathscr{B}(e^{-\int_0^s \mathscr{L}_*(t,s')ds'} \bar{v}_{(W)}, \bar{v}_{(M,PV_e)})\right] \vec{e}_1 ds \tag{4.19}$$

$$= \int_0^\tau [\vec{u}_{(W')}(\vec{x},t,s)\cdot\nabla M(\vec{x},t)]\vec{e}_1 ds \tag{4.20}$$

where $\vec{u}_{(W')}$ is a fast velocity since W_1', W_2', u_m', and v_m' are fast and depend on τ (see (4.16)). The last two terms on the right-hand-side of (4.15) ('slow-fast' and 'fast-fast') are zero:

$$\mathscr{B}\left(\begin{pmatrix} M \\ PV_e \\ 0 \\ 0 \\ 0 \\ 0 \end{pmatrix}, \begin{pmatrix} 0 \\ 0 \\ W_1' \\ W_2' \\ u_m' \\ v_m' \end{pmatrix}\right) = \mathscr{B}\left(\begin{pmatrix} 0 \\ 0 \\ W_1' \\ W_2' \\ u_m' \\ v_m' \end{pmatrix}, \begin{pmatrix} 0 \\ 0 \\ W_1' \\ W_2' \\ u_m' \\ v_m' \end{pmatrix}\right) = 0, \tag{4.21}$$

as can be seen directly from (4.11).

Finally, combining all the details together, the evolution equation for the slow variable M may be written as

$$\frac{\partial M(\vec{x},t)}{\partial t} = -\lim_{\tau\to\infty}\left(\frac{1}{\tau}\int_0^\tau \vec{u}_{(M,PV_e)}(\vec{x},t,s)ds + \frac{1}{\tau}\int_0^\tau \vec{u}_{(W')}(\vec{x},t,s)ds\right)\cdot\nabla M(\vec{x},t), \tag{4.22}$$

where ∇M does not depend on τ, and thus may be taken outside of the integrals. To aid in the interpretation of (4.22), we use the notation $\langle f\rangle$ to define the time average of any function $f(\vec{x},t,\tau)$, as follows:

$$\langle f\rangle(\vec{x},t) = \lim_{\tau\to\infty}\frac{1}{\tau}\int_0^\tau f(\vec{x},t,s)ds. \tag{4.23}$$

Using the bracket $\langle\rangle$ notation, the M-evolution equation (4.22) becomes

$$\frac{\partial M(\vec{x},t)}{\partial t} = -\langle\vec{u}_{(M,PV_e)}\rangle(\vec{x},t)\cdot\nabla M(\vec{x},t) - \langle\vec{u}_{(W')}\rangle(\vec{x},t)\cdot\nabla M(\vec{x},t), \tag{4.24}$$

in which there are two different contributions involving time-averaged velocity fields: one may refer to the terms as 'slow-slow' and 'fast-slow,' respectively, but this is an abuse of the dry language as explained. In contrast to the dry and single-phase saturated cases, *all* velocity

fields may have a fast component arising from Heaviside jumps at phase boundaries. Even the velocity field $\vec{u}_{(M,PV_e)}$ obtained *only* from slow variables M and PV_e has variation on the fast time scale τ, and thus one must analyze the average $\langle \vec{u}_{(M,PV_e)} \rangle$ as $\tau \to \infty$ in order to know the evolution of of the slow variable M.

With $V_r = 1$ and purely saturated environment (see Section 5.1), $\mathscr{L}_0$ in (2.34) is modified to include some extra entries in the first row of the matrix. These new entries represent the rainfall term $\dfrac{\partial q_t}{\partial z}$ in the q_t equation (2.6). As shown in Section 5.1, additional slow and fast terms will arise in (4.24) through the linear impact from $\mathscr{L}_0$.

4.4 Evolution of PV_e

A projection of (4.8) onto the PV_e-component may be analyzed in a manner similar to analysis of the M-equation in Section 4.3. Isolating the second component of (4.8), one finds:

$$\lim_{\tau\to\infty} -\tau \frac{\partial}{\partial t} \begin{pmatrix} 0 \\ PV_e(\vec{x},t) \\ 0 \\ 0 \\ 0 \\ 0 \end{pmatrix} = \lim_{\tau\to\infty} \int_0^\tau \left[\vec{e}_2^{\,\mathsf{T}} \cdot \mathscr{B}(\bar{v}_{(M,PV_e)}, \bar{v}_{(M,PV_e)}) \right] \begin{pmatrix} 0 \\ 1 \\ 0 \\ 0 \\ 0 \\ 0 \end{pmatrix} ds +$$

$$+ \lim_{\tau\to\infty} \int_0^\tau [\vec{e}_2^{\,\mathsf{T}} \cdot \mathscr{B}(e^{-\int_0^s \mathscr{L}_*(t,s')ds'} \bar{v}_{(W)}, \bar{v}_{(M,PV_e)})] \begin{pmatrix} 0 \\ 1 \\ 0 \\ 0 \\ 0 \\ 0 \end{pmatrix} ds +$$

$$+\lim_{\tau\to\infty}\int_0^\tau [\vec{e}_2^{\,\mathsf{T}}\cdot\mathscr{B}(\bar{v}_{(M,PV_e)}, e^{-\int_0^s \mathscr{L}_*(t,s')ds'}\bar{v}_{(W)})]\begin{pmatrix}0\\1\\0\\0\\0\\0\end{pmatrix}ds +$$

$$+\lim_{\tau\to\infty}\int_0^\tau [\vec{e}_2^{\,\mathsf{T}}\cdot\mathscr{B}(e^{-\int_0^s \mathscr{L}_*(t,s')ds'}\bar{v}_{(W)}, e^{-\int_0^s \mathscr{L}_*(t,s')ds'}\bar{v}_{(W)})]\begin{pmatrix}0\\1\\0\\0\\0\\0\end{pmatrix}ds, \tag{4.25}$$

where $\vec{e}_2^{\,\mathsf{T}} = (0,1,0,0,0,0)$. Now the calculation of the bi-linear term $\vec{e}_2^{\,\mathsf{T}}\cdot\mathscr{B}(\vec{v}^{\,a},\vec{v}^{\,b})$ is more complicated because it has four different groups:

$$\vec{u}^{\,a}\cdot\nabla PV_e^b + \frac{\partial\vec{u}^{\,a}}{\partial z}\cdot\nabla\theta_e^b + \xi^a(-w_z^b) + (w_x^a v_z^b - w_y^a u_z^b). \tag{4.26}$$

Using (4.26), the first term ('slow-slow') on the right hand side of (4.25) becomes

$$\int_0^\tau \left[\vec{e}_2^{\,\mathsf{T}}\cdot\mathscr{B}(\bar{v}_{(M,PV_e)},\bar{v}_{(M,PV_e)})\right]\vec{e}_2 ds$$

$$\begin{aligned}
&= \int_0^\tau \left\{[\vec{u}_{(M,PV_e)}(\vec{x},t,s)\cdot\nabla PV_e(\vec{x},t)] + [\frac{\partial\vec{u}_{(M,PV_e)}}{\partial z}(\vec{x},t,s)\cdot\nabla\theta_{e(M,PV_e)}(\vec{x},t,s)]\right\}\vec{e}_2 ds \\
&= \tau\left\{\langle\vec{u}_{(M,PV_e)}\rangle(\vec{x},t)\cdot\nabla PV_e(\vec{x},t) + \langle\frac{\partial\vec{u}_{(M,PV_e)}}{\partial z}\cdot\nabla\theta_{e(M,PV_e)}\rangle(\vec{x},t)\right\}\vec{e}_2,
\end{aligned} \tag{4.27}$$

and where we have used the bracket notation (4.23) to denote τ-averages. We have also used the fact that ∇PV_e does not depend on the fast time scale, and thus can be taken outside of

the integral. Compared with equation (4.26), only two of the terms survive in (4.27) because $W_1^a = W_1^b = 0$ and the inversion formula for w is $w = \nabla^{-2} W_1$ (see Appendix C). The second 'fast-slow' term on the right hand side of (4.25) is given by

$$\int_0^\tau \left[\vec{e}_2^{\,\mathsf{T}} \cdot \mathscr{B}(e^{-\int_0^s \mathscr{L}_*(t,s')ds'} \bar{v}_{(W)}, \bar{v}_{(M,PV_e)})\right] \vec{e}_2 ds \tag{4.28}$$

$$\begin{aligned} = \int_0^\tau \Big\{ & [\vec{u}_{(W')}(\vec{x},t,s) \cdot \nabla PV_e(\vec{x},t)] + [\frac{\partial \vec{u}_{(W')}}{\partial z}(\vec{x},t,s) \cdot \nabla \theta_{e(M,PV_e)}(\vec{x},t,s)] + \\ & + [w_{x(W')} v_{z(M,PV_e)} - w_{y(W')} u_{z(M,PV_e)}](\vec{x},t,s) \Big\} \vec{e}_2 ds \\ = \tau \Big\{ & \langle \vec{u}_{(W')} \rangle (\vec{x},t) \cdot \nabla PV_e(\vec{x},t) + \langle \frac{\partial \vec{u}_{(W')}}{\partial z} \cdot \nabla \theta_{e(M,PV_e)} \rangle (\vec{x},t) + \\ & + \langle w_{x(W')} v_{z(M,PV_e)} - w_{y(W')} u_{z(M,PV_e)} \rangle (\vec{x},t) \Big\} \vec{e}_2. \end{aligned} \tag{4.29}$$

In arriving at (4.29), we use the bi-linear form (4.26) and notice that the third group of terms $\xi^a(-w_z^b) = 0$ since $W_1^b = 0$. Following analogous calculations, we find the third and fourth terms of (4.25), respectively given by (4.30) and (4.31) below:

$$\text{('slow-fast')} \quad \int_0^\tau \left[\vec{e}_2^{\,\mathsf{T}} \cdot \mathscr{B}(\bar{v}_{(M,PV_e)}, e^{-\int_0^s \mathscr{L}_*(t,s')ds'} \bar{v}_{(W)})\right] \vec{e}_2 ds$$

$$= \int_0^\tau \left[\vec{e}_2^{\,\mathsf{T}} \cdot \mathscr{B}\left(\begin{pmatrix} M \\ PV_e \\ 0 \\ 0 \\ 0 \\ 0 \end{pmatrix}, e^{-\int_0^s \mathscr{L}_*(t,s')ds'} \begin{pmatrix} 0 \\ 0 \\ W_1 \\ W_2 \\ u_m \\ v_m \end{pmatrix} \right) \right] \vec{e}_2 ds$$

$$= \int_0^\tau \Big\{ [\frac{\partial \vec{u}_{(M,PV_e)}}{\partial z}(\vec{x},t,s) \cdot \nabla \theta_{e(W')}(\vec{x},t,s)] + [\xi_{(M,PV_e)}(\vec{x},t,s)(-w_{z(W')}(\vec{x},t,s))] \Big\} \vec{e}_2 ds$$

$$= \tau \Big\{ \langle \frac{\partial \vec{u}_{(M,PV_e)}}{\partial z} \cdot \nabla \theta_{e(W')} \rangle (\vec{x},t) + \langle \xi_{(M,PV_e)}(-w_{z(W')}) \rangle (\vec{x},t) \Big\} \vec{e}_2; \tag{4.30}$$

('fast-fast') $$\int_0^\tau \left[\vec{e}_2^{\,\intercal} \cdot \mathscr{B}(e^{-\int_0^s \mathscr{L}_*(t,s')ds'} \bar{v}_{(W)}, e^{-\int_0^s \mathscr{L}_*(t,s')ds'} \bar{v}_{(W)}) \right] \vec{e}_2 ds$$

$$= \int_0^\tau \left[\vec{e}_2^{\,\intercal} \cdot \mathscr{B}(e^{-\int_0^s \mathscr{L}_*(t,s')ds'} \begin{pmatrix} 0 \\ 0 \\ W_1 \\ W_2 \\ u_m \\ v_m \end{pmatrix}, e^{-\int_0^s \mathscr{L}_*(t,s')ds'} \begin{pmatrix} 0 \\ 0 \\ W_1 \\ W_2 \\ u_m \\ v_m \end{pmatrix}) \right] \vec{e}_2 ds$$

$$= \int_0^\tau \Big\{ [\frac{\partial \vec{u}_{(W')}}{\partial z}(\vec{x},t,s) \cdot \nabla \theta_{e(W')}(\vec{x},t,s)] + [\xi_{(W')}(\vec{x},t,s)(-w_{z(W')}(\vec{x},t,s))] +$$

$$+ [w_{x(W')} v_{z(W')} - w_{y(W')} u_{z(W')}](\vec{x},t,s) \Big\} \vec{e}_2 ds$$

$$= \tau \Big\{ \langle \frac{\partial \vec{u}_{(W')}}{\partial z} \cdot \nabla \theta_{e(W')} \rangle (\vec{x},t) + \langle \xi_{(W')}(-w_{z(W')}) \rangle (\vec{x},t) +$$

$$+ \langle w_{x(W')} v_{z(W')} - w_{y(W')} u_{z(W')} \rangle (\vec{x},t) \Big\} \vec{e}_2. \tag{4.31}$$

Finally, combining (4.27)-(4.31), the evolution equation of the variable PV_e has been derived from the fast-wave-averaging equation (4.8), and may be written as

$$\begin{aligned}
-\frac{\partial PV_e(\vec{x},t)}{\partial t} &= \frac{1}{\tau}((4.27)+(4.29)+(4.30)+(4.31)) \\
&= \langle \vec{u}_{(M,PV_e)} \rangle(\vec{x},t) \cdot \nabla PV_e(\vec{x},t) + \langle \vec{u}_{(W')} \rangle(\vec{x},t) \cdot \nabla PV_e(\vec{x},t) + \\
&+ \langle \frac{\partial \vec{u}_{(M,PV_e)}}{\partial z} \cdot \nabla \theta_{e(M,PV_e)} \rangle(\vec{x},t) + \langle \frac{\partial \vec{u}_{(W')}}{\partial z} \cdot \nabla \theta_{e(M,PV_e)} \rangle(\vec{x},t) + \\
&+ \langle \frac{\partial \vec{u}_{(M,PV_e)}}{\partial z} \cdot \nabla \theta_{e(W')} \rangle(\vec{x},t) + \langle \frac{\partial \vec{u}_{(W')}}{\partial z} \cdot \nabla \theta_{e(W')} \rangle(\vec{x},t) + \\
&+ \langle \xi_{(M,PV_e)}(-w_{z(W')}) \rangle(\vec{x},t) + \langle \xi_{(W')}(-w_{z(W')}) \rangle(\vec{x},t) + \\
&+ \langle w_{x(W')} v_{z(M,PV_e)} - w_{y(W')} u_{z(M,PV_e)} \rangle(\vec{x},t) + \\
&+ \langle w_{x(W')} v_{z(W')} - w_{y(W')} u_{z(W')} \rangle(\vec{x},t). \qquad (4.32)
\end{aligned}$$

4.5 The effects of phase changes

The effects of phase changes on the limiting, slow dynamics may now be assessed by comparison of the M-equation (4.24) and the PV_e-equation (4.32) to the evolution of dry PV described by (3.7)-(3.10). Of course, when water is present, a major difference from the outset is the necessity of including of a second slow variable M, in addition to a PV-variable, as has been described in Section 2.4.

When incorporating phase changes, a fundamental difference is the nature of the velocity field $\vec{u}_{(M,PV_e)}$ and the potential temperature field $\theta_{e(M,PV_e)}$ obtained from (M, PV_e)-inversion. In contrast to their analogous dry counterparts, these fields are not purely slow, because of the presence of Heaviside functions in the inversion relation (2.39) (see also (C.8), (C.18), and (C.19) in Appendix C). The Heaviside functions representing phase boundaries are determined by the full flow, including the fast component, and thus $\vec{u}_{(M,PV_e)}$ and $\theta_{e(M,PV_e)}$ are functions of the fast time scale $\tau = t/\varepsilon$. Now the fast time average $\langle \vec{u}_{(M,PV_e)} \rangle$ appears as an advection velocity in the M, PV_e-equations in place of $\vec{u}_{(M,PV_e)}$. Indeed, all terms on the right-hand-sides of (4.24) and (4.32) involve fast-averages $\langle \cdot \rangle$.

Thus we see that closure of the (M, PV_e)-equations in terms of slow variables only cannot be achieved when describing phase interfaces as fixed Heaviside operators that depend on total water. This is in contrast to the limiting dry dynamics, for which the single conservation equation (3.7) for PV involves only the slow advection velocity $\vec{u}_{(PV)}$, which is closed in terms of PV by (3.9)-(3.10). With phase changes present, coupling to fast components arises through $\langle \vec{u}_{(M,PV_e)} \rangle$, and also through an additional, time-averaged advection velocity $\langle \vec{u}_{(W')} \rangle$. Moreover, the PV_e-equation (4.32) contains time averages of 'fast-slow', 'slow-fast' and 'fast-fast' products.

Finally, a time-averaged 'slow-slow' nonlinear term $\langle (\partial \vec{u}_{(M,PV_e)}/\partial z) \cdot \nabla \theta_{e(M,PV_e)} \rangle$ appears on the right-hand-side of the PV_e-equation (4.32), whose analog is identically zero in dry and purely saturated cases (see Sections 5.1 and 5.2 below for discusion of purely saturated cases). This slow-slow nonlinearity has value zero in saturated regions, and 'turns on' after crossing phase interfaces and entering into unsaturated regions. It thus reflects slowly varying behavior of the large-scale, mid-latitude atmosphere that is directly associated with phase changes of water.

Chapter 5

Effects of rainfall, and reduced M and PV_e limiting dynamics

The fast-wave averaging equations (4.24) for M and (4.32) for PV_e were derived assuming general initial conditions with waves present, where we set $V_r = 0$ for ease of the computations. Here we add back rainfall $V_r \neq 0$, and ask: What is the influence of rainfall? For instance, does rainfall/precipitation possibly induce coupling between slow and fast components? We consider rainfall within two types of simplified settings. First, one may confine the dynamics to a purely saturated environment, and second, one may consider balanced initial conditions without waves. All of the cases considered in this section lead to closed systems for slow dynamics.

5.1 A purely saturated environment with $V_r = 1$

5.1.1 Evolution of M.

In a purely saturated region, the operator $\mathscr{L}_*$ in (2.34) will reduce to the simpler form:

$$\mathscr{L}_* = \begin{pmatrix} 0 & 0 & 0 & 0 & 0 & 0 \\ 0 & 0 & 0 & 0 & 0 & 0 \\ 0 & 0 & 0 & 1 & 0 & 0 \\ 0 & 0 & -1 & 0 & 0 & 0 \\ 0 & 0 & 0 & 0 & 0 & -1 \\ 0 & 0 & 0 & 0 & 1 & 0 \end{pmatrix}, \tag{5.1}$$

where we have set the Heaviside functions $H_s = 1$ and $H_u = 0$. The matrix $\mathscr{L}_0$ is also free of complications due to Heaviside functions. With $V_r = 1$, $\mathscr{L}_0$ now has non-zero entries in the first row to represent the rainfall term $\dfrac{\partial q_t}{\partial z}$ appearing in the q_t-equation (2.6) which will be finally inserted into the M equation after the change of variables process, to yield

$$\mathscr{L}_0 = \begin{pmatrix} -\partial_z & \partial_z^2\nabla^{-2} & 0 & \partial_z^3\nabla^{-2}\nabla_h^{-2} - \partial_z\nabla_h^{-2} & 0 & 0 \\ 0 & 0 & 0 & 0 & 0 & 0 \\ 0 & 0 & 0 & 0 & 0 & 0 \\ 0 & 0 & -\nabla_h^2\nabla^{-2} & 0 & 0 & 0 \\ 0 & 0 & 0 & 0 & 0 & 0 \\ 0 & 0 & 0 & 0 & 0 & 0 \end{pmatrix}. \tag{5.2}$$

One can observe that the entries in the first row of (5.2) are directly related to the inversion formula $q_t = M - \partial_z\nabla^{-2}(PV_e + \partial_z\nabla_h^{-2}W_2) + \nabla_h^{-2}W_2$ with $H_s = 1$, $H_u = 0$ (For details, see (C.8) and (C.20), which indicates $\theta_e = \partial_z\nabla^{-2}(PV_e + \partial_z\nabla_h^{-2}W_2) - \nabla_h^{-2}W_2$.) and represent $\dfrac{\partial q_t}{\partial z}$ in the M equation. Similarly, rainfall also has an impact on the W_2-equation, but the new terms arise at $O(\varepsilon)$ and hence do not appear in $\mathscr{L}_0$ (see (B.33) and (B.35)).

As described in Section 4.3 above, the fast-wave-averaging equation (4.8) may be projected onto the M-mode to find its evolution in a purely saturated domain. The evolution is structurally the same as (4.24) with extra linear, rainfall terms:

$$\frac{\partial M(\vec{x},t)}{\partial t} = -\langle\vec{u}_{(M,PV_e)}\rangle(\vec{x},t)\cdot\nabla M(\vec{x},t) - \langle\vec{u}_{(W')}\rangle(\vec{x},t)\cdot\nabla M(\vec{x},t) +$$

$$+ \langle\frac{\partial q_{t(M,PV_e)}}{\partial z}\rangle(\vec{x},t) + \langle\frac{\partial q_{t(W')}}{\partial z}\rangle(\vec{x},t). \tag{5.3}$$

However, the terms on the right-hand-side involving fast variables $\langle\vec{u}_{(W')}\rangle$ and $\langle\dfrac{\partial q_{t(W')}}{\partial z}\rangle$ are identically zero, as explained below. The remaining slow terms are independent of the fast time scale τ, and thus they are invariant under the averaging operator $\langle\cdot\rangle$. Hence (5.3) reduces to

$$\frac{\partial M(\vec{x},t)}{\partial t} = -\vec{u}_{(M,PV_e)}(\vec{x},t)\cdot\nabla M(\vec{x},t) + \frac{\partial q_{t(M,PV_e)}}{\partial z}(\vec{x},t). \tag{5.4}$$

It remains to demonstrate that the terms $\langle \vec{u}_{(W')} \rangle \cdot \nabla M$ and $\langle \frac{\partial q_{t(W')}}{\partial z} \rangle$ in (5.3) arising from fast components (W_1', W_2', u_m', v_m') will vanish under the averaging operation $\langle \cdot \rangle$. As a concrete example consider $\langle \frac{\partial q_{t(W')}}{\partial z} \rangle$, which can be obtained from the single-phase inversion formula $F(\cdot)$ for $q_t = F(M, PV_e, W_1, W_2, u_m, v_m) = M - \partial_z \nabla^{-2}(PV_e + \partial_z \nabla_h^{-2} W_2) + \nabla_h^{-2} W_2$. To isolate the fast components, one may filter the slow components by setting $M = PV_e = 0$, such that

$$q_{t(W')} = F(0, 0, W_1', W_2', u_m', v_m') = \partial_z \nabla^{-2}(\partial_z \nabla_h^{-2} W_2') + \nabla_h^{-2} W_2'. \tag{5.5}$$

Then applying the fast-averaging-operator $\langle \cdot \rangle$, we obtain

$$\langle q_{t(W')} \rangle = \langle \partial_z \nabla^{-2}(\partial_z \nabla_h^{-2} W_2') + \nabla_h^{-2} W_2' \rangle = \partial_z \nabla^{-2}(\partial_z \nabla_h^{-2} \langle W_2' \rangle) + \nabla_h^{-2} \langle W_2' \rangle. \tag{5.6}$$

By the definition of (W_1', W_2', u_m', v_m') from (4.16), these are purely oscillatory variables associated with the non-zero eigenvalues of $\mathscr{L}_*$ in (5.1). Thus the conclusion $\langle W_1' \rangle = 0$, $\langle W_2' \rangle = 0$, $\langle u_m' \rangle = 0$, and $\langle v_m' \rangle = 0$ is straightforward, which implies $\langle q_{t(W')} \rangle = 0$. A similar argument shows that $\langle \vec{u}_{(W')} \rangle \cdot \nabla M = 0$.

5.1.2 Evolution of PV_e.

Using the single-phase operators $\mathscr{L}_*$ and $\mathscr{L}_0$ given by (5.1) and (5.2), we now project (4.8) onto the PV_e mode. Apart from the first row of $\mathscr{L}_0$, all other entries in both $\mathscr{L}_*$ and $\mathscr{L}_0$ are the same as for the more general case with phase changes, except with the simplification $H_s = 1$ and $H_u = 0$ for a purely saturated domain. Although $\mathscr{L}_0$ has entries in its first row to account for rainfall with $V_r = 1$, only its *second* row impacts the projection of (4.8) onto the PV_e mode. Hence, we conclude that PV_e evolution in the saturated domain has exactly the same structural form as (4.32), even for $V_r = 1$.

As explained in Section 5.1.1 for the single-phase M-equation, slow variables are invariant under the fast-averaging operation $\langle \cdot \rangle$, while fast variables average to zero. Implementation of these results in (4.32) leads to a reduced PV_e-equation without any slow-fast or fast-slow

interaction terms:

$$
\begin{aligned}
-\frac{\partial PV_e(\vec{x},t)}{\partial t} &= \vec{u}_{(M,PV_e)}(\vec{x},t)\cdot\nabla PV_e(\vec{x},t) + \frac{\partial \vec{u}_{(M,PV_e)}}{\partial z}(\vec{x},t)\cdot\nabla\theta_{e(M,PV_e)}(\vec{x},t) \\
&+ \langle\frac{\partial \vec{u}_{(W')}}{\partial z}\cdot\nabla\theta_{e(W')}\rangle(\vec{x},t) + \langle\xi_{(W')}(-w_{z(W')})\rangle(\vec{x},t) \\
&+ \langle w_{x(W')}v_{z(W')} - w_{y(W')}u_{z(W')}\rangle(\vec{x},t). \qquad (5.7)
\end{aligned}
$$

Rigorous analysis of the fast-fast nonlinear interactions has been performed by transforming the physical variables to Fourier space (see Appendix D and Appendix E). The Fourier analysis reveals that the sum of the 4 terms is identically zero, which is not obvious to see in physical space. Finally, the slow-slow term $\frac{\partial \vec{u}_{(M,PV_e)}}{\partial z}\cdot\nabla\theta_{e(M,PV_e)}$ also vanishes identically, as can be shown by Fourier analysis or vector algebra using the relations $\vec{u}_{(M,PV_e)} = (-\partial\psi/\partial y, \partial\psi/\partial x, 0)$ and $\theta_{e(M,PV_e)} = \partial\psi/\partial z$, where ψ is a streamfunction given by

$$\nabla^2\psi = PV_e. \qquad (5.8)$$

The inversion equation (5.8) is the special case of the general inversion formula (2.39) with $W_2 = 0$ and vorticity-streamfunction relation $\xi = \nabla_h^2\psi$. (see (C.20)–(C.24))

5.1.3 Summary of the slow dynamics in a saturated domain with $V_r = 1$.

Gathering together the M-equation , PV_e-equation, and inversion relations for the saturated phase, one arrives at the closed system:

$$\frac{\partial PV_e(\vec{x},t)}{\partial t} + \vec{u}_{(M,PV_e)}(\vec{x},t)\cdot\nabla PV_e(\vec{x},t) = 0, \qquad (5.9)$$

$$\frac{\partial M(\vec{x},t)}{\partial t} + \vec{u}_{(M,PV_e)}(\vec{x},t)\cdot\nabla M(\vec{x},t) = \frac{\partial q_{t(M,PV_e)}}{\partial z}(\vec{x},t), \qquad (5.10)$$

$$\nabla^2\psi = PV_e \qquad (5.11)$$

$$\vec{u}_{(M,PV_e)} = (-\frac{\partial\psi}{\partial y}, \frac{\partial\psi}{\partial x}, 0), \quad \theta_{e(M,PV_e)} = \frac{\partial\psi}{\partial z}, \quad q_{t(M,PV_e)} = M - \frac{\partial\psi}{\partial z}. \qquad (5.12)$$

Notice that $\vec{u}_{(M,PV_e)}$ and $\theta_{e(M,PV_e)}$ are actually determined from PV_e alone. Furthermore, one sees that q_t and M do not feed back on the dynamics of PV_e, although PV_e can influence the evolution of q_t and M [14, 15].

This case illustrates that the slow modes evolve independently from the fast wave modes, even in the presence of rainfall/precipitation (by itself, without phase changes).

5.2 A purely saturated environment with $V_r = O(\varepsilon^{-1})$

The case of $V_r = \varepsilon^{-1}$ corresponds to a large but still realistic value of the dimensional rainfall speed $V_T = 1$ m/s ($V_r = V_T/w$, where w is a reference vertical velocity scale; thus $V_r = \varepsilon^{-1}$ corresponds to $V_T = 1$ m/s and $w = 0.1$ m/s). Now V_r appears in $\mathscr{L}_*$ and hence M is no longer a purely slow variable, but nevertheless, one can proceed to analyze the dynamics of the slow mode PV_e.

With rainfall included in the ε^{-1} balance of terms, the operators $\mathscr{L}_*$, $\mathscr{L}_0$ are given by

$$\mathscr{L}_* = \begin{pmatrix} -\partial_z & \partial_z^2\nabla^{-2} & 0 & \partial_z^3\nabla^{-2}\nabla_h^{-2} - \partial_z\nabla_h^{-2} & 0 & 0 \\ 0 & 0 & 0 & 0 & 0 & 0 \\ 0 & 0 & 0 & 1 & 0 & 0 \\ 0 & 0 & -1 & 0 & 0 & 0 \\ 0 & 0 & 0 & 0 & 0 & -1 \\ 0 & 0 & 0 & 0 & 1 & 0 \end{pmatrix} \tag{5.13}$$

$$\mathscr{L}_0 = \begin{pmatrix} 0 & 0 & 0 & 0 & 0 & 0 \\ 0 & 0 & 0 & 0 & 0 & 0 \\ 0 & 0 & 0 & 0 & 0 & 0 \\ -\nabla_h^2\partial_z & \nabla_h^2\partial_z^2\nabla^{-2} & -\nabla_h^2\nabla^{-2} & \partial_z^3\nabla^{-2} - \partial_z & 0 & 0 \\ 0 & 0 & 0 & 0 & 0 & 0 \\ 0 & 0 & 0 & 0 & 0 & 0 \end{pmatrix}, \tag{5.14}$$

where the influence of V_r appears in the first row of $\mathscr{L}_*$ and forth row of $\mathscr{L}_0$ (compare to (5.1)

and (5.2)). Similar to Section 5.1, these extra entries are used to represent the term $\frac{\partial q_t}{\partial z}$, which appears in the q_t-equation, and thus to determine both M and W_2 (see more details in (B.36), (B.37)).

A projection of (4.8) onto the PV_e mode involves only the second rows of (5.13) and (5.14). Following from the projection, the resulting closed system for PV_e is structurally the same as (3.7) and (5.9):

$$\frac{D}{Dt}PV_e = (\frac{\partial}{\partial t} + \vec{u}_{(PV_e)} \cdot \nabla)PV_e = 0 \tag{5.15}$$

$$\nabla^2\psi = PV_e, \quad \vec{u}_{(PV_e)} = \left(-\frac{\partial\psi}{\partial y}, \frac{\partial\psi}{\partial x}, 0\right), \quad \theta_{e(PV_e)} = \frac{\partial\psi}{\partial z}. \tag{5.16}$$

5.3 The PQG equations with phase changes for balanced initial conditions

As a moist model for evolution from balanced initial conditions, the precipitating quasi-geostrophic equations [50] retain phase changes, but filter wave motions from the outset. Consequently, all 'slow-fast,' 'fast-slow,' and 'fast-fast' nonlinearities are absent from the associated version of the PV_e-equation (4.32). Furthermore, the Heaviside functions representing phase boundaries can only be a function of the balanced dynamics. Thus (M, PV_e)-inversion recovers a purely slow streamfunction, such that the advection velocity $\vec{u}_{(M,PV_e)}$ appearing in the (M, PV_e)-equation is slow and invariant under the fast-averaging operation $\langle\cdot\rangle$. The signature 'slow-slow' nonlinear term $(\partial\vec{u}_{(M,PV_e)}/\partial z) \cdot \nabla\theta_{e(M,PV_e)}$ in (4.32) is also invariant under fast-averaging, and it becomes nonzero in unsaturated regions of the environment, representing the change in functional form of the buoyancy at phase interfaces. In the notation of the current paper, the PQG model is reproduced here as:

$$\frac{\partial PV_e(\vec{x},t)}{\partial t} + \vec{u}_{(M,PV_e)}(\vec{x},t) \cdot \nabla PV_e(\vec{x},t) = \frac{\partial\vec{u}_{(M,PV_e)}}{\partial z}(\vec{x},t) \cdot \nabla\theta_{e(M,PV_e)}(\vec{x},t), \tag{5.17}$$

$$\frac{\partial M(\vec{x},t)}{\partial t} + \vec{u}_{(M,PV_e)}(\vec{x},t) \cdot \nabla M(\vec{x},t) = \frac{\partial q_{t(M,PV_e)}}{\partial z}(\vec{x},t), \tag{5.18}$$

$$\nabla_h^2\psi + \frac{\partial}{\partial z}\left[\frac{1}{2}H_u\left(\frac{\partial\psi}{\partial z} + M\right)\right] + \frac{\partial}{\partial z}\left[H_s\frac{\partial\psi}{\partial z}\right] = PV_e \tag{5.19}$$

$$\vec{u}_{(M,PV_e)} = (-\frac{\partial\psi}{\partial y}, \frac{\partial\psi}{\partial x}, 0), \quad \theta_{e(M,PV_e)} = \frac{1}{2}H_u\left(\frac{\partial\psi}{\partial z}+M\right)+H_s\left(\frac{\partial\psi}{\partial z}\right), \quad q_{t(M,PV_e)} = M-\theta_{e(M,PV_e)}. \tag{5.20}$$

Chapter 6

Methodology

6.1 Numerical method

The 3D moist Boussinesq equations with two phases of water (vapor and liquid) are simulated in a 2π-periodic domain using a dealiased, pseudo-spectral code. Calculations with spatial resolutions $128 \times 128 \times 128$ and $256 \times 256 \times 256$ are compared to ensure that the results are insensitive to resolution, e.g., for the $O(1)$ time averages in (4.24) contributing to the evolution of the slow variable M. The comparison provides confidence in the robustness of our results, especially for smallest value of the Rossby and Froude numbers ($\varepsilon \sim O(10^{-3})$).

After transferring the physical space equations into Fourier space, a third-order Rung-Kutta time-stepping scheme solves the coupled system of ODEs resulting from discretization of the wavevector. Linear rotation and buoyancy terms are treated explicitly, and the nonlinear terms are calculated in physical space with implementation of FFTW. A pressure-solver enforces the incompressibility constraint, and viscous linear terms are included using an integrating factor. A hyperviscosity is used instead of the normal viscosity to induce dissipation only at the smallest scales. For example, in the momentum equation, the hyperviscosity takes the form

$$(-1)^{p+1}\nu(\nabla^2)^p\vec{v}, \tag{6.1}$$

where we use $p = 8$. The coefficient ν has the structure

$$\nu = 2.5(\frac{E_\nu(k_m, t)}{k_m})^{1/2}k_m^{2-2p}, \tag{6.2}$$

where k_m is highest available wavenumber and E_ν is the kinetic energy in k_m shell. Similar expressions are used in the equations for equivalent potential temperature θ_e and water q_t [23, 53].

6.2 Discussion of time scales and values of the parameter ε

In the multiscale method to derive the fast-wave-averaging equation (4.8), two time scales (short and long) arise naturally. The model equations have been nondimensionalized so that $t = O(\varepsilon)$ is closely linked to the fast waves (time scale τ), while $t = O(1)$ is associated with slow motions (time scale t). The wave frequencies in the unsaturated and saturated domains are, respectively, given by

$$\sigma_u(\vec{k}) = \frac{(Fr_u^{-2}k_h^2 + Ro^{-2}k_z^2)^{1/2}}{k}, \qquad \sigma_s(\vec{k}) = \frac{(Fr_s^{-2}k_h^2 + Ro^{-2}k_z^2)^{1/2}}{k}, \tag{6.3}$$

where Fr_u, Fr_s are defined in (2.15). Given $Fr_s = Ro = \varepsilon$, then $\sigma_s = \varepsilon^{-1}$ and the time period of waves in the purely saturated region is $T' = 2\pi/\sigma_s = O(\varepsilon)$. Time steps in the numerical simulations are chosen small enough to simultaneously satisfy the CFL condition and to resolve the fast-wave oscillations.

We consider the special case $Fr_1 = Fr_2 = Ro = \varepsilon$ and corresponding $(Fr_u, Fr_s) = (\varepsilon/\sqrt{2}, \varepsilon)$, $(\sigma_u, \sigma_s) = (\sqrt{2}\varepsilon^{-1}, \varepsilon^{-1})$, with $10^{-3} \leq \varepsilon \leq 1$. The values of (Ro, Fr_u, Fr_s) are monitored in time by calculating the non-dimensional quantities (2.11) and (2.15), where $L = H = 2\pi$ and U is maximum magnitude of velocity field. During $O(1)$ time intervals of our decay simulations with hyperviscosity, the values of (Ro, Fr_u, Fr_s) do not change significantly, helping to essentially 'freeze' the value of ε for any given run.

6.3 Cloud fraction

As mentioned in Chapter 2, phase changes enter the model through the buoyancy and to simplify the dynamics for fast-wave averaging framework (Chapter 4) the phase boundaries are defined as locations where the anomalous total water q_t is zero. In the simplified dynamics

under consideration there (Chapter 4), the total water is solely water vapor in unsaturated regions such that $q_t = q_v$; in saturated regions, excess water above the saturation level is entirely liquid water such that $q_t = q_r$. In order to consider the effects of cloud fraction, a constant value of $q_{vs,0}$ will be used in our numerical simulations such that $\tilde{q}_t = \tilde{q}_v = q_{vs} - q_{vs,0}$, with linear saturation profile $q_{vs}(z)$ [10, 23, 42]. Hence the more general expressions (including the impact of cloud fraction) for the unsaturated buoyancy b_u and the saturated buoyancy b_s are given by

$$b_u = [\theta_e + (\varepsilon - 1)q_t], \qquad b_s = [\theta_e + (\varepsilon - 1)q_{vs,0} - \epsilon q_r]. \tag{6.4}$$

The anomalous water constituents are found from the relations

$$q_v = q_t,\ q_r = 0 \quad \text{if} \quad q_t < q_{vs,0}, \quad \text{and} \quad q_v = q_{vs,0},\ q_r = q_t - q_{vs,0} \quad \text{if} \quad q_t \geq q_{vs,0}, \tag{6.5}$$

which define vapor q_v and rain q_r in terms of total water q_t and saturation threshold $q_{vs,0}$. In the simulations, the value of $q_{vs,0}$ will be adjusted to vary the initial cloud fraction. The formulas $q_v = \min(q_t, q_{vs,0})$, $q_r = \max(0, q_t - q_{vs,0})$ are used to determine vapor q_v and liquid water q_r from total water q_t and saturation threshold $q_{vs,0}$ (To reduce the parameter space, the rainfall parameter V_r is here set to zero, such that the liquid water q_r does not fall.) . By adjusting the constant parameter $q_{vs,0}$, one may control the initial cloud fraction quantified by cloud indicator $H_s(q_t - q_{vs,0})$. In Chapter 7, the cloud fraction will be calculated as L^1 norm of cloud indicator $H_s(q_t - q_{vs,0})$. During the $O(1)$-time evolution, for small amount of initial $||H_s(q_t - q_{vs,0})||_1$ with value less than $\leq 30\%$ of the domain, the fluctuation of $||H_s(q_t - q_{vs,0})||_1$ over time is quite small (1% to 2%). Thus, for all practical purposes, the cloud fraction can be considered as fixed for the discussion in Section 7.1. We note that large initial $||H_s(q_t - q_{vs,0})||_1$, with value $\geq 70\%$ of the domain, leads to significant fluctuations of $||H_s(q_t - q_{vs,0})||_1$ in time.

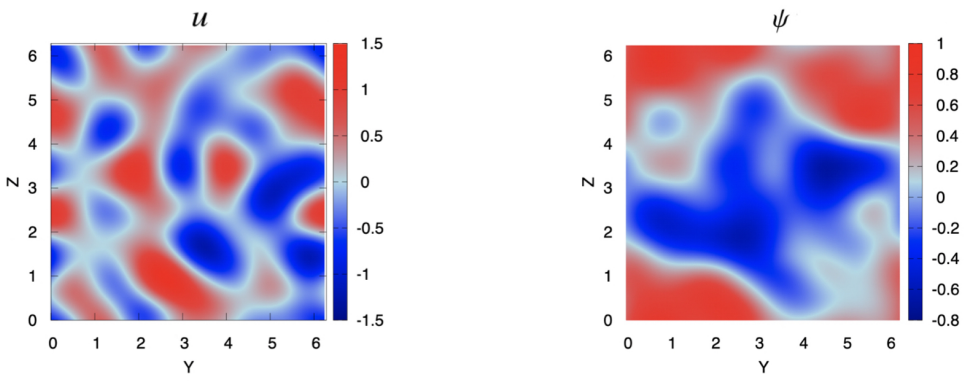

Figure 6.1: Random large-scale initial conditions: velocity u (left) and stream function ψ (right). 2D slices are shown with $x = \pi$ held fixed.

6.4 Large-scale, random initial conditions

For most cases in Chapter 7, we consider decay from large-scale, random initial conditions. The spectral density for all variables (u, v, w, θ_e, q_t) is a Gaussian function given by

$$F(k) = \varepsilon_f \frac{\exp(-0.5(k - k_f)^2/s^2)}{(2\pi)^{1/2} s} \tag{6.6}$$

where $s = 1$ is standard deviation, $k_f = 3$ is the peak wave number of the force and $\varepsilon_f = O(1)$ is the energy input rate. Furthermore, the k-values are restricted to the interval $[1, 5]$. Upon the change of variable from (u, v, w, θ_e, q_t) to $(M, PV_e, W_1, W_2, u_m, v_m)$, the slow (M, PV_e) and fast (W) components have comparable spectral density levels in wavenumbers $[1, 5]$. For specific choices of the initial distinguished parameter ε (based on maximum magnitude of the initial velocity) and saturation threshold $q_{vs,0}$, the system evolves according to moist Boussinesq dynamics with phase changes of water. Figure 6.1 shows 2D slices of the initial variables u and ψ constructed from aforementioned random initial condition.

6.5 Evaluation of nonlinear terms in PV_e evolution equation

As discussed in Chapter 4, the (M, PV_e)-evolution equations derived from fast-wave-averaging have the explicit expressions (4.24) and (4.32). With a closer look at the PV_e-equation, the nonlinear terms appearing in the right hand side of (4.32) contain slow-slow, fast-slow, slow-fast, fast-fast interactions. For the limiting ($\varepsilon \to 0$) dry dynamics, only the slow-slow term $\vec{u}_{(PV)} \cdot \nabla PV$ is non-zero and there is complete decoupling between the slowly varying components and the fast waves [16, 17, 38, 40]. Similarly, starting from balanced initial conditions without waves, only slow-slow terms appear in the (M, PV_e) limiting dynamics [50]. However in (4.24) and (4.32), one cannot, a priori, show that all of the coupling terms are zero. Thus, phases changes lead to potential sources of feedback from fast oscillations onto the evolution of the slow modes (M, PV_e). The feedback may originate directly from the fast components (W), or indirectly at phase interfaces through (M, PV_e)-inversion, and is manifested through time averages over fast time scales.

Here we perform a numerical assessment for small values of ε, and investigate trends for decreasing ε. For the PV_e-equation, the averages to be measured in the simulations at finite ε are the following:

Slow-Slow:

$$\frac{1}{T}\int_0^T \vec{u}_{(M,PV_e)}(\vec{x},t') \cdot \nabla PV_e(\vec{x},t')dt' \tag{6.7}$$

$$\frac{1}{T}\int_0^T \frac{\partial \vec{u}_{(M,PV_e)}(\vec{x},t')}{\partial z} \cdot \nabla \theta_{(M,PV_e)}(\vec{x},t')dt' \tag{6.8}$$

Fast-Slow:

$$\frac{1}{T}\int_0^T \vec{u}_{(W')}(\vec{x},t') \cdot \nabla PV_e(\vec{x},t')dt' \tag{6.9}$$

$$\frac{1}{T}\int_0^T \frac{\partial \vec{u}_{(W')}(\vec{x},t')}{\partial z} \cdot \nabla \theta_{(M,PV_e)}(\vec{x},t')dt' \tag{6.10}$$

$$\frac{1}{T}\int_0^T [w_{x(W')}v_{z(M,PV_e)} - w_{y(W')}u_{z(M,PV_e)}](\vec{x},t')dt' \tag{6.11}$$

Slow-Fast:

$$\frac{1}{T}\int_0^T \frac{\partial \vec{u}_{(M,PV_e)}(\vec{x},t')}{\partial z}\cdot\nabla\theta_{(W')}(\vec{x},t')dt' \tag{6.12}$$

$$\frac{1}{T}\int_0^T -\xi_{(M,PV_e)}w_{z(W')}(\vec{x},t')dt' \tag{6.13}$$

Fast-Fast:

$$\frac{1}{T}\int_0^T \{\frac{\partial \vec{u}_{(W')}(\vec{x},t')}{\partial z}\cdot\nabla\theta_{(W')}(\vec{x},t')$$
$$+ [-\xi_{(W')}w_{z(W')} + w_{x(W')}v_{z(W')} - w_{y(W')}u_{z(W')}](\vec{x},t')\}dt' \tag{6.14}$$

The numerical quantities we monitor are discrete versions of integration over total time T, which means that we collect data starting from $t' = 0$ and record the values after each step until the stopping time $t' = T$. Then we compute the L^2 norm for the spatial domain, resulting in a single non-dimensional number for each term (6.7) - (6.14), e.g., $||\langle\vec{u}_{(M,PV_e)}\cdot\nabla PV_e\rangle||_2$. Since the time-averaged quantities enter statistically steady state when $T \approx 0.3$, the data for fixed $T = 0.6$ is presented in tabular form for the main results (Chapter 7), and $T = 0.67$ is used in Section 8.1. Note that long-time averages reflect loss of energy due to viscous decay in all variables, obscuring trends.

6.6 (M, PV_e)-inversion for finite ε

After each time step of the numerical simulation, the updated state vector (u, v, w, θ_e, q_t) may be used in a post-processing step to find the updated fields (M, PV_e, H_u, H_s). Then to compute the slow components $\vec{u}_{(M,PV_e)}$, $\theta_{e(M,PV_e)}$ and $q_{t(M,PV_e)}$, we use the finite-ε PV-M-inversion of

(5.19) (with saturation threshold $q_{vs,0}$) given by

$$\nabla_h^2\psi+\frac{\partial}{\partial z}[H_u(\frac{1}{2-\varepsilon}\frac{\partial\psi}{\partial z}+\frac{1-\varepsilon}{2-\varepsilon}M)]+\frac{\partial}{\partial z}[H_s(\frac{1}{1+\varepsilon}\frac{\partial\psi}{\partial z}+\frac{\varepsilon}{1+\varepsilon}M+(1-2\varepsilon)q_{vs,0})]=PV_e. \quad (6.15)$$

Following inversion of (6.15) to find the streamfuntion ψ, finite-ε version of relations (5.20) is used to obtain $\vec{u}_{(M,PV_e)}$, $\theta_{e(M,PV_e)}$. Finally, the definition of M given by (2.21), together with $\theta_{e(M,PV_e)}$, gives $q_{t(M,PV_e)}$.

For the numerical solution of (6.15), a centered-difference method was used, which, owing to the discontinuous coefficients introduced by phase boundaries (H_u, H_s), is similar to the ghost fluid approach [35, 36, 55]. The conjugate gradient method is then used to solve the discretized symmetric linear system and determine the streamfunction ψ. Here we adopt a simple version of the ghost-fluid method that does not use subcell information about the interface location, and a Gaussian smoothing of the resulting ψ is used, such that gradient fields may be reliably computed in (6.7) - (6.14). A 1D version of the Gaussian filter is given by

$$W[\psi](x)=\frac{1}{\sqrt{4\pi s}}\int_{-\infty}^{\infty}\psi(x-y)\exp\frac{-y^2}{4s}dy, \quad (6.16)$$

where (6.16) is also known as a Weierstrass transformation. For the 3D version we use the Gaussian-Weierstrass kernel $s = 500$ in all three directions for resolution 256^3 ($s = 200$ in all directions for resolution 128^3). A simplified test case shows quantitative agreement between this method and a subcell-location version of the ghost-fluid approach.

Chapter 7

Results of numerical simulations

In this section, numerical simulations are used to test the fast-wave averaging theory with phase changes. The most attention will be given to a scenario where the initial conditions are large-scale and randomly selected (section 7.1). Then some additional sensitivity studies are also conducted to assess the robustness of the results (section 7.2).

7.1 A first assessment: fast-wave averaging with phase changes

The setup is as follows. This first assessment will use random initial conditions, which are generated as described above in Chapter 6. The parameter of interest is ε, and small values are considered as a numerical investigation of the limit $\varepsilon \to 0$. All other parameters are held fixed, including the duration $T = 0.6$ of the time-averaging window and also the cloud fraction $||H_s(q_t - q_{vs,0})||_1 = 22\%$. Strictly speaking, the cloud indicator H_s and distinguished parameter ε are dynamic quantities; nevertheless, the simulation is run for only a time of $O(1)$, and on these time scales, the fluctuations of these two quantities are somewhat small. Hence it is reasonable to use the initial values of ε and cloud fraction $||H_s(q_t - q_{vs,0})||_1$ to represent these two dynamic quantities, and to use these two quantities to help characterize the physical setting of each simulation.

Figure 7.1 shows the results of the numerical simulations for several different values of ε ranging from 1 to 10^{-3}. In this figure, the particular quantity of interest is $\langle \vec{u}_{(W')} \cdot \nabla PV_e \rangle$ ("fast-slow"), which is from the right hand side of the PV_e evolution equation in (4.32). The L^2 norm of this quantity is plotted against the value of ε on a log–log plot. (The L^2 norm is normalized by taking a ratio of the target quantity's L^2 norm after $T = 0.6$ divided by its

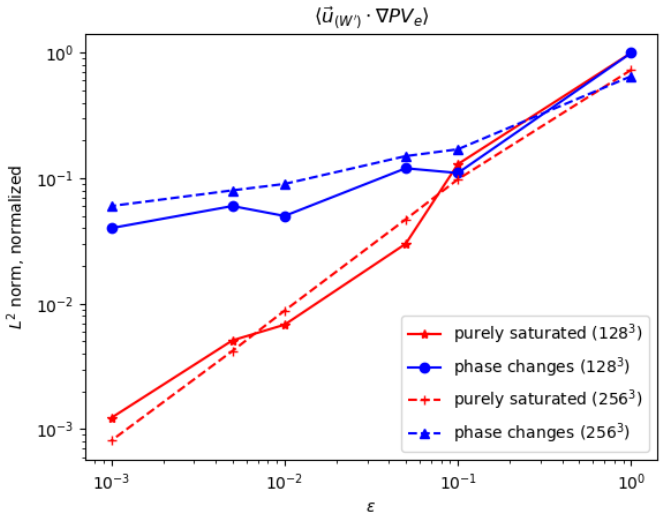

Figure 7.1: Behavior of the fast–slow term $\langle \vec{u}_{(W')} \cdot \nabla PV_e \rangle$ as ε tends toward zero, for the case of a randomly selected initial condition. The duration for the time averaging is $T = 0.6$, and for the phase-change cases the cloud fraction is $||H_s(q_t - q_{vs,0})||_1 = 22\%$. The L^2 norm of $\langle \vec{u}_{(W')} \cdot \nabla PV_e \rangle$ is plotted and is normalized by dividing by the initial L^2 norm of $\vec{u}_{(W')} \cdot \nabla PV_e$.

initial L^2 norm.)

As a baseline, the purely saturated case (without phase changes) is shown in figure 7.1 in red. In this baseline case, the L^2 norm of $\langle \vec{u}_{(W')} \cdot \nabla PV_e \rangle$ decays proportional to ε as $\varepsilon \to 0$. Such a result is in agreement with the dry theory [16, 38], and it provides a demonstration of the soundness of the numerical experiments. Two different numerical resolutions, 128^3 and 256^3, are also shown here to support the numerical robustness. Physically, this plot indicates that the velocity $\vec{u}_{(W')}$, which is associated with fast waves, is "averaged out" for small values of ε.

Are the fast waves also 'averaged out' in the case with phase changes? The results are shown in figure 7.1 in blue. For $\varepsilon = 0.1$, the L^2 norm of $\langle \vec{u}_{(W')} \cdot \nabla PV_e \rangle$ is also approximately 0.1, and its magnitude is similar in the phase-change case and the purely saturated case. Hence, from this $\varepsilon = 0.1$ experiment, one sees an indication that the fast waves are indeed averaged out, to the extent possible for $\varepsilon = 0.1$. For smaller values of $\varepsilon = 0.01$ and 0.001, the L^2 norm of

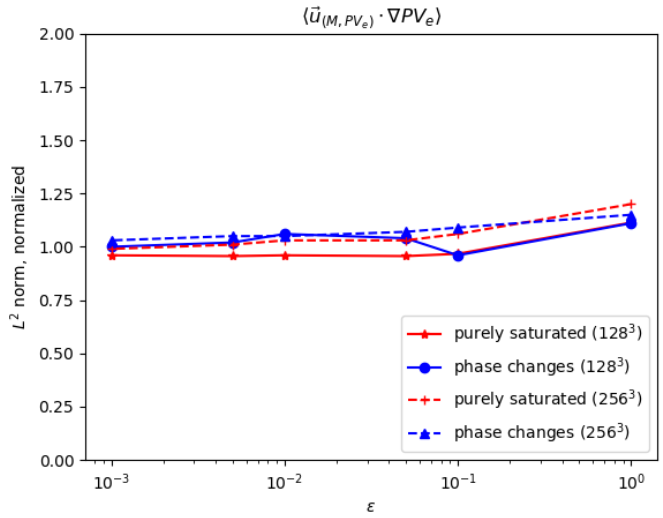

Figure 7.2: Same as Figure 7.1, except for the slow-slow term $\langle \vec{u}_{(M,PV_e)} \cdot \nabla PV_e \rangle$.

$\langle \vec{u}_{(W')} \cdot \nabla PV_e \rangle$ remains somewhat small and in the range of roughly 0.03 to 0.1, and it appears to continue to decay as $\varepsilon \to 0$, but the decay rate is either very slow or not decaying. In particular, the decay rate is much slower with phase changes (blue color) than the decay rate that is proportional to ε in the purely saturated case (red color). The phase changes appear to cause the velocity $\vec{u}_{(W')}$, which is associated with fast waves, to acquire a time-averaged component that is somewhat small but possibly non-negligible.

For comparison, figure 7.2 shows the L^2 norm of $\langle \vec{u}_{(M,PV_e)} \cdot \nabla PV_e \rangle$ for different values of ε. This is a slow-slow term, in contrast to the fast-slow term shown earlier in figure 7.1. Here, in figure 7.2, for all values of ε, the (normalized) L^2 norm is approximately equal to 1, indicating that the time-averaged quantity has essentially the same L^2 norm as its initial value. Hence, the term $\langle \vec{u}_{(M,PV_e)} \cdot \nabla PV_e \rangle$ is not averaged out, and it contributes to the important mechanism of PV advection, in both the phase-change case and the purely saturated case.

To provide further details, table 7.1 shows the behavior of some of the other nonlinear terms from (6.7 - 6.14) in the moist Boussinesq simulations with phase changes. The table shows three values of ε as it tends toward zero: 0.1, 0.01, and 0.001. As a comparison, table 7.2 shows the corresponding results for the dry case. By comparing tables 7.1 and 7.2, we now

	$\varepsilon = O(0.1)$	$\varepsilon = O(0.01)$	$\varepsilon = O(0.001)$
$\|\|\langle \vec{u}_{(M,PV_e)} \cdot \nabla PV_e \rangle\|\|_2$	0.96	1.06	1.00
$\|\|\langle \vec{u}_{(W')} \cdot \nabla PV_e \rangle\|\|_2$	0.11	0.05	0.04
$\|\|\langle \frac{\partial \vec{u}_{(M,PV_e)}}{\partial z} \cdot \nabla \theta_{e(M,PV_e)} \rangle\|\|_2$	0.92	0.91	0.88
$\|\|\langle \frac{\partial \vec{u}_{(W')}}{\partial z} \cdot \nabla \theta_{e(W')} - \xi_{(W')} w_{z(W')} + w_{x(W')} v_{z(W')} - w_{y(W')} u_{z(W')} \rangle\|\|_2$	0.14	0.42	0.30

Table 7.1: Behavior of terms in the PV_e evolution equation from (6.7)–(6.14) in the moist Boussinesq simulations with phase changes, for the case of a randomly selected initial condition. The duration for the time averaging is $T = 0.6$, the resolution is 128^3, and the cloud fraction is $||H_s(q_t - q_{vs,0})||_1 = 22\%$. The L^2 norm of $\langle f \rangle$ is normalized by dividing by the initial L^2 norm of f, where f represents the various terms displayed.

summarize some additional main points.

First, consider the two nonlinear terms that contain wave influence: $||\langle \vec{u}_{(W')} \cdot \nabla PV_e \rangle||_2$, and $||\langle \frac{\partial \vec{u}_{(W')}}{\partial z} \cdot \nabla \theta_{e(W')} - \xi_{(W')} w_{z(W')} + w_{x(W')} v_{z(W')} - w_{y(W')} u_{z(W')} \rangle||_2$. In table 7.1 for the phase-change case, these two wave-influence terms are relatively small and have norms in the range of 0.04 to 0.4. Hence, relative to the slow-slow terms $||\langle \vec{u}_{(M,PV_e)} \cdot \nabla PV_e \rangle||_2$ and $||\langle \frac{\partial \vec{u}_{(M,PV_e)}}{\partial z} \cdot \nabla \theta_{e(M,PV_e)} \rangle||_2$, which have norms of 0.9 to 1.0, the wave-influence terms are somewhat small. Consequently, the slow modes evolve *nearly* independent of the fast wave influence.

Second, notice the difference between the fast-fast term $||\langle \frac{\partial \vec{u}_{(W')}}{\partial z} \cdot \nabla \theta_{e(W')} - \xi_{(W')} w_{z(W')} + w_{x(W')} v_{z(W')} - w_{y(W')} u_{z(W')} \rangle||_2$ that is grouped together, versus one of its components, such as $||\langle \frac{\partial \vec{u}_{(W')}}{\partial z} \cdot \nabla \theta_{e(W')}||_2$, which is also shown by itself in table 7.2. In particular, the separate component $||\langle \frac{\partial \vec{u}_{(W')}}{\partial z} \cdot \nabla \theta_{e(W')}||_2$ does not average out as ε tends to zero; instead, its norm remains nearly constant for all values of ε. In contrast, the sum of all four terms grouped together does tend toward zero as ε tends toward zero. This phenomenon can be understood in the purely saturated case by referring to Fourier analysis. More specifically, when there is no

	$\varepsilon = O(0.1)$	$\varepsilon = O(0.01)$	$\varepsilon = O(0.001)$
$\|\|\langle \vec{u}_{(M,PV_e)} \cdot \nabla PV_e \rangle\|\|_2$	0.97	0.96	0.96
$\|\|\langle \vec{u}_{(W')} \cdot \nabla PV_e \rangle\|\|_2$	$1.29{*}10^{-1}$	$0.68{*}10^{-2}$	$1.23{*}10^{-3}$
$\|\|\langle \frac{\partial \vec{u}_{(M,PV_e)}}{\partial z} \cdot \nabla \theta_{e(M,PV_e)} \rangle\|\|_2$	null	null	null
$\|\|\langle \frac{\partial \vec{u}_{(W')}}{\partial z} \cdot \nabla \theta_{e(W')} - \xi_{(W')} w_{z(W')} + w_{x(W')} v_{z(W')} - w_{y(W')} u_{z(W')} \rangle\|\|_2$	$0.46{*}10^{-1}$	$0.48{*}10^{-2}$	$0.85{*}10^{-3}$
$\|\|\langle \frac{\partial \vec{u}_{(W')}}{\partial z} \cdot \nabla \theta_{e(W')} \|\|_2$	0.58	0.64	0.62

Table 7.2: Same as table 7.1, except for the purely saturated case, which has a cloud fraction of 100%.

phase change present, the Fourier analysis shows that the fast-fast nonlinear coefficient C_{kpq} in Fourier space [24] is identically zero. Thus, when viewed in physical space rather than Fourier space, one may need to combine all four terms together to get the Fourier inversion of C_{kpq}, and to see the budget terms tending toward zero as ε tends toward zero. This is in contrast to the fast-slow terms, such as $||\langle \vec{u}_{(W')} \cdot \nabla PV_e \rangle||_2$, which is seen in table 7.2 to decay proportional to ε as a separate term on its own; in this case, it is the Riemann–Lebesgue lemma, a different mechanism, that is responsible for the decay as ε tends toward zero.

7.2 Sensitivity studies and robustness tests

Following the results from the previous section 7.1, naturally one may ask about the robustness of the results. For instance, are the same results seen for different initial conditions? Does the cloud fraction have any impact on the outcome? The above questions are answered in this section with some additional tests.

While the use of randomly selected initial conditions already provides some generality, we now test another type of initial condition of a different type (see also [53,59]). In particular, the goal is to create some initial conditions that are somewhat simple while also involving the

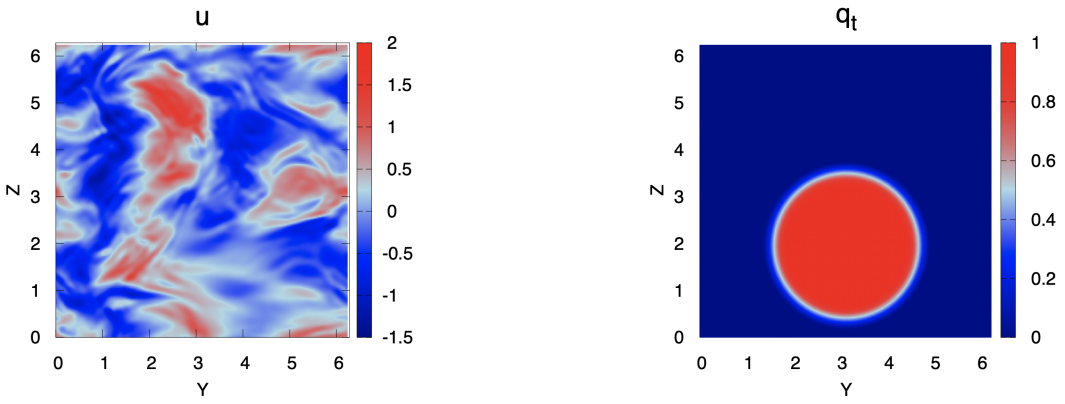

Figure 7.3: Initial conditions for a sensitivity study, with initial turbulent velocity u (left) and a moist bubble in total water q_t (right). 2D slices are shown with $x = \pi$ held fixed. The bubble of q_t has initial moisture perturbation centred at $\vec{x}_0 = (\pi, \pi, 0.625\pi)$.

influence of a turbulent flow. To do this, the model is initialized using a dry turbulent state that is first generated without the influence of moisture. To generate the dry turbulent state, a large-scale random forcing is first imposed, and the simulation is run to a statistical steady state, thereby providing a dry turbulent state. The velocity field $\vec{u}^{\top} = (u, v, w)$ generated from this turbulent state will then be utilized as the desired initial condition for velocity. Simultaneously a new stable temperature background (hot inside bubble; cold outside) will be constructed artificially. Now moisture in the initial state is included in a simple way; at a new time $t = 0$ a bubble of water vapor is added to the turbulent velocity field and stable temperature background at the lower center of the domain. The system is then allowed to evolve according to moist Boussinesq dynamics with phase changes of water. To illustrate the initial conditions, figure 7.3 shows 2D slices of two of the variables: u, q_t. When the dynamics have run for 1 time unit and the moisture and the turbulence have begun mixing, we begin to collect data for the time-averaged budget analysis. Mathematically, for equation (6.9), we set time $T = 0.6$ and choose data from $t' \in [1, 1.6]$ together with frozen cloud fraction (28% at $t' = 1$). The results are shown in figures 7.4 and 7.5, which demonstrate that essentially the same conclusion and phenomenon are seen as in the case of randomly selected initial condition from earlier figures 7.1 and 7.2.

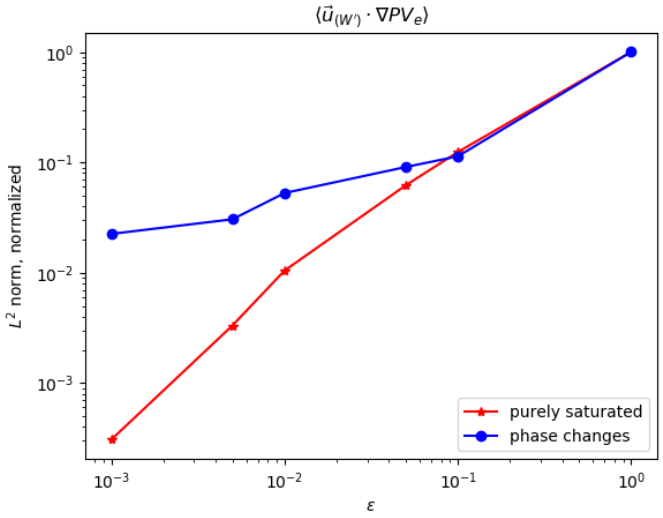

Figure 7.4: Same as figure 7.1, except for initial conditions of a turbulent velocity field and a moist bubble, and for only a resolution of 128^3.

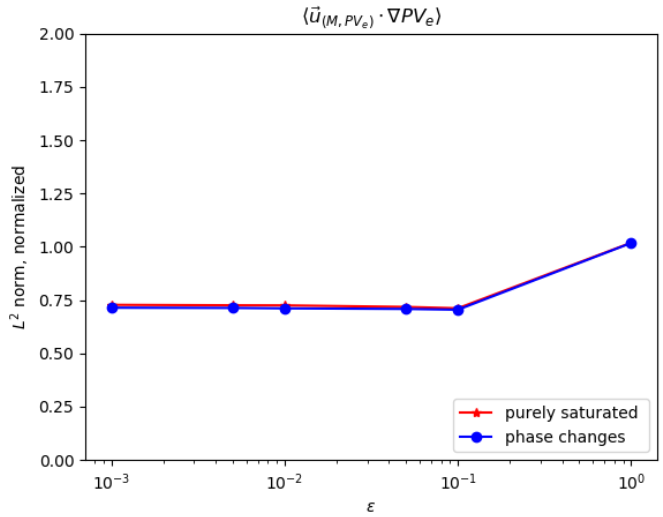

Figure 7.5: Same as figure 7.2, except for initial conditions of a turbulent velocity field and a moist bubble, and for only a resolution of 128^3.

As another set of sensitivity studies, we now discuss the impact of cloud fraction. In particular, recall that figures 7.1 and 7.2 showed results for a particular value of cloud fraction of 22%, as well as the purely saturated case where cloud fraction is 100%. We now ask: Do the results change for different values of cloud fraction? For simplicity, attention will be focused on $||\langle \vec{u}_{(W')} \cdot \nabla PV_e \rangle||_2$ only. For this exploration, we freeze $\varepsilon = O(0.01), T = 0.6$ and then vary the initial $q_{vs,0}$ value to control different initial cloud fractions. The results of the analysis are shown in figure 7.6. For the two boundary points of 0% and 100% cloud fraction, for which no phase changes are present, notice that the L^2 norm is $O(0.01)$ and proportional to ε, which indicates that the fast waves are averaged out in these two cases. On the other hand, for other values of cloud fraction between 0% and 100%, the normalized $||\langle \vec{u}_{(W')} \cdot \nabla PV_e \rangle||_2$ values are larger and do not seem to be proportional to an ε value of $O(0.01)$, which is consistent with the main conclusion in section 7.1. As a finer detail, notice that the value of $||\langle \vec{u}_{(W')} \cdot \nabla PV_e \rangle||_2$ increases as cloud fraction increases (away from the two boundary values of 0% and 100% cloud fraction). In other words, fast waves appear to be averaged out to a greater degree when the cloud fraction is in the range of 0% to 20%, which is also the most relevant range for cloud fractions in nature. When the cloud fraction is higher, the fast waves are averaged out less, and the value of $||\langle \vec{u}_{(W')} \cdot \nabla PV_e \rangle||_2$ is higher.

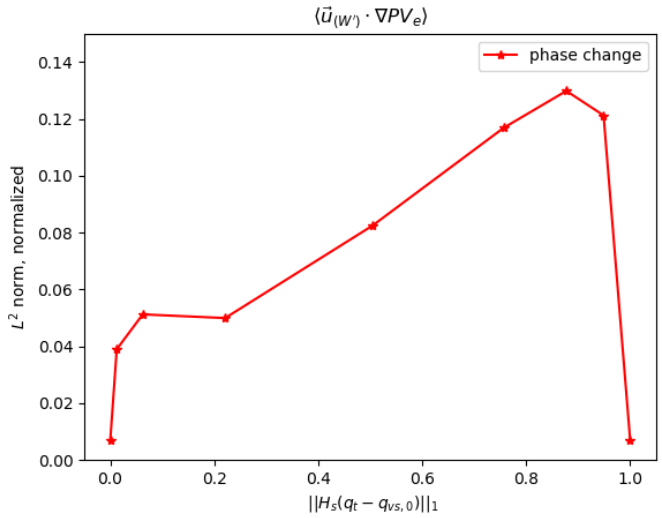

Figure 7.6: Behavior of the fast–slow term $\langle \vec{u}_{(W')} \cdot \nabla PV_e \rangle$ for the case of a randomly selected initial condition, for different values of the cloud fraction, $||H_s(q_t - q_{vs,0})||_1$. The duration for the time averaging is $T = 0.6$, and $\varepsilon = O(0.01)$. The L^2 norm of $\langle \vec{u}_{(W')} \cdot \nabla PV_e \rangle$ is plotted and is normalized by dividing by the initial L^2 norm of $\vec{u}_{(W')} \cdot \nabla PV_e$.

Chapter 8

Explanation and physical interpretation

8.1 A closer look at simulated data

To explain the mechanism by which phase changes impact fast-wave averaging, we isolate points in the simulations where $O(1)$ time averages are larger than $O(\varepsilon)$. We use the simulation with $\varepsilon = O(0.01)$, random large-scale initial conditions and cloud fraction 22%. The goal is to explore the physical properties of these 'bad' points where the time-average of fast-slow interactions are $O(0.1)$ instead of $\varepsilon = O(0.01)$.

Specifically, we monitor the fast-slow term $\langle \vec{u}_{(W')} \rangle (\vec{x}, t) \cdot \nabla M(\vec{x}, t)$ in M-evolution equation (4.24), starting form random initial conditions. After time averaging, instead of taking L^2 norm, we check all points (x_0, y_0, z_0) in the 3D-domain. A post-processing routine computes the absolute value $|\frac{1}{T}\int_0^T \vec{u}_{(W')}(\vec{x}, t') \cdot \nabla M(\vec{x}, t')dt'|$ for $T = 0.67$, and highlights every point whose time-averaged absolute value is greater than $O(0.1)$ (see the third panel in figure 8.1). Meanwhile, in order to observe the relationship between phase changes and these 'bad' points, we also plot the initial cloud distribution (first panel in figure 8.1), and the the time-average $\langle H_s \rangle$ of the cloud indicator function H_s (second panel in figure 8.1). Note that H_s is shorthand for $H_s(q_t - q_{vs,0})$. From the figure, one may observe the following: if the value $\langle H_s(x_0, y_0, z_0) \rangle$ is near 0 or 1, then this position (x_0, y_0, z_0) is away from a phase interface (blue color in the second panel); values $\langle H_s(x_0, y_0, z_0) \rangle \in [0.2, 0.8]$ indicate that this position experiences frequent change of phase (yellow color in the second panel).

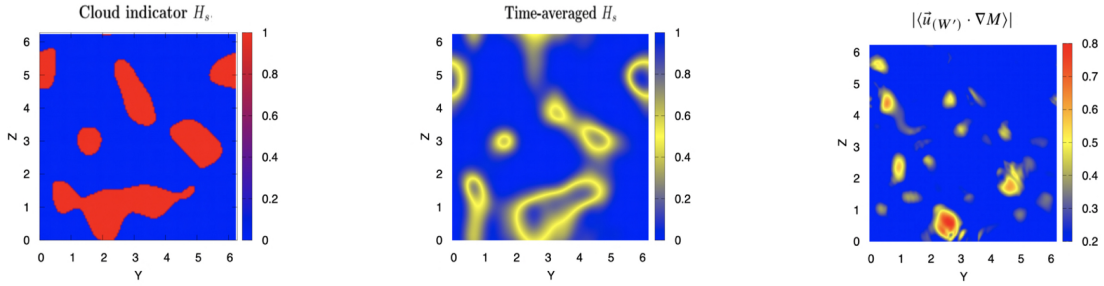

Figure 8.1: From left to right are initial H_s at $t = 0$, $\langle H_s\rangle$ and $|\langle\vec{u}_{(W')}\cdot\nabla M\rangle|$. 2D slices are shown for $x = \pi$ held fixed. Red areas in the first panel represents clouds (liquid water). Yellow patterns in second panel indicate the regions where phase changes happen frequently. Hot spots (yellow to red) in the third panel indicate high values of the fast-slow coupling term.

A closer look at the hot spots in third panel of figure 8.1 reveals interesting physical properties of the flow. For a specific point (x_0, y_0, z_0), figure 8.2 demonstrates how the location alternates between unsaturated and saturated states (top panel). During the time $t \in [0, 0.67]$, there are 23 time windows with $H_s(t, x_0, y_0, z_0) = 1$, and 22 time windows with $H_s(t, x_0, y_0, z_0) = 0$. Furthermore, the bottom panel shows the time ratio that the wave spends in those two different states as a function of time window (time ratio = time in each window$/T$, where $T = 0.67$). One can see that more time is spent in the saturated state. Quantitatively, 58% of the time is spent in the saturated state, compared to 42%-time in the unsaturated state. Close to a phase boundary, a wave spends more time in the saturated state because the frequencies have the relationship $(\sigma_u, \sigma_s) = (\sqrt{2}\varepsilon^{-1}, \varepsilon^{-1})$ (see (6.3) and recall that $Fr_1 = Fr_2 = \varepsilon$, therefore the non-zero frequency σ_u in the unsaturated state is greater than σ_s in the saturated state). Finally, figure 8.3 shows that q_t has wave fluctuations crossing the phase boundary, and it spends more time in the saturated state. Other physical variables exhibit the similar behavior. Since more time is spent in one phase than the other, or more time is spent in the wave crest than the wave valley, it is possible that the wave has a time average that is nonzero, and the wave is therefore possibly not "averaged out."

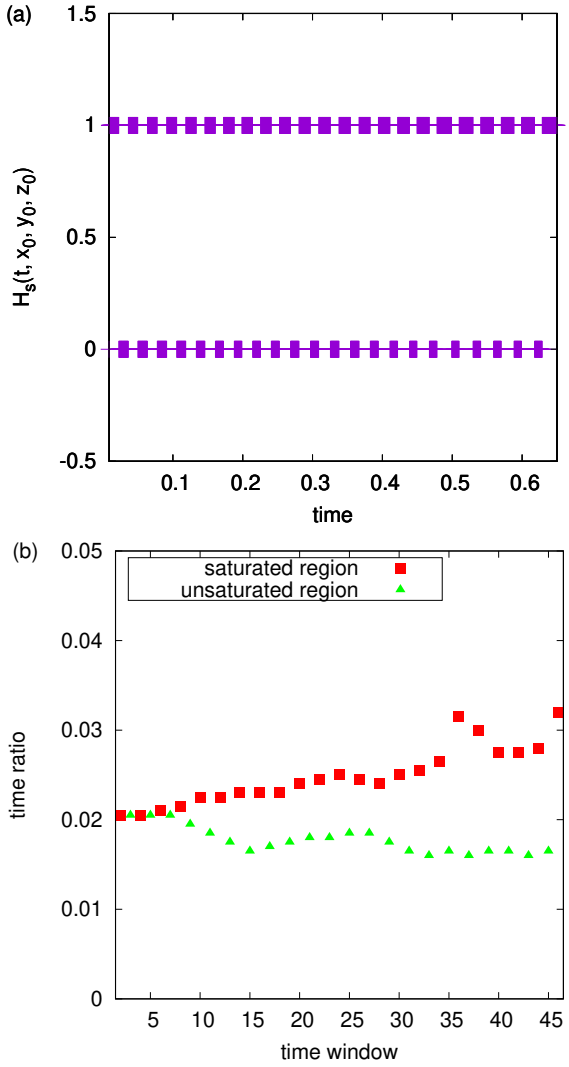

Figure 8.2: (Top) $H_s(t, x_0, y_0, z_0)$ vs. time t for $t \in [0, 0.67]$, with H_s measured from a red-spot position (x_0, y_0, z_0) in figure 8.1. There are 45 total alternating time windows: 23 for the saturated state, and 22 for the unsaturated state. Quantitatively, 58% of the time is spent in the saturated state, compared to 42% time in the unsaturated state. (Bottom) The green triangles represent the time ratio spent in unsaturated windows, while the red squares correspond to time spent in saturated windows (time ratio = time in each window/T, where $T = 0.67$).

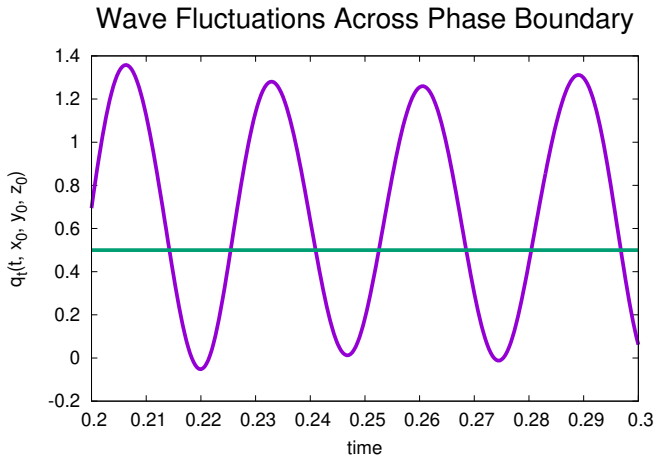

Figure 8.3: The purple curve is the time evolution of water $q_t(t, x_0, y_0, z_0)$, for fixed (x_0, y_0, z_0) chosen from a red spot position in figure 8.1. The green line is the saturation threshold $q_{vs,0} = 0.5$.

8.2 ODE system

In this section, we look for a simple nonlinear system to help in understanding section 8.1. In particular, we will introduce the ODE system that arises from the 3-D Boussinesq moist dynamics if spatial variations are neglected:

$$\frac{dw}{dt} = b = N_u b_u H_u + N_s b_s H_s \tag{8.1}$$

$$\frac{db_u}{dt} + N_u w = 0 \tag{8.2}$$

$$\frac{db_s}{dt} + N_s w = 0 \tag{8.3}$$

Among the velocity components, we only keep the w equation, which is the simplest setup that still retains waves. Also, according to equation (6.3), we retain the main properties of waves with different frequencies (N_u, N_s) in different phases (b_u, b_s), and introduce the conditions for phase change $(H_s = H(b_s - b_u))$. Finally, when we discuss the time-averaged of analytical solution and associated asymptotic theory of ODE, we will make the N_u, N_s parameter go to ∞ which plays the role of ε^{-1} in (2.3 - 2.6). We continue to use the special parameter settings $N_1 = N_2$ as in the numerical simulation, recalling (2.14), and retain the buoyancy

frequencies that are associated with unsaturated regions (N_u) and saturated regions (N_s) to have the relationships

$$N_u{}^2 = 2N_s{}^2 \tag{8.4}$$

where $N_u \neq N_s$ and are both positive.

8.2.1 General Solution for ODE System in Different Phases

In order to solve the aforementioned ODE analytically, the key point is to define the invariant variable $M = N_u^{-1}b_u - N_s^{-1}b_s$, which satisfies $dM/dt = 0$. Hence M is a parameter and then $b_s = \dfrac{N_s}{N_u}b_u - MN_s$. With the replacement of b_s in the ODE system, we only need 2 variables at any given time to describe the evolution as

$$\frac{dw}{dt} = N_u b_u H_u + N_s(\frac{N_s}{N_u}b_u - MN_s)H_s, \tag{8.5}$$

$$\frac{db_u}{dt} + N_u w = 0. \tag{8.6}$$

The phase change condition $H_s = H(b_s - b_u)$ follows from the earlier condition $H_s = H(q_t - q_{vs,0})$ [42], where $b_s \geq b_u$ gives a saturated region while $b_s < b_u$ represents an unsaturated region. For an unsaturated region, $b_u > \dfrac{MN_sN_u}{N_s - N_u}$ yields

$$b_u'' + N_u^2 b_u = 0, \tag{8.7}$$

followed by the general solution

$$b_u = c_{u1}\sin(N_u t) + c_{u2}\cos(N_u t). \tag{8.8}$$

For a saturated region, $b_u \leq \dfrac{MN_sN_u}{N_s - N_u}$ leads to

$$b_u'' + N_s^2 b_u = MN_s^2 N_u, \tag{8.9}$$

followed by the general solution

$$b_u = c_{s1}\sin(N_s t) + c_{s2}\cos(N_s t) + MN_u. \tag{8.10}$$

To find a nonlinear solution that switches phase, as a piece-wise sine function, the main idea is to use variables (w, b_u) in the unsaturated phase and then evolve the system forward in time until we hit saturation. After that we switch to using variables (w, b_s) while in the saturated phase.

8.2.2 A simple solution example with $M = 0$

A simple solution of the nonlinear wave in the ODE system is now presented, for any $(b_u(t_0), w(t_0), M)$, where t_0 is the initial time. The interesting case will be an alternating piecewise wave, which crosses the phase boundary repeatedly, passing back and forth between unsaturated and saturated regions. For simplicity, we demonstrate using an example with $M = 0$, which means that the phase boundary is exactly at $y = 0$ or $b_u = 0$.

Without loss of generality, assume an initial buoyancy exactly at the phase boundary such that $b_u(t_0) = 0$, and set the initial vertical velocity $w(t_0) = a$, where a is arbitrary positive number. Note that $b_u'(t_0) = -N_u w(t_0) = -N_u a < 0$, which indicates that the solution will enter the saturated region first. The analytical solution for this initial condition is given by

$$b_u(t) = \begin{cases} -\dfrac{aN_u}{N_s}\sin(N_s(t-t_0)) & t \in [t_0 + n\mathcal{T}, t_0 + \dfrac{\pi}{N_s} + n\mathcal{T}] \\ a\sin(N_u(t - t_0 - \dfrac{\pi}{N_s})) & t \in [t_0 + \dfrac{\pi}{N_s} + n\mathcal{T}, t_0 + (n+1)\mathcal{T}], \end{cases} \tag{8.11}$$

where $\mathcal{T} = \dfrac{\pi}{N_u} + \dfrac{\pi}{N_s}$ and $n = 0, 1, 2\cdots$. Then, after one half period at $t = t_0 + \pi/N_s$, the solution meets the phase interface at $y = 0$ with $b_u(t_0 + \pi/N_s) = 0, b_u'(t_0 + \pi/N_s) = aN_u > 0$, which is the starting point for wave propagation in the unsaturated region.

Using formula (8.11), we can now calculate the time-averaged value $|\frac{1}{T}\int_0^T b_u(t)dt|$, to determine if there is a non-zero average when a phase boundary is present. Without loss of

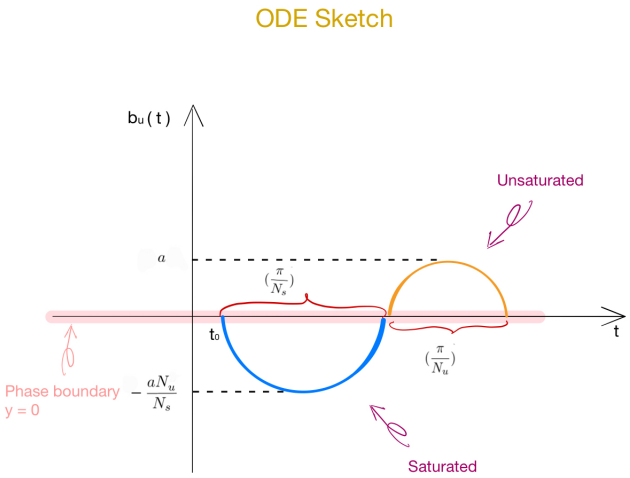

Figure 8.4: Piecewise solution of (8.11) for $M = 0$ such that the phase interface is at $y = 0$.

generality, we choose $a = 1$ and $N_u = \sqrt{2}N_s$ as in (8.4). On the one hand, consider the purely unsaturated case without phase changes, in which case the analytical solution for $b_u(t)$ is a simple sine function with frequency N_u. In that case, for fixed averaging interval T, the average $|\frac{1}{T}\int_0^T b_u(t)dt| \leq \dfrac{2}{N_u T} \to 0$ as $N_u \to \infty$. On the other hand, if the phase interface is present, then we find the relations:

$$\frac{2}{\pi(1+\sqrt{2})} - \frac{2}{N_u T} \leq |\frac{1}{T}\int_0^T b_u(t)dt| \leq \frac{2}{\pi(1+\sqrt{2})} + \frac{2}{N_u T}, \quad N_u \to \infty, \tag{8.12}$$

which is strictly bounded away from zero. Figure 8.4 displays the solution (8.11), and clearly illustrates how different frequencies $N_u \neq N_s$ lead to non-zero time average of $b_u(t)$ as in (8.12). Most importantly, the same essential mechanism is observed in the 3D Boussinesq simulations, as seen in figure 8.3.

Chapter 9

Conclusions and Discussion

9.1 Asympotic analysis

In the context of moist atmospheric dynamics, we have adapted fast-wave averaging to include moisture, rainfall and phase changes between water vapor and liquid water. The ultimate goal is to better understand the limiting dynamics for small Rossby and Froude numbers, and the nature of possible coupling between slow and fast components of the system. The analysis assumes a distinguished limit in which all small parameters (Rossby, Froude, etc.) are related to one parameter $\varepsilon \to 0$. Including an additional equation for total water leads to an additional slow mode M, which is absent in the dry dynamics. Thus the main objective was to obtain limiting dynamics for (M, PV_e) as $\varepsilon \to 0$.

Phase interfaces between unsaturated and saturated regions of the environment lead mathematically to the presence of Heaviside functions in the governing Boussinesq equations. These Heaviside functions delineate phase boundaries where the buoyancy changes its functional form, and they depend on both fast and slow variables. Consequently, the linear operator of the dry system becomes a nonlinear operator in the moist system with phase changes.

Here we have presented a formulation of fast-wave averaging, in which the Heaviside functions are treated as known, determined from the Boussinesq family of solutions at fixed value of ε. Then the nonlinear phase-change operator becomes a piece-wise linear operator, and much progress can be achieved. Notably, a linear version of (M, PV_e)-inversion may be used to evaluate linear and nonlinear interaction terms in the fast-wave averaging equations. Although closure of the (M, PV_e)-equations is not obtained, important insight is gained regarding the

nature of the slow dynamics and possible coupling to the fast variables (W_1, W_2, u_m, v_m).

As derived in Chapter 4, condensation and evaporation at phase interfaces lead to a 'slow-slow' non-linearity $\langle(\partial\vec{u}_{(M,PV_e)}/\partial z)\cdot\nabla\theta_{e(M,PV_e)}\rangle$ in the PV_e-equation that is nonzero in unsaturated regions of the flow. Such a term is present in the PQG reduced dynamics without waves, but obviously absent in purely saturated dynamics formulations. As also identified in Chapter 4 and discussed in Chapter 5, the phase-change analysis reveals several potential sources of feedback from fast oscillations onto the evolution of the slow modes (M, PV_e). The feedback may originate directly from the fast components (W_1, W_2, u_m, v_m), or indirectly at phase interfaces through (M, PV_e)-inversion. Feedback onto (M, PV_e) is manifested through time averages over fast time scales.

Finally, we note that numerical simulations of the moist Boussinesq system can be used to provide further insight in Chapter 6, 7. For instance, simulations could be used to probe the slow-fast, fast-slow and fast-fast terms appearing in the (M, PV_e)-equations. By applying time averages to the simulation data, one can infer whether or not the time-averaged terms are tending to zero, and therefore infer whether or not there is coupling between fast and slow modes. Such information from simulations could also complement the formal asymptotic analysis (Chapter 4, 5) and together aid the formulation of rigorous proofs in future.

9.2 Numerical assessment

Phase changes of water in atmospheric flows are as fundamental as the presence of fast inertia-gravity waves generated by the effects of rotation and stable stratification. In Chapter 2, all these effects are combined in an idealized model with a Boussinesq dynamical core and simplified thermodynamics allowing for phase changes of water, from vapor to liquid and vice versa. We conduct moist Boussinesq simulations (Chapter 6) designed to support asymptotic theory in the limit of vanishing Rossby and Froude numbers: $Ro = Fr_1 = Fr_2 = \varepsilon \to 0$ (asymptotically large rotation and strong stable stratification). The theory separates the state space of the Boussinesq dynamics into fast waves evolving on short times $t = O(\varepsilon)$, and slowly

varying (M, PV_e) components evolving on times $t = O(1)$. Furthermore, the initial conditions are assumed to contain fast waves. Then the central goal is to assess the coupling between fast and slow components on $O(1)$ time scales as $\varepsilon \to 0$. Such coupling is explicitly represented by terms in the fast-wave-averaging equation (4.8). For example, in the PV_e-equation (4.32), the fast-slow, slow-fast and fast-fast terms (6.9) - (6.14) do not a priori vanish in an environment with phase changes. This situation is in contrast to the the case of dry dynamics, for which rigorous proofs establish decoupling between the dry PV and the fast waves [16, 17, 38, 40]. On the other hand, all of the terms (6.7) - (6.14) can be measured in numerical simulations at finite ε, and thus our companion numerical calculations investigate trends in their behaviors for decreasing ε in the range $10^{-3} \leq \varepsilon \leq 1$.

The main suite of simulations starts from random, large-scale initial conditions and varies the distinguished parameter ε, along with the saturation threshold $q_{vs,0}$ (which determines the resulting cloud fraction). For example, when the cloud fraction is roughy 22% of the domain, the results show that the fast-fast term (6.14) does not decay with ε (table 7.1), and the fast-slow term $||\langle \vec{u}_{(W')} \cdot \nabla PV_e \rangle||_2$ decays significantly slower with ε than the analogous term in the dry dynamics (figure 7.1). For fixed ε, robustness studies indicate that fast-slow coupling increases with cloud fraction, up to cloud fractions of at least 80% of the domain (figure 7.6). Altogether, the results suggest that coupling of (M, PV_e)-dynamics with fast-waves may persist as $\varepsilon \to 0$ when the cloud fraction is in the range $[10\%, 85\%]$.

The limiting equations (4.24) and (4.32) for (M, PV_e) may contain nonzero averages arising mathematically from two sources. Feedback from waves onto (M, PV_e) may originate directly from the fast components (W), or indirectly at phase interfaces through (M, PV_e)-inversion (5.19, 6.15). To gain insight into behavior of waves near a phase interface, we use a coupled ODE system for vertical velocity $w(t)$, together with unsaturated buoyancy $b_u(t)$ and saturated buoyancy $b_s(t)$. In this model, the saturation condition is given by $b_u = b_s$, and the saturation threshold is given in terms of the parameter M. The buoyancies b_u and b_s evolve according to different oscillator equations associated with different frequencies N_u and N_s. To solve the ODE system from an unsaturated initial b_u, one may first integrate the oscillator

equation for b_u until the saturation condition $b_u = b_s$ is reached, and then proceed to integrate the oscillator equation for b_s until $b_s = b_u$, and so on. For $N_u \neq N_s$, the exact solution consists of a piecewise wave solution as in figure 8.4. By virtue of the different frequencies and wavelengths on either side of the phase boundary, the time average of b_u over $t = O(1)$ is bounded away from zero for asymptotically large N_u. Such piecewise waves are indeed observed in the Boussinesq simulations, e.g., as seen in the solution for $q_t(t, \vec{x}_0)$ for fixed location $\vec{x}_0$ close to a phase boundary (figure 8.3).

For Boussinesq dynamics with phase changes, the formal asymptotic theory (Chapter 4), PDE numerical simulations (Chapter 7), and model-ODE exact solutions (Chapter 8) together indicate that feedback from waves onto slowly varying flow components may have an impact even as the Rossby and Froude numbers tend to zero. Especially given the importance of phase changes for atmospheric applications, several follow-up studies are planned. Theoretically, the longer term goal is to perform rigorous analysis in which the phase boundaries are determined as part of the solution. Future numerical simulations will investigate convergence of the fast-wave-averaging equations to the PQG equations, starting from balanced initial conditions, as well as the effects of fast-wave coupling for turbulence steady states with phase changes.

Appendix A

Non-dimensional equations and distinguished limit

For the moist Boussinesq equations with phase changes, the dimensional form is shown in (1a)-(1d) of [50], and a non-dimensional version is described in the appendix of [50] in terms of buoyancy variables b_u and b_s. Here, a different, but equivalent, non-dimensional version is described, using θ_e and q_t as the moist thermodynamic variables:

$$\frac{D_h\vec{u}_h}{Dt} + w\frac{\partial u_h}{\partial z} + R_0^{-1}u_h^{\perp} + E_u\nabla_h\phi = 0 \tag{A.1}$$

$$A^2\left(\frac{D_h w}{Dt} + w\frac{\partial w}{\partial z}\right) + E_u\frac{\partial\phi}{\partial z} - \Gamma A^2 b = 0 \tag{A.2}$$

$$\nabla_h \cdot u_h + \frac{\partial w}{\partial z} = 0 \tag{A.3}$$

$$\frac{D_h\theta_e}{Dt} + w\frac{\partial\theta_e}{\partial z} + {Fr_1}^{-2}(\Gamma A^2)^{-1}w = 0 \tag{A.4}$$

$$\frac{D_h q_t}{Dt} + w\frac{\partial q_t}{\partial z} - {Fr_2}^{-2}(\Gamma A^2)^{-1}w - V_r C_{cl}\frac{\partial q_r}{\partial z} = 0 \tag{A.5}$$

along with the relationships

$$b = b_u H_u + b_s H_s, \quad b_u = \theta_e + (\frac{c_p\theta_0}{L_v} - 1)q_t, \quad b_s = \theta_e - \frac{c_p\theta_0}{L_v}q_t, \tag{A.6}$$

where (Ro, Eu, A, Γ, V_r) are the Rossby number, Euler number, aspect ratio, buoyancy parameter, and rain fall speed, respectively. Note that there are two moist thermodynamic

variables (θ_e and q_t) and two phases, as opposed to the dry case with one Froude number, one thermodynamic variable (θ), and one phase. The two "Froude" numbers used here are

$$Fr_1 = U(N_1 H)^{-1} \qquad L_{d_1} = \frac{N_1 H}{f}, \tag{A.7}$$

$$Fr_2 = U(N_2 H)^{-1} \qquad L_{d_2} = \frac{N_2 H}{f}, \tag{A.8}$$

$$N_1{}^2 = \frac{g}{\theta_0}\frac{d\tilde{\theta}_e}{dz} = \frac{g}{\theta_0}\frac{d}{dz}(\tilde{\theta} + \frac{L_v}{c_p}\tilde{q}_v) = \frac{g}{\theta_0}\left(B + \frac{L_v}{c_p}B_{vs}\right), \tag{A.9}$$

$$N_2{}^2 = -\frac{g}{\theta_0}\frac{L_v}{c_p}\frac{d\tilde{q}_t}{dz} = -\frac{g}{\theta_0}(\frac{L_v}{c_p}B_{vs}), \tag{A.10}$$

where L_{d1} and L_{d2} are Rossby radii of deformation, and N_1 and N_2 are buoyancy frequencies. Note that the notation Fr_2, L_{d2}, N_2 is used in analogy to Froude number, Rossby radius of deformation, and buoyancy frequency, respectively, although Fr_2, L_{d2}, and N_2 are defined in terms of not buoyancy but total water. More detail information of reference scales and the non-dimensional quantities can be found in [50] (Table A1, Table A2).

To define the distinguished limit, we consider the asymptotic scalings of (A.1 – A.5) with respect to small Froude and small Rossby number (a rapid rotating and strongly stably stratified flow), which gives

$$Ro = Eu^{-1} = \varepsilon, \quad Fr_1 = Ro\frac{L}{L_{d_1}} = O(\varepsilon), \quad Fr_2 = Ro\frac{L}{L_{d_2}} = O(\varepsilon), \quad \Gamma A^2 = {Fr_1}^{-1}. \tag{A.11}$$

Also, from [50] (equation (A7)), we have $\frac{c_p\theta_0}{L_v} = C_{cl}Ro$. For simplicity, setting $C_{cl} = 1$, we have $\frac{c_p\theta_0}{L_v} = \varepsilon$.

With aforementioned asymptotic scaling and distinguished limit relationship, the non-dimensional model is displayed as:

$$\frac{D_h\vec{u}_h}{Dt} + w\frac{\partial\vec{u}_h}{\partial z} + \varepsilon^{-1}\vec{u}_h^{\perp} + \varepsilon^{-1}\nabla_h\phi = 0 \tag{A.12}$$

$$A^2\left(\frac{D_h w}{Dt}+w\frac{\partial w}{\partial z}\right)+\varepsilon^{-1}\frac{\partial \phi}{\partial z}=\varepsilon^{-1}\frac{L_{d_1}}{L}b \tag{A.13}$$

$$\nabla_h \vec{u}_h+\frac{\partial w}{\partial z}=0 \tag{A.14}$$

$$\frac{D_h \theta_e}{Dt}+w\frac{\partial \theta_e}{\partial z}+\varepsilon^{-1}\frac{L_{d_1}}{L}w=0 \tag{A.15}$$

$$\frac{D_h q_t}{Dt}+w\frac{\partial q_t}{\partial z}-\varepsilon^{-1}\frac{L_{d_2}}{L}w-V_r\frac{\partial q_r}{\partial z}=0 \tag{A.16}$$

Apart from the key non-dimensional parameter ε^{-1} shown above, $\varepsilon_1^{-1}=\varepsilon^{-1}\frac{L_{d_1}}{L}, \varepsilon_2^{-1}=\varepsilon^{-1}\frac{L_{d_2}}{L}$ will be defined, which are related to two Froude numbers. Furthermore, picking $L=L_{d_1}=L_{d_2}$ (implying $\varepsilon=\varepsilon_1=\varepsilon_2$) and $A=1$ allows simple notation and gives:

$$\frac{D_h \vec{u}_h}{Dt}+w\frac{\partial \vec{u}_h}{\partial z}+\varepsilon^{-1}\vec{u}_h^{\perp}+\varepsilon^{-1}\nabla_h \phi=0 \tag{A.17}$$

$$\frac{D_h w}{Dt}+w\frac{\partial w}{\partial z}+\varepsilon^{-1}\frac{\partial \phi}{\partial z}=\varepsilon^{-1}b \tag{A.18}$$

$$\nabla_h \vec{u}_h+\frac{\partial w}{\partial z}=0 \tag{A.19}$$

$$\frac{D_h \theta_e}{Dt}+w\frac{\partial \theta_e}{\partial z}+\varepsilon^{-1}w=0 \tag{A.20}$$

$$\frac{D_h q_t}{Dt}+w\frac{\partial q_t}{\partial z}-\varepsilon^{-1}w-V_r\frac{\partial q_r}{\partial z}=0 \tag{A.21}$$

Note that $V_r=0$, $V_r=1$ or $V_r=\varepsilon^{-1}$ is remained to be specified, since we consider different scenarios for rainfall (no rainfall, or normal speed $V_T=0.1$ m/s or large speed $V_T=1$ m/s). With the special choices above, where all $O(1)$ constants were set equal to unity, we arrive at the advantageous situation where only one distinguished parameter ε appears, to help simplify the notation.

Appendix B

Change of Variables in Different Environments

In this appendix, we will demonstrate a change of variables to a 4-dimensional state vector $\vec{v}^{\,\intercal} = (M, PV_e, W_1, W_2)$, which separates the zero-frequency variables M, PV_e from the wave variables W_1, W_2, starting from the 5-d state vector $\vec{v}^{\,\intercal} = (u, v, w, \theta_e, q_t)$ (which is actually 4-dimensional due to the additional constraint of incompressibility, $u_x + v_y + w_z = 0$ and the special horizontal mean flow case u_m, v_m has been discussed in (2.30),(2.31)). Two cases will be considered: $V_r = 0$ and $V_r \neq 0$.

$V_r = 0$ with phase changes

The starting point is the moist Boussinesq system with phase changes, which has a 5-d state vector $\vec{v}^{\,\intercal} = (u, v, w, \theta_e, q_t)$ with evolution equations

$$\frac{D_h \vec{u}_h}{Dt} + w\frac{\partial \vec{u}_h}{\partial z} + \varepsilon^{-1}\vec{u}_h^{\perp} + \varepsilon^{-1}\nabla_h \phi = 0 \tag{B.1}$$

$$\frac{D_h w}{Dt} + w\frac{\partial w}{\partial z} + \varepsilon^{-1}\frac{\partial \phi}{\partial z} = \varepsilon_1^{-1}\left(b_u H_u + b_s H_s\right) \tag{B.2}$$

$$\nabla_h \cdot \vec{u}_h + \frac{\partial w}{\partial z} = 0 \tag{B.3}$$

$$\frac{D_h \theta_e}{Dt} + w\frac{\partial \theta_e}{\partial z} + \varepsilon_1^{-1} w = 0 \tag{B.4}$$

$$\frac{D_h q_t}{Dt} + w\frac{\partial q_t}{\partial z} - \varepsilon_2^{-1} w = 0 \tag{B.5}$$

$$\text{where } b_u = [\theta_e + \varepsilon q_t - q_t], \qquad b_s = [\theta_e - \varepsilon q_t]. \tag{B.6}$$

Applying the curl operator ($\nabla_h \times$) on equation (B.1) leads to

$$\frac{\partial \xi}{\partial t} + \nabla_h \times \left(\vec{u}_h \cdot \nabla_h \vec{u}_h + w \frac{\partial \vec{u}_h}{\partial z} \right) + \varepsilon^{-1} \delta = 0, \tag{B.7}$$

and applying the divergence operator ($\nabla_h \cdot$) on equation (B.1) leads to

$$\Rightarrow \frac{\partial \delta}{\partial t} + \nabla_h \cdot \left(\vec{u}_h \cdot \nabla_h \vec{u}_h + w \frac{\partial \vec{u}_h}{\partial z} \right) - \varepsilon^{-1} \xi + \varepsilon^{-1} \nabla_h^2 \phi = 0, \tag{B.8}$$

$$\text{where } \delta = \nabla_h \times \vec{u}_h^{\perp} = u_x + v_y, \qquad \xi = \nabla_h \times \vec{u}_h = v_x - u_y, \tag{B.9}$$

$$u_h^{\perp} = \begin{pmatrix} -v \\ u \end{pmatrix}, \qquad \nabla_h \cdot u_h^{\perp} = -v_x + u_y = -\xi. \tag{B.10}$$

For simplicity, the usage of notation NL_ξ denotes the nonlinear term in equation (B.7). Meanwhile, with the incompressibility condition given by equation (B.3), one may replace δ by $-w_z$, and thus (B.7) becomes

$$\frac{\partial \xi}{\partial t} + NL_\xi - \varepsilon^{-1} w_z = 0. \tag{B.11}$$

By introducing a new variable M,

$$M = q_t + G_m \theta_e, \qquad G_m = \frac{\varepsilon_2}{\varepsilon_1}, \tag{B.12}$$

and adding (B.4) and (B.5) together, one finds

$$\frac{\partial M}{\partial t} + \vec{u} \cdot \nabla M = 0, \quad \text{or} \quad \frac{DM}{Dt} = 0. \tag{B.13}$$

By introducing a new variable PV_e,

$$PV_e = \xi + F \frac{\partial \theta_e}{\partial z}, \qquad F = \frac{\varepsilon}{\varepsilon_1}, \tag{B.14}$$

and applying the operator (∂_z) on equation (B.4), one finds

$$\frac{\partial\left(\partial_z\theta_e\right)}{\partial t}+\partial_z\left(\vec{u}\cdot\nabla\theta_e\right)+\varepsilon_1^{-1}w_z=0. \tag{B.15}$$

Adding (B.11) and (B.15) together leads to

$$\frac{\partial PV_e}{\partial t}+\partial_z\left(\vec{u}\cdot\nabla\theta_e\right)+NL_\xi=0. \tag{B.16}$$

This completes the derivation of the M, PV_e equations.

The next step is to present variables W_1 and W_2. Similarly one could substitute $-w_z$ for δ in equation (B.8) to arrive at

$$\frac{\partial w_z}{\partial t}-\nabla_h\cdot\left(\vec{u}_h\cdot\nabla_h\vec{u}_h+w\frac{\partial\vec{u}_h}{\partial z}\right)+\varepsilon^{-1}\xi=\varepsilon^{-1}\nabla_h^2\phi,$$

$$\Rightarrow\frac{\partial w_{zz}}{\partial t}-\partial_z\nabla_h\cdot\left(\vec{u}_h\cdot\nabla_h\vec{u}_h+w\frac{\partial\vec{u}_h}{\partial z}\right)+\varepsilon^{-1}\xi_z=\varepsilon^{-1}\partial_z\nabla_h^2\phi. \tag{B.17}$$

By applying the operator (∇_h^2) on equation (B.2), one finds

$$\frac{\partial\nabla_h^2 w}{\partial t}+\nabla_h^2\left(\vec{u}\cdot\nabla w\right)+\varepsilon^{-1}\nabla_h^2\frac{\partial\phi}{\partial z}-\varepsilon_1^{-1}\nabla_h^2\underbrace{\left(b_uH_u+b_sH_s\right)}_{b}=0. \tag{B.18}$$

Combining (B.17) and (B.18) together will then cancel the pressure terms and yield:

$$\frac{\partial\nabla^2 w}{\partial t}+\varepsilon^{-1}\xi_z-\varepsilon_1^{-1}\nabla_h^2 b+\nabla_h^2\left(\vec{u}\cdot\nabla w\right)-\partial_z\nabla_h\cdot\left(\vec{u}_h\cdot\nabla_h\vec{u}_h+w\frac{\partial\vec{u}_h}{\partial_z}\right)=0. \tag{B.19}$$

Based on the linear part of equation (B.19), we naturally generate two variables:

$$W_1=\nabla^2 w, \tag{B.20}$$

$$W_2=\xi_z-F\nabla_h^2 b,\qquad\qquad F=\frac{\varepsilon}{\varepsilon_1}. \tag{B.21}$$

When W_1, W_2 are inserted into the liner part of (B.19); the result is

$$\frac{\partial W_1}{\partial t} + \varepsilon^{-1} W_2 + \nabla_h^2 \left(\vec{u} \cdot \nabla w\right) - \partial_z \nabla_h \cdot \left(\vec{u}_h \cdot \nabla_h \vec{u}_h + w \frac{\partial \vec{u}_h}{\partial_z}\right) = 0. \tag{B.22}$$

In order to close the system, taking the time derivative of W_2 will lead to its evolution equation. Since the W_2 term contains b, we first focus attention on $\dfrac{\partial b}{\partial t}$ (note $b = H_u b_u + H_s b_s$). Recall the non-dimensional forms of b_u, b_s in (B.6), which are just combinations of θ_e, q_t. Hence $\dfrac{\partial b_u}{\partial t}$, $\dfrac{\partial b_s}{\partial t}$ easily yield following two equations for b_u and b_s:

$$\frac{\partial b_u}{\partial t} + \vec{u} \cdot \nabla b_u + \varepsilon_u^{-1} \cdot w = 0, \tag{B.23}$$

$$\frac{\partial b_s}{\partial t} + \vec{u} \cdot \nabla b_s + \varepsilon_s^{-1} \cdot w = 0, \tag{B.24}$$

where ε_u^{-1}, ε_s^{-1} are non-dimensional forms of the buoyancy frequencies and the corresponding dimensional forms are N_u^2, N_s^2 mentioned in (2.13). Thereby, together with (B.4) and (B.5), we can relate ε_u^{-1}, ε_s^{-1} with ε_1^{-1}, ε_2^{-1} as follows:

$$\varepsilon_u^{-1} = \varepsilon_1^{-1} + \varepsilon_2^{-1} - \frac{\varepsilon}{\varepsilon_2}, \qquad \varepsilon_s^{-1} = \varepsilon_1^{-1} + \frac{\varepsilon}{\varepsilon_2}. \tag{B.25}$$

Next, write down the time derivative for buoyancy,

$$\frac{\partial b}{\partial t} = \frac{\partial \left(b_u H_u + b_s H_s\right)}{\partial t} = \frac{\partial b_u}{\partial t} H_u + \frac{\partial b_s}{\partial t} H_s + \left(b_u - b_s\right) \partial_t H_u. \tag{B.26}$$

Note that $\left(b_u - b_s\right) \partial_t H_u$ becomes zero because $\partial_t H_u$ is a Dirac delta function at the phase interface, and $b_u = b_s$ at the phase interface. As a result, and using (B.23) and (B.24) described above, we find

$$\begin{aligned} & \frac{\partial b}{\partial t} = -H_u \varepsilon_u^{-1} w - H_s \varepsilon_s^{-1} w - H_u \vec{u} \cdot \nabla b_u - H_s \vec{u} \cdot \nabla b_s, \\ \text{or} \quad & \frac{\partial b}{\partial t} + C_{(H)} w + H_u \vec{u} \cdot \nabla b_u + H_s \vec{u} \cdot \nabla b_s = 0, \\ \text{where} \quad & C_{(H)} = H_u \varepsilon_u^{-1} + H_s \varepsilon_s^{-1} = H_u (\varepsilon_1^{-1} + \varepsilon_2^{-1} - \frac{\varepsilon}{\varepsilon_2}) + H_s (\varepsilon_1^{-1} + \frac{\varepsilon}{\varepsilon_2}). \end{aligned} \tag{B.27}$$

Note that $C_{(H)}$ as the coefficient of the linear part in (B.27) contains not only $O(\varepsilon^{-1})$ terms but also $O(1)$ terms. Pulling out the ε^{-1} part, one arrives at the following version of (B.27):

$$\frac{\partial b}{\partial t} + \varepsilon^{-1}[H_u(\frac{\varepsilon}{\varepsilon_1} + \frac{\varepsilon}{\varepsilon_2} - \frac{\varepsilon^2}{\varepsilon_2}) + H_s(\frac{\varepsilon}{\varepsilon_1} + \frac{\varepsilon^2}{\varepsilon_2})]w + H_u\vec{u}\cdot\nabla b_u + H_s\vec{u}\cdot\nabla b_s = 0. \tag{B.28}$$

Apply operator (∇_h^2) on equation (B.27) leads to

$$\frac{\partial \nabla_h^2 b}{\partial t} + \nabla_h^2\left(C_{(H)}w\right) + \nabla_h^2\left(H_u\vec{u}\cdot\nabla b_u + H_s\vec{u}\cdot\nabla b_s\right) = 0. \tag{B.29}$$

With this information in hand, we can now return to W_2 itself. Taking the time derivative of variable $W_2 = \xi_z - F\nabla_h^2 b$ and combining the information from equation (B.11) and (B.29), we find

$$\begin{aligned}\frac{\partial\left(\xi_z - F\nabla_h^2 b\right)}{\partial t} &= \varepsilon^{-1}\partial_z^2(w) + F\nabla_h^2\left(C_{(H)}w\right) \\ &\quad - \partial_z(NL_\xi) + F\nabla_h^2\left(H_u\vec{u}\cdot\nabla b_u + H_s\vec{u}\cdot\nabla b_s\right).\end{aligned} \tag{B.30}$$

With the replacement of $W_1 = \nabla^2 w$, $W_2 = \xi_z - F\nabla_h^2 b$ in linear part, one could update the previous equation as

$$\begin{aligned}\frac{\partial W_2}{\partial t} &= \varepsilon^{-1}\partial_z^2\left(\nabla^{-2}W_1\right) + F\nabla_h^2\left(C_{(H)}\nabla^{-2}W_1\right) \\ &\quad - \partial_z(NL_\xi) + F\nabla_h^2\left(H_u\vec{u}\cdot\nabla b_u + H_s\vec{u}\cdot\nabla b_s\right).\end{aligned} \tag{B.31}$$

This concludes the derivation for the case of $V_r = 0$ with phase changes.

$V_r = 1$ within purely saturated region

In now considering $V_r \neq 0$, in the following discussion, attention will be confined to purely saturated region, so that $H_u = 0$ and $H_s = 1$, without phase changes, but with the presence of rainfall in consideration. Consequently, the q_t equation in (B.5) will have an extra $\dfrac{\partial q_t}{\partial z}$ term,

as shown in

$$\frac{D_h q_t}{Dt} + w\frac{\partial q_t}{\partial z} - \varepsilon_2^{-1} w = \frac{\partial q_t}{\partial z}. \tag{B.32}$$

The above modification of the q_t equation will go through in the derivations of the M equation and W_2 equation, which are constructed based on the variable q_t. By the definition in (B.12), one may rewrite (B.13) as

$$\frac{\partial M}{\partial t} + \vec{u} \cdot \nabla M = \frac{\partial q_t}{\partial z}, \quad \text{or} \quad \frac{DM}{Dt} = \frac{\partial q_t}{\partial z}. \tag{B.33}$$

Since in a purely saturated region we have $b_s = \theta_e - \varepsilon q_t$, we observe that the impact of rainfall on the W_2 equation will emerge through (B.28). After inserting the rainfall term into the original (B.28), and restricting attention to the saturated, single-phase scenario, we find

$$\frac{\partial b_s}{\partial t} + \varepsilon^{-1}(\frac{\varepsilon}{\varepsilon_1} + \frac{\varepsilon^2}{\varepsilon_2})w + \vec{u} \cdot \nabla b_s = -\varepsilon \frac{\partial q_t}{\partial z}. \tag{B.34}$$

Then we find the form of the W_2 equation in a purely saturated region, with rainfall impact:

$$\frac{\partial W_2}{\partial t} = \varepsilon^{-1}\partial_z^2\left(\nabla^{-2}W_1\right) + \varepsilon^{-1}F\nabla_h^2\left((\frac{\varepsilon}{\varepsilon_1} + \frac{\varepsilon^2}{\varepsilon_2})\nabla^{-2}W_1\right) + \varepsilon F\nabla_h^2(\frac{\partial q_t}{\partial z})$$

$$- \partial_z\left(NL_\xi\right) + F\nabla_h^2\left(\vec{u} \cdot \nabla b_s\right). \tag{B.35}$$

Though the $\dfrac{\partial q_t}{\partial z}$ term has been introduced into this equation, it arises at order $O(\varepsilon)$, which will not explicitly show up in the leading orders of behavior of W_2 related to $\mathscr{L}_*$, $\mathscr{L}_0$. Nevertheless, the rainfall term still impacts the M evolution at leading order, as shown in (B.33).

$V_r = O(\varepsilon^{-1})$ within purely saturated region

A similar argument can be implemented here with $V_r = O(\varepsilon^{-1})$. The corresponding adjusted M, W_2 equations are given by

$$\frac{\partial M}{\partial t} + \vec{u} \cdot \nabla M = \varepsilon^{-1}\frac{\partial q_t}{\partial z}, \tag{B.36}$$

$$\frac{\partial W_2}{\partial t} = \varepsilon^{-1}\partial_z^2\left(\nabla^{-2}W_1\right) + \varepsilon^{-1}F\nabla_h^2\left((\frac{\varepsilon}{\varepsilon_1} + \frac{\varepsilon^2}{\varepsilon_2})\nabla^{-2}W_1\right) + F\nabla_h^2(\frac{\partial q_t}{\partial z})$$
$$- \partial_z\left(NL_\xi\right) + F\nabla_h^2\left(\vec{u}\cdot\nabla b_s\right). \tag{B.37}$$

Appendix C

Inverse change of variables to recover (u, v, w, θ_e, q_t)

In this appendix, we show how to recover the variables (u, v, w, θ_e, q_t), given the variables $(PV_e, M, W_1, W_2, u_m, v_m)$. In a sense, this is a type of PV inversion, although also including M and waves W_1, W_2, u_m, v_m.

The definition of b_u, and W_2 give

$$b_u = (\theta_e + \varepsilon q_t - q_t), \quad b_s = (\theta_e - \varepsilon q_t), \tag{C.1}$$

$$W_2 = \xi_z - F\nabla_h^2 (H_u b_u + H_s b_s), \tag{C.2}$$

and when b_u, b_s are inserted into (C.2), the W_2 equation in terms of θ_e, q_t yields

$$W_2 = \xi_z - F\nabla_h^2 (H_u (\theta_e + \varepsilon q_t - q_t) + H_s (\theta_e - \varepsilon q_t)), \tag{C.3}$$

or

$$\xi_z - W_2 = F\nabla_h^2 (\theta_e - H_u q_t + \varepsilon q_t). \tag{C.4}$$

Through neglecting εq, we only put $O(1)$ balanced terms into consideration, implying leading order inversion formula in the end. Replacing q_t by $M - G_m\theta_e$ (for simplicity setting $G_m = 1$,

$F = 1$) shows

$$\xi_z - W_2 = \nabla_h^2 \left(\theta_e - H_u \left(M - \theta_e\right)\right), \tag{C.5}$$

$$\nabla_h^{-2} \left(\xi_z - W_2\right) = \left(1 + H_u\right) \theta_e - H_u M, \tag{C.6}$$

$$\nabla_h^{-2} \left(\xi_z - W_2\right) + H_u M = \left(1 + H_u\right) \theta_e, \tag{C.7}$$

$$\theta_e = \frac{1}{2} H_u [\nabla_h^{-2} \left(\xi_z - W_2\right) + M] + H_s [\nabla_h^{-2} \left(\xi_z - W_2\right)]. \tag{C.8}$$

The aforementioned straightforward work only depends on definitions of buoyancy b_u, b_s, W_2, and M, which simply express θ_e in terms of M, ξ, W_2. The next goal is to write down the inversion of ξ with respect to M, PV_e and W_2.

To find the inversion PDE, we first apply operator (∂_z) to (C.8), and we see that $\partial_z(\theta_e)$ equals

$$\frac{\partial}{\partial z} \{ \frac{1}{2} H_u [\nabla_h^{-2} \left(\xi_z - W_2\right) + M] + H_s [\nabla_h^{-2} \left(\xi_z - W_2\right)] \}. \tag{C.9}$$

Now recall the definition of $PV_e = \xi + F \dfrac{\partial \theta_e}{\partial z}$ (for simplicity setting $F = 1$), and notice that $\dfrac{\partial \theta_e}{\partial z}$ could be replaced by (C.9) to yield

$$\xi + \frac{\partial}{\partial z} \{ \frac{1}{2} H_u [\nabla_h^{-2} \left(\xi_z - W_2\right) + M] + H_s [\nabla_h^{-2} \left(\xi_z - W_2\right)] \} = PV_e. \tag{C.10}$$

If a streamfunction $\psi = (\nabla_h^{-2})\xi$ is introduced, which also implies $\xi = (\nabla_h^2)\psi$, $(\nabla_h^{-2})\xi_z = \psi_z$, one can rewrite (C.10) as

$$\nabla_h^2 \psi + \frac{\partial}{\partial z} \{ \frac{1}{2} H_u [\partial_z \psi - \nabla_h^{-2} W_2 + M] + H_s [\partial_z \psi - \nabla_h^{-2} W_2] \} = PV_e. \tag{C.11}$$

This is an elliptic PDE for the streamfunction ψ, given PV_e, M, and W_2. It is an extension of PV-and-M inversion [58, 59] and now includes the influence of waves via W_2.

An important point is that the PDE (C.11) illustrates how ψ is influenced by fast waves in two ways. First, as mentioned above, the presence of W_2 is one clear influence of waves. Second, recall that the Heaviside functions H_u, H_s also introduce t, τ dependence. In fact, even

if one considers the recovery of $\psi_{(M,PV_e)}$ (by considering a case of recovery from given M, PV_e with setting $W_1 = 0, W_2 = 0$), the τ-dependence of H_u, H_s will introduce a fast τ-dependence to $\psi_{(M,PV_e)}$, even though M and PV_e themselves have no τ-dependence. It shows how waves can influence $\psi_{(M,PV_e)}$ via phase changes.

Solving the elliptic PDE in (C.11) provides ψ in terms of (M, PV_e, W_2). Accordingly, knowledge of ψ helps us to derive the inversion formulas for the velocity field $\vec{u}^{\intercal} = (u, v, w)$, which could be determined from ψ, W_1 and finally be expressed as $(M, PV_e, W_1, W_2, u_m, v_m)$ only.

Similarly, the definition of $W_1 = \nabla^2 w$ demonstrates

$$w = \nabla^{-2} W_1. \tag{C.12}$$

With the incompressibility condition

$$u_x + v_y = -w_z = -(\partial_z \nabla^{-2}) W_1, \tag{C.13}$$

and the definition of $\xi = v_x - u_y$, we arrive at

$$v_{xx} + v_{yy} = \xi_x - \left(\partial_y \partial_z \nabla^{-2}\right) W_1, \tag{C.14}$$

$$u_{xx} + u_{yy} = -\xi_y - \left(\partial_x \partial_z \nabla^{-2}\right) W_1. \tag{C.15}$$

The results of u, v are expressed as

$$v = \left(\nabla_h^{-2}\right)(\xi_x - \left(\partial_y \partial_z \nabla^{-2}\right) W_1), \tag{C.16}$$

$$u = \left(\nabla_h^{-2}\right)(-\xi_y - \left(\partial_x \partial_z \nabla^{-2}\right) W_1). \tag{C.17}$$

As a more physically revealing form, one can rewrite (C.16)–(C.17) as

$$v - v_m = \partial_x \psi - \partial_y \partial_z \left(\nabla_h^{-2} \nabla^{-2} W_1 \right), \tag{C.18}$$

$$u - u_m = -\partial_y \psi - \partial_x \partial_z \left(\nabla_h^{-2} \nabla^{-2} W_1 \right), \tag{C.19}$$

where u_m, v_m are mean velocities and subscript m denotes the horizontal average. (C.18)-(C.19) displays the contributions from the streamfunction ψ, mean velocities and from the velocity potential $-\nabla_h^{-2}\nabla^{-2}W_1$ that is due to waves. Since ψ could be found from (C.11) and written in terms of (M, PV_e, W_2), we see that the velocity field $\vec{u}^{\intercal} = (u, v, w)$ could be obtained through inverting state vector $\vec{v}^{\intercal} = (M, PV_e, W_1, W_2, u_m, v_m)$.

The following contents offer a special inversion formula for the single phase case (purely saturated region with $H_u = 0, H_s = 1$), under no presence of wave ($W_1 = 0, W_2 = 0, u_m = 0, v_m = 0$), which supports conclusions demonstrated on Chapter 5. In a purely saturated region ($H_s = 1, H_u = 0$), (C.10) becomes

$$\xi + \partial_z \left(\nabla_h^{-2} \right) (\xi_z - W_2) = PV_e. \tag{C.20}$$

The remaining work is to introduce the streamfunction $\psi = (\nabla_h^{-2})\xi$, which implies $\xi = (\nabla_h^2)\psi$, $(\nabla_h^{-2})\xi_{zz} = \psi_{zz}$ in (C.20). Without considering the impact of waves, setting $W_2 = 0$ in (C.20) leads to

$$\nabla^2 \psi = PV_e. \tag{C.21}$$

Then $\vec{u}_{(M,PV_e)}$, as the slow part velocity field, coming from (C.12, C.18, C.19) with $W_1 = 0$, $u_m = v_m = 0$, and $\xi = (\nabla_h^2)\psi$, is given by

$$u_{(M,PV_e)} = -\psi_y, \quad v_{(M,PV_e)} = \psi_x, \quad w_{(M,PV_e)} = 0. \tag{C.22}$$

The slow thermaldynamic variable $\theta_{e(M,PV_e)}$, with contributions from M, PV_e slow components

only, is derived through (C.8), with $H_u = 0, H_s = 1, W_2 = 0, \xi = (\nabla_h^2)\psi$:

$$\theta_{e(M,PV_e)} = \psi_z. \tag{C.23}$$

Finally, the definition of $M = \theta_e + q_t$ directly expresses slow variable $q_{t(M,PV_e)}$ as

$$q_{t(M,PV_e)} = M - \psi_z. \tag{C.24}$$

Appendix D

Fourier decomposition of $\mathscr{L}_*$

Two different scenarios will be presented here corresponding to the purely saturated region with two different rainfall speeds $V_r = 1$ and $V_r = \varepsilon^{-1}$ (these two cases may be generalized to $V_r = O(1)$ and $V_r = O(\varepsilon^{-1})$, respectively). The Fourier analysis in following D, E will answer the main question: Will the slow component $\bar{v}_{slow}(t, \vec{x})$ evolve independently from the fast component, as in (3.7)-(3.8), even in the presence of precipitation V_r? Or will precipitation V_r introduce an influence of the fast waves on the evolution of the slow component? Eventually, exactly analogous equations for suitably-defined potential vorticity variables displayed in E clarifies that independence between slow and fast components. In other words, there is no impact from rainfall on slow modes evolution.

Working through the Fourier decomposition of $\mathscr{L}_*$, we use dimensional variables in order to make explicit the appearance of the dimensional frequencies N_1, N_2 described in (2.12), Coriolis parameter f and dimensional rainfall speed V_T, helping to elucidate the dominant physics and to make contact with previous literature, e.g. [5, 17, 33, 40, 43, 45]. Based on the dimensional system (1a)–(1d) of [50] (see also 17(b) in [50] with $q_{vs}(z) = 0$), it's convenient to use rescaled variables

$$\theta_e' = \frac{g}{\theta_0}\frac{\theta_e}{N_1}, \text{ and } q_t' = \frac{gL_v}{\theta_0 c_p}\frac{q_t}{N_2}. \tag{D.1}$$

Then the modified dynamic system in dimensional form will be given:

$$\frac{D\vec{u}}{Dt} + f\hat{z} \times \vec{u} = -\nabla\frac{\phi}{\rho_0} + \hat{z}(N_1\theta_e' - \frac{\theta_0 c_p}{L_v}N_2 q_t') \tag{D.2}$$

$$\nabla \cdot \vec{u} = 0 \tag{D.3}$$

$$\frac{D\theta_e'}{Dt} + N_1 w = 0 \tag{D.4}$$

$$\frac{Dq_t'}{Dt} - N_2 w - V_T \frac{\partial q_t'}{\partial z} = 0 \tag{D.5}$$

With the assumption of periodic boundary conditions in the spatial domain, we try to seek dispersion relation, writing special eigenfunction wave solution as

$$\vec{v} = e^{(i\vec{k}\cdot\vec{x} - i\sigma(\vec{k})t)}\vec{\phi}, \tag{D.6}$$

where $\vec{k}$ is the wave number, $\sigma(\vec{k})$ is the eigenfrequencies, $\vec{\phi}$ is the eigenvector, and $\vec{v}$ should satisfy the incompressibility condition. Similarly, as described in Section 2.1, after non-dimensional process, one could fill previous system (D.2 – D.5) in abstract formulation (2.2) to construct concrete $\mathscr{L}_*$ and $\mathscr{L}_0$ as follow. (Note that the pressure term is rewritten using the expression $\Delta\phi = -\varepsilon\nabla\cdot(\vec{u}\cdot\nabla\vec{u}) + \partial\theta_e/\partial z - \varepsilon\partial q_t/\partial z + \xi$.)

$V_r = 1$**:**

$$\mathscr{L}_*(\vec{v}) = \begin{pmatrix} -\partial_x\Delta^{-1}\partial_y & -1+\partial x\Delta^{-1}\partial_x & 0 & \partial_x\Delta^{-1}\partial_z & 0 \\ 1-\partial_y\Delta^{-1}\partial_y & \partial_y\Delta^{-1}\partial_x & 0 & \partial_y\Delta^{-1}\partial_z & 0 \\ -\partial_z\Delta^{-1}\partial_y & \partial_z\Delta^{-1}\partial_x & 0 & \partial_z\Delta^{-1}\partial_z - 1 & 0 \\ 0 & 0 & 1 & 0 & 0 \\ 0 & 0 & -1 & 0 & 0 \end{pmatrix} \begin{pmatrix} u \\ v \\ w \\ \theta_e \\ q_t \end{pmatrix} \tag{D.7}$$

$$\mathscr{L}_0(\vec{v}) = \begin{pmatrix} 0 & 0 & 0 & 0 & -\partial_x\Delta^{-1}\partial_z \\ 0 & 0 & 0 & 0 & -\partial_y\Delta^{-1}\partial_z \\ 0 & 0 & 0 & 0 & 1-\partial_z\Delta^{-1}\partial_z \\ 0 & 0 & 0 & 0 & 0 \\ 0 & 0 & 0 & 0 & -\partial_z \end{pmatrix} \begin{pmatrix} u \\ v \\ w \\ \theta_e \\ q_t \end{pmatrix} \tag{D.8}$$

$V_r = \varepsilon^{-1}$**:**

$$\mathscr{L}_*(\vec{u}) = \begin{pmatrix} -\partial x\Delta^{-1}\partial y & -1+\partial x\Delta^{-1}\partial x & 0 & \partial x\Delta^{-1}\partial z & 0 \\ 1-\partial y\Delta^{-1}\partial y & \partial y\Delta^{-1}\partial x & 0 & \partial y\Delta^{-1}\partial z & 0 \\ -\partial z\Delta^{-1}\partial y & \partial z\Delta^{-1}\partial x & 0 & \partial z\Delta^{-1}\partial z-1 & 0 \\ 0 & 0 & 1 & 0 & 0 \\ 0 & 0 & -1 & 0 & -\partial z \end{pmatrix} \begin{pmatrix} u \\ v \\ w \\ \theta_e \\ q_t \end{pmatrix} \tag{D.9}$$

$$\mathscr{L}_0(\vec{u}) = \begin{pmatrix} 0 & 0 & 0 & 0 & -\partial x\Delta^{-1}\partial z \\ 0 & 0 & 0 & 0 & -\partial y\Delta^{-1}\partial z \\ 0 & 0 & 0 & 0 & 1-\partial z\Delta^{-1}\partial z \\ 0 & 0 & 0 & 0 & 0 \\ 0 & 0 & 0 & 0 & 0 \end{pmatrix} \begin{pmatrix} u \\ v \\ w \\ \theta_e \\ q_t \end{pmatrix} \tag{D.10}$$

The implementation of Fourier transform $\mathscr{F} : (x, y, z, t) \to (k, l, m, \sigma)$ on the ε^{-1} balance part of abstract equation (2.2), which is $\dfrac{\partial \vec{v}}{\partial t} + \varepsilon^{-1}\mathscr{L}_*(\vec{v}) = 0$, will directly give following matrix equation

$$-i\sigma\vec{\phi} = -\tilde{A}_*\vec{\phi}. \tag{D.11}$$

The associated matrix $\tilde{A}_*$, $\tilde{A}_0$ with respect to the dimensional form of $\varepsilon^{-1}\mathscr{L}_*$, $\mathscr{L}_0$ are displayed below. (Note that $A_* = -|\,\vec{k}\,|^2\tilde{A}_*$, $A_0 = -|\,\vec{k}\,|^2\tilde{A}_0$.)

$V_r = 1$**:**

$$A_* = \begin{pmatrix} klf & (|\,\vec{k}\,|^2 - k^2)f & 0 & -kmN_1 & 0 \\ (-|\,\vec{k}\,|^2 + l^2)f & -klf & 0 & -lmN_1 & 0 \\ lmf & -kmf & 0 & {k_h}^2N_1 & 0 \\ 0 & 0 & -|\,\vec{k}\,|^2N_1 & 0 & 0 \\ 0 & 0 & |\,\vec{k}\,|^2N_2 & 0 & 0 \end{pmatrix} \tag{D.12}$$

$$A_0 = \begin{pmatrix} 0 & 0 & 0 & 0 & km\frac{\theta_0 c_p}{L_v}N_2 \\ 0 & 0 & 0 & 0 & lm\frac{\theta_0 c_p}{L_v}N_2 \\ 0 & 0 & 0 & 0 & -k_h^2\frac{\theta_0 c_p}{L_v}N_2 \\ 0 & 0 & 0 & 0 & 0 \\ 0 & 0 & 0 & 0 & im|\vec{k}|^2 V_T \end{pmatrix} \tag{D.13}$$

$V_r = \varepsilon^{-1}$**:**

$$A_* = \begin{pmatrix} klf & (|\vec{k}|^2 - k^2)f & 0 & -kmN_1 & 0 \\ (-|\vec{k}|^2 + l^2)f & -klf & 0 & -lmN_1 & 0 \\ lmf & -kmf & 0 & {k_h}^2 N_1 & 0 \\ 0 & 0 & -|\vec{k}|^2 N_1 & 0 & 0 \\ 0 & 0 & |\vec{k}|^2 N_2 & 0 & im|\vec{k}|^2 V_T \end{pmatrix} \tag{D.14}$$

$$A_0 = \begin{pmatrix} 0 & 0 & 0 & 0 & km\frac{\theta_0 c_p}{L_v}N_2 \\ 0 & 0 & 0 & 0 & lm\frac{\theta_0 c_p}{L_v}N_2 \\ 0 & 0 & 0 & 0 & -k_h^2\frac{\theta_0 c_p}{L_v}N_2 \\ 0 & 0 & 0 & 0 & 0 \\ 0 & 0 & 0 & 0 & 0 \end{pmatrix} \tag{D.15}$$

By the incompressibility condition, notice that

$$k\hat{u} + l\hat{v} + m\hat{w} = 0, \Rightarrow kl\hat{u} + l^2\hat{v} + lm\hat{w} = 0, k^2\hat{u} + kl\hat{v} + km\hat{w} = 0, \tag{D.16}$$

and simple algebra presents

$$-|k|^2 N_1\hat{w} = -m^2 N_1\hat{w} - k_h^2 N_1\hat{w} = kmN_1\hat{u} + lmN_1\hat{v} - k_h^2 N_1\hat{w}. \tag{D.17}$$

Similarly, $|k|^2 N_2\hat{w}$ could be expressed as

$$|k|^2 N_2\hat{w} = -kmN_2\hat{u} - lmN_2\hat{v} + {k_h}^2 N_2\hat{w}. \tag{D.18}$$

Complete the symmetrization for the 4×4 sub-matrix of A_*, giving analogous structure (see (D.19)) with previous literature [17, 40, 45], so as the corresponding eigen-vectors. Since the last column entries of A_* are different from dry case, which breaks the symmetrizing process for full matrix. In an abuse of notation, we use ϕ to replace $\vec{\phi}$ in following content, if there is no misunderstanding and contradiction.

For $V_r = 1$ case, new matrix A_{s*} and associated eigenvalues, eigenvectors are given as:

$$A_{s*} = \begin{pmatrix} 0 & m^2 f & -lmf & -kmN_1 & 0 \\ -m^2 f & 0 & kmf & -lmN_1 & 0 \\ lmf & -kmf & 0 & k_h^2 N_1 & 0 \\ kmN_1 & lmN_1 & -k_h^2 N_1 & 0 & 0 \\ 0 & 0 & N_2|\vec{k}|^2 & 0 & 0 \end{pmatrix} \tag{D.19}$$

$$\sigma = 0 \text{ (triple)} \qquad \sigma^2 = \frac{N_1^2 k_h^2 + f^2 m^2}{|k|^2} \ \ (\sigma = |\sigma^{\pm}|) \tag{D.20}$$

$$\phi^0 = \frac{1}{\sqrt{N_1^2 k_h^2 + f^2 m^2}} \begin{pmatrix} -N_1 l \\ N_1 k \\ 0 \\ mf \\ 0 \end{pmatrix} \qquad \phi^q = \begin{pmatrix} 0 \\ 0 \\ 0 \\ 0 \\ 1 \end{pmatrix} \qquad \phi^{\pm} = \begin{pmatrix} \frac{m}{k_h}(\sigma k \pm ilf) \\ \frac{m}{k_h}(\sigma l \mp ikf) \\ -\sigma k_h \\ \pm iN_1 k_h \\ \mp iN_2 k_h \end{pmatrix} \tag{D.21}$$

A special case must be considered, which is $k_h = 0$:

$$\sigma = 0 \text{ (triple)} \qquad \sigma^2 = f^2 \ \ (\sigma = |\sigma^{\pm}|) \tag{D.22}$$

$$\phi^0 = \begin{pmatrix} 0 \\ 0 \\ 0 \\ 1 \\ 0 \end{pmatrix} \quad \phi^q = \begin{pmatrix} 0 \\ 0 \\ 0 \\ 0 \\ 1 \end{pmatrix} \quad \phi^{\pm} = \begin{pmatrix} \frac{1+i}{2} \\ \frac{1-i}{2} \\ 0 \\ 0 \\ 0 \end{pmatrix} \tag{D.23}$$

The first two eigenvectors have 0 eigenfrequencies, called as slow modes, while fast modes represent the rest of two vectors with nonzero frequencies. Meanwhile, one eigenvector corresponding to 0 eigenvalue has been abandoned, since it violates the incompressibility condition. Orthogonality of the associated eigenvectors is not guaranteed. Nevertheless, one may process to analyse one of the slow modes (ϕ^0 mode also known as PV_e mode) by projecting (3.6) into ϕ^0 mode in Fourier space, since ϕ^0 is perpendicular to the rest of three modes ϕ^q, ϕ^+, ϕ^-.

For $V_r = \varepsilon^{-1}$ case, with similar argument we simply demonstrate the results of matrix A_*, eigenvalues and eigenvectors as follow:

$$A_* = \begin{pmatrix} klf & (\mid \vec{k} \mid^2 - k^2)f & 0 & -kmN_1 & 0 \\ (-\mid \vec{k} \mid^2 + l^2)f & -klf & 0 & -lmN_1 & 0 \\ lmf & -kmf & 0 & {k_h}^2 N_1 & 0 \\ 0 & 0 & -\mid \vec{k} \mid^2 N_1 & 0 & 0 \\ 0 & 0 & \mid \vec{k} \mid^2 N_2 & 0 & im \mid \vec{k} \mid^2 V_T \end{pmatrix} \tag{D.24}$$

$$\sigma^0 = 0 \text{ (double)} \quad \sigma^q = -mV_T \quad \sigma^2 = \frac{N_1^2 k_h^2 + f^2 m^2}{|\vec{k}|^2} \ \ (\sigma = |\sigma^{\pm}|) \tag{D.25}$$

$$\phi^0 = \frac{1}{\sqrt{N_1^2 k_h^2 + f^2 m^2}} \begin{pmatrix} -N_1 l \\ N_1 k \\ 0 \\ mf \\ 0 \end{pmatrix} \quad \phi^q = \begin{pmatrix} 0 \\ 0 \\ 0 \\ 0 \\ 1 \end{pmatrix} \quad \phi^{\pm} = \begin{pmatrix} \frac{m}{k_h}(\sigma k \pm ilf) \\ \frac{m}{k_h}(\sigma l \mp ikf) \\ -\sigma k_h \\ \pm i N_1 k_h \\ -\frac{iN_2 k_h \sigma}{mV_T \pm \sigma} \end{pmatrix} \tag{D.26}$$

And the special case $k_h = 0$ yields

$$\sigma = 0 \text{ (double)} \quad \sigma^q = -mV_T \quad \sigma^2 = f^2 \ \ (\sigma = |\sigma^{\pm}|) \tag{D.27}$$

$$\phi^0 = \begin{pmatrix} 0 \\ 0 \\ 0 \\ 1 \\ 0 \end{pmatrix} \quad \phi^q = \begin{pmatrix} 0 \\ 0 \\ 0 \\ 0 \\ 1 \end{pmatrix} \quad \phi^{\pm} = \begin{pmatrix} \frac{1+i}{2} \\ \frac{1-i}{2} \\ 0 \\ 0 \\ 0 \end{pmatrix}. \tag{D.28}$$

It's worth to remind reader here, under $V_r = \varepsilon^{-1}$ and $m \neq 0$ circumstance, there is only one slow mode ϕ^0 since ϕ^q is no longer to be slow due to the nonzero eigenvalue σ^q.

Appendix E

Analysis of Resonant Interaction for Slow Dynamics

Based on the well constructed eigenvectors described above, we start to build the concrete form of the average equation (3.6) in Fourier space. In the end, through the analysis of resonant triad interactions arising from bi-linear operator ($\mathscr{B}$) one could verify whether the decoupling property between slow and fast modes is still valid in the limit $\varepsilon \to 0$ under the presence water(q_t) and rainfall(V_T).

Initial condition $\bar{v}(\vec{x},t)$ in (3.2) is written in terms of the aforementioned eigenvectors $\phi^{(\alpha)}_{(\vec{k})}$(D.21 or D.26) together with amplitude function $a^{(\alpha)}_{(\vec{k})}(t)$,

$$\bar{v}(\vec{x},t) = \sum_{\vec{k}\in\mathbb{Z}^3}\sum_{\alpha\in\mathscr{A}} e^{i\vec{k}\cdot\vec{x}} a^{(\alpha)}_{(\vec{k})}(t)\phi^{(\alpha)}_{(\vec{k})}, \qquad \mathscr{A} = \{0,q,+,-\}. \tag{E.1}$$

Plugging (E.1) into $\mathscr{B}$, thus the bi-linear term could be represented explicitly

$$\begin{aligned} &\mathscr{B}(e^{-s\mathscr{L}_*}\bar{v}, e^{-s\mathscr{L}_*}\bar{v}) = \\ &= \sum_{\vec{k}\in\mathbb{Z}^3}\sum_{\alpha\in\mathscr{A}} \left\{ \sum_{(\vec{k}'+\vec{k}''=\vec{k})} \sum_{(\alpha',\alpha''\in\mathscr{A})} e^{i(\vec{k}\cdot\vec{x} - s(\sigma^{(\alpha')}_{(\vec{k}')} + \sigma^{(\alpha'')}_{(\vec{k}'')}))} B^{(\alpha',\alpha'',\alpha)}_{(\vec{k}',\vec{k}'',\vec{k})} a^{(\alpha')}_{(\vec{k}')}(t) a^{(\alpha'')}_{(\vec{k}'')}(t) \right\} \phi^{(\alpha)}_{(\vec{k})}, \end{aligned} \tag{E.2}$$

where the coefficient B arrives to be

$$B^{(\alpha',\alpha'',\alpha)}_{(\vec{k}',\vec{k}'',\vec{k})} = \frac{i}{2}\left[(\vec{u}^{(\alpha')}_{(\vec{k}')}\cdot\vec{k}'')(\vec{\phi}^{(\alpha'')}_{(\vec{k}'')}\cdot\vec{\phi}^{(\alpha)}_{(\vec{k})}) + (\vec{u}^{(\alpha'')}_{(\vec{k}'')}\cdot\vec{k}')(\vec{\phi}^{(\alpha')}_{(\vec{k}')}\cdot\vec{\phi}^{(\alpha)}_{(\vec{k})}) \right]. \tag{E.3}$$

Hence the quadratic contribution due to bi-linear operator $\mathscr{B}$ in the abstract averaging equation (3.6) are given as

$$\lim_{\tau\to\infty}\frac{1}{\tau}\int_0^\tau e^{s\mathscr{L}_*}\left(\mathscr{B}(e^{-s\mathscr{L}_*}\bar{v},e^{-s\mathscr{L}_F}\bar{v})\right)ds =$$
$$=\lim_{\tau\to\infty}\frac{1}{\tau}\int_0^\tau\sum_{\vec{k}\in\mathbb{Z}^3}\sum_{\alpha\in\mathscr{A}}\left\{\sum_{\vec{k'}+\vec{k''}=\vec{k}}\sum_{\alpha',\alpha''\in\mathscr{A}}e^{i(\vec{k}\cdot\vec{x}-s(\sigma^{(\alpha')}_{(\vec{k'})}+\sigma^{(\alpha'')}_{(\vec{k''})}-\sigma^{(\alpha)}_{(\vec{k})}))}\times\right.$$
$$\left.\times B^{(\alpha',\alpha'',\alpha)}_{(\vec{k'},\vec{k''},\vec{k})}a^{(\alpha')}_{(\vec{k'})}(t)a^{(\alpha'')}_{(\vec{k''})}(t)\right\}\phi^{(\alpha)}_{(\vec{k})}. \tag{E.4}$$

Only three wave resonances can survive inside the fast averaging equation, and we define the set $\mathscr{S}_{\alpha,\vec{k}}$ as survival index set:

$$\mathscr{S}_{\alpha,\vec{k}}=\left\{(\vec{k'},\vec{k''},\alpha',\alpha'')|\vec{k'}+\vec{k''}=\vec{k},\sigma^{(\alpha')}_{(\vec{k'})}+\sigma^{(\alpha'')}_{(\vec{k''})}=\sigma^{(\alpha)}_{(\vec{k})}\right\}. \tag{E.5}$$

Directly projecting (3.6) onto the slow mode ϕ^0 will focus our attention on the analysis of slow component dynamics and its evolution equation. Verification on resonant triad interactions under the index set $\mathscr{S}_{0,\vec{k}}$ will be operated as follow (for both $V_r=1$ and $V_r=\varepsilon^{-1}$), which will illuminate the decoupling relationship between slow and fast components.

For $V_r=1$ case, we turn to eigenvectors set (D.21), where $\phi^{(0)},\phi^{(q)}$ are known as slow modes while $\phi^{(+)},\phi^{(-)}$ are fast since previous two are associated with zero frequencies and later two own non-zero frequencies. When we confine that the resonant triad interactions involve at least one slow mode $\phi^{(0)}$ ($slow-(*)-(*)$ impact), all possible resonant interactions coefficient B under the survival index set $\mathscr{S}_{0,\vec{k}}$ are

$$B^{(+,-,0)}_{(\vec{k'},\vec{k''},\vec{k})}=B^{(-,+,0)}_{(\vec{k'},\vec{k''},\vec{k})}=B^{(q,q,0)}_{(\vec{k'},\vec{k''},\vec{k})}=B^{(q,0,0)}_{(\vec{k'},\vec{k''},\vec{k})}=B^{(0,q,0)}_{(\vec{k'},\vec{k''},\vec{k})}=0. \tag{E.6}$$

Similar concrete form can be formulated for the linear operator $\mathscr{L}_0$ and simply yields

$$\lim_{\tau\to\infty}\frac{1}{\tau}\int_0^\tau e^{s\mathscr{L}_*}\mathscr{L}_0(e^{-s\mathscr{L}_*}\bar{v}(\vec{x},t))ds=\sum_{\vec{k}\in\mathbb{Z}^3}\sum_{\sigma^{(\alpha')}_{(\vec{k})}=\sigma^{(\alpha)}_{(\vec{k})}}L^{(\alpha',\alpha)}_{(\vec{k})}a^{(\alpha')}_{(\vec{k})}(t)e^{i\vec{k}\vec{x}}\phi^{(\alpha)}_{(\vec{k})}, \tag{E.7}$$

where $L^{(\alpha',\alpha)}_{(\vec{k})}=\left\langle A_0(\vec{k})\phi^{(\alpha')}_{(\vec{k})},\phi^{(\alpha)}_{(\vec{k})}\right\rangle$ is the coefficient for linear operator $\mathscr{L}_0$ and $A_0(\vec{k})$ is (D.13). Direct calculation gives following two inner product for $\alpha=0$ (Note that we only need to check two cases $\alpha'=q$ and $\alpha'=0$ when $\alpha=0$ since only $\sigma^{(0)}_{(\vec{k})}-\sigma^{(0)}_{(\vec{k})}=0$ and $\sigma^{(0)}_{(\vec{k})}-\sigma^{(q)}_{(\vec{k})}=0$.)

$$\left\langle A_0(\vec{k})\phi^{(0)}_{(\vec{k})}\,,\,\phi^{(0)}_{(\vec{k})}\right\rangle=\left\langle A_0(\vec{k})\phi^{(q)}_{(\vec{k})}\,,\,\phi^{(0)}_{(\vec{k})}\right\rangle=0\Rightarrow L^{(q,0)}_{(\vec{k})}=L^{(0,0)}_{(\vec{k})}=0. \tag{E.8}$$

Finally for ϕ^0 mode, the explicit limiting dynamic evolution equation (derived from projecting (3.6) into ϕ^0 mode) expressed as an ODE of its amplitude $a^0_{\vec{k}}$ are given as follow (by setting $\alpha=0$ in (E.4, E.7)),

$$\frac{da^{(0)}_{(\vec{k})}}{dt}+\sum_{\substack{k'+\vec{k''}=\vec{k}\\ \sigma^{(\alpha')}_{(\vec{k'})}+\sigma^{(\alpha'')}_{(\vec{k''})}=\sigma^{(0)}_{(\vec{k})}}}B^{(\alpha',\alpha'',0)}_{(\vec{k'},\vec{k''},\vec{k})}a^{(\alpha')}_{(\vec{k'})}a^{(\alpha'')}_{(\vec{k''})}+\sum_{\sigma^{(\alpha')}_{(\vec{k})}=\sigma^{(0)}_{(\vec{k})}}L^{(\alpha',0)}_{(\vec{k})}a^{(0)}_{(\vec{k})}=0. \tag{E.9}$$

We remind reader that orthogonality is not guaranteed in previous eigenvectors (D.21), however, the reason one could still process the ODE analysis of $a^0_{\vec{k}}$ by successfully projecting (3.6) on ϕ^0 mode is because that ϕ^0 is perpendicular to the rest of three modes ϕ^q,ϕ^+,ϕ^-. Together with the resonant coefficient calculation showed above in (E.6) and liner term coefficient (E.8), one may observe that the slow mode (ϕ^0) is free of interactions with the fast modes. In other words, the amplitudes $a^0_{\vec{k}}$ is well determined only by itself in the limiting fast wave averaging equation (3.6):

$$\frac{da^{(0)}_{(\vec{k})}}{dt}+\sum_{\substack{k'+\vec{k''}=\vec{k}\\ \sigma^{(0)}_{(\vec{k'})}+\sigma^{(0)}_{(\vec{k''})}=\sigma^{(0)}_{(\vec{k})}}}B^{(0,0,0)}_{(\vec{k'},\vec{k''},\vec{k})}a^{(0)}_{(\vec{k'})}a^{(0)}_{(\vec{k''})}=0. \tag{E.10}$$

An inversion transformation of the Fourier-space equation for slow mode ϕ^0 leads to the conservation of equivalent potential voriticity. Technically speaking, the fast-wave-averaging equation for PV_e in purely saturated region with $V_r = 1$ are given by

$$\frac{D}{Dt}PV_e = (\frac{\partial}{\partial t} + \vec{u}_{(PV_e)} \cdot \nabla)PV_e = 0, \tag{E.11}$$

implying that slow mode (PV_e or ϕ^0) evolve independently from fast mode (waves or $\phi^{\pm}$) under the presence of water and rainfall. The subscript (PV_e) indicates that a variable has been computed by inverting from $(M, PV_e, W_1, W_2, u_m, v_m)$ to $(\vec{u}, \theta_e, q_t)$ using (PV_e) only. From the perspective of Fourier space, one may treat $\vec{u}_{(PV_e)}$ as the contribution only from the entries in slow mode ϕ^0.

For $V_r = \varepsilon^{-1}$ case, eigenvectors set (D.26) will be used to process analysis. In contrast with $V_r = 1$ case, only one mode ϕ^0 with zero eigenvalue remains to be slow. Similar algebra states the following resonant interactions coefficient B under the survival index set $\mathscr{S}_{0,\vec{k}}$ and linear term coefficient L as follow

$$B^{(+,-,0)}_{(\vec{k'},\vec{k''},\vec{k})} = B^{(-,+,0)}_{(\vec{k'},\vec{k''},\vec{k})} = B^{(+,q,0)}_{(\vec{k'},\vec{k''},\vec{k})} = B^{(q,+,0)}_{(\vec{k'},\vec{k''},\vec{k})} = 0, \tag{E.12}$$

$$\left\langle A_0(\vec{k})\phi^{(0)}_{(\vec{k})} \, , \, \phi^{(0)}_{(\vec{k})} \right\rangle = 0 \Rightarrow L^{(0,0)}_{(\vec{k})} = 0. \tag{E.13}$$

Hence, in the remarkable resonant triad interactions only slow-slow-slow impact survives. The possibility of slow-fast-fast has been eliminated by (E.12), meanwhile, slow-fast-slow, slow-slow-fast aren't counted since no resonant interaction is generated from them ($(\vec{k'}, \vec{k''}, slow, fast) \notin \mathscr{S}_{0,\vec{k}}$). In conclusion, $V_r = \varepsilon^{-1}$ gives the same result as (E.10) and (E.11).

Bibliography

[1] A. Babin, A. Mahalov, and B. Nicolaenko, *Global splitting, integrability and regularity of 3d euler and navier-stokes equations for uniformly rotating fluids*, European Journal of Mechanics, B/Fluids, 15 (1996), pp. 291–300.

[2] A. Babin, A. Mahalov, and B. Nicolaenko, *On nonlinear baroclinic waves and adjustment of pancake dynamics*, Theoretical and computational fluid dynamics, 11 (1998), pp. 215–235.

[3] A. Babin, A. Mahalov, and B. Nicolaenko, *Fast singular oscillating limits and global regularity for the 3d primitive equations of geophysics*, ESAIM: Mathematical Modelling and Numerical Analysis, 34 (2000), pp. 201–222.

[4] A. Babin, A. Mahalov, B. Nicolaenko, and Y. Zhou, *On the asymptotic regimes and the strongly stratified limit of rotating boussinesq equations*, Theoretical and computational fluid dynamics, 9 (1997), pp. 223–251.

[5] P. Bartello, *Geostrophic adjustment and inverse cascades in rotating stratified turbulence*, Journal of the atmospheric sciences, 52 (1995), pp. 4410–4428.

[6] A. Bousquet, M. C. Zelati, and R. Temam, *Phase transition models in atmospheric dynamics*, Milan Journal of Mathematics, 82 (2014), pp. 99–128.

[7] Y. Cao, M. Hamouda, R. Temam, J. Tribbia, and X. Wang, *The equations of the multi-phase humid atmosphere expressed as a quasi variational inequality*, Nonlinearity, 31 (2018), p. 4692.

[8] S. Chen, A. J. Majda, and S. N. Stechmann, *Multiscale asymptotics for the skeleton of the Madden–Julian oscillation and tropical–extratropical interactions*, Math. Clim.

Weather Forecast., 1 (2015), pp. 43–69.

[9] ——, *Tropical–extratropical interactions with the MJO skeleton and climatological mean flow*, J. Atmos. Sci., 73 (2016), pp. 4101–4116.

[10] Q. Deng, L. M. Smith, and A. J. Majda, *Tropical cyclogenesis and vertical shear in a moist Boussinesq model*, J. Fluid Mech., 706 (2012), pp. 384–412.

[11] A. Dutrifoy and A. Majda, *The dynamics of equatorial long waves: a singular limit with fast variable coefficients*, Commun. Math. Sci., 4 (2006), pp. 375–397.

[12] ——, *Fast wave averaging for the equatorial shallow water equations*, Communications in Partial Differential Equations, 32 (2007), pp. 1617–1642.

[13] A. Dutrifoy, A. J. Majda, and S. Schochet, *A simple justification of the singular limit for equatorial shallow-water dynamics*, Communications on Pure and Applied Mathematics, 62 (2009), pp. 322–333.

[14] T. K. Edwards, L. M. Smith, and S. N. Stechmann, *Atmospheric rivers and water fluxes in precipitating quasi-geostrophic turbulence*, Quarterly Journal of the Royal Meteorological Society, 146 (2020), pp. 1960–1975.

[15] T. K. Edwards, L. M. Smith, and S. N. Stechmann, *Spectra of atmospheric water in precipitating quasi-geostrophic turbulence*, Geophysical & Astrophysical Fluid Dynamics, (2020), p. in press.

[16] P. F. Embid and A. J. Majda, *Averaging over fast gravity waves for geophysical flows with arbitary potential vorticity*, Comm. PDEs, 21 (1996), pp. 619–658.

[17] ——, *Low Froude number limiting dynamics for stably stratified flow with small or finite Rossby numbers*, Geophys. Astrophys. Fluid Dynam., 87 (1998), pp. 1–50.

[18] A. E. Gill, *Atmosphere–Ocean Dynamics*, vol. 30 of International Geophysics Series,

Academic Press, 1982.

[19] W. W. Grabowski, *Representation of turbulent mixing and buoyancy reversal in bulk cloud models*, J. Atmos. Sci., 64 (2007), pp. 3666–3680.

[20] W. W. Grabowski and P. K. Smolarkiewicz, *Monotone finite-difference approximations to the advection-condensation problem*, Monthly Weather Review, 118 (1990), pp. 2082–2098.

[21] W. W. Grabowski and P. K. Smolarkiewicz, *Two-time-level semi-Lagrangian modeling of precipitating clouds*, Mon. Wea. Rev., 124 (1996), pp. 487–497.

[22] H. Greenspan, *On the nonlinear interaction of inertial modes*, J. Fluid. Mech., 36 (1969), pp. 257–264.

[23] G. Hernandez-Duenas, A. J. Majda, L. M. Smith, and S. N. Stechmann, *Minimal models for precipitating turbulent convection*, J. Fluid Mech., 717 (2013), pp. 576–611.

[24] G. Hernandez-Duenas, L. M. Smith, and S. N. Stechmann, *Investigation of Boussinesq dynamics using intermediate models based on wave–vortical interactions*, J. Fluid Mech., 747 (2014), pp. 247–287.

[25] ——, *Stability and instability criteria for idealized precipitating hydrodynamics*, J. Atmos. Sci., 72 (2015), pp. 2379–2393.

[26] S. Hittmeir and R. Klein, *Asymptotics for moist deep convection i: refined scalings and self-sustaining updrafts*, Theoretical and Computational Fluid Dynamics, 32 (2018), pp. 137–164.

[27] S. Hittmeir, R. Klein, J. Li, and E. S. Titi, *Global well-posedness for passively transported nonlinear moisture dynamics with phase changes*, Nonlinearity, 30 (2017), p. 3676.

[28] ——, *Global well-posedness for the primitive equations coupled to nonlinear moisture dynamics with phase changes*, Nonlinearity, 33 (2020), pp. 3206–3236.

[29] B. Khouider, A. J. Majda, and S. N. Stechmann, *Climate science in the tropics: waves, vortices and PDEs*, Nonlinearity, 26 (2013), pp. R1–R68.

[30] S. Klainerman and A. Majda, *Singular limits of quasilinear hyperbolic systems with large parameters and the incompressible limit of compressible fluids*, Comm. Pure Appl. Math., 34 (1981), pp. 481–524.

[31] ——, *Compressible and incompressible fluids*, Comm. Pure Appl. Math., 35 (1982), pp. 629–651.

[32] R. Klein and A. Majda, *Systematic multiscale models for deep convection on mesoscales*, Theor. Comp. Fluid Dyn., 20 (2006), pp. 525–551.

[33] M. Lelong and J. Riley, *Internal wave-vortical mode interactions in strongly stratified flows*, Journal of Fluid Mechanics, 232 (1991), pp. 1–19.

[34] J. Li and E. S. Titi, *A tropical atmosphere model with moisture: global well-posedness and relaxation limit*, Nonlinearity, 29 (2016), p. 2674.

[35] X.-D. Liu, R. P. Fedkiw, and M. Kang, *A boundary condition capturing method for Poisson's equation on irregular domains*, J. Comput. Phys., 160 (2000), pp. 151–178.

[36] X.-D. Liu and T. Sideris, *Convergence of the ghost fluid method for elliptic equations with interfaces*, Math. Comput., 72 (2003), pp. 1731–1746.

[37] A. Majda, *Compressible Fluid Flow and Systems of Conservation Laws in Several Space Variables*, vol. 53 of Applied Mathematical Sciences, Springer-Verlag, New York, 1984.

[38] A. J. Majda, *Introduction to PDEs and Waves for the Atmosphere and Ocean*, vol. 9 of Courant Lecture Notes in Mathematics, American Mathematical Society, Providence,

2003.

[39] ——, *Multiscale models with moisture and systematic strategies for superparameterization*, J. Atmos. Sci., 64 (2007), pp. 2726–2734.

[40] A. J. Majda and P. Embid, *Averaging over fast gravity waves for geophysical flows with unbalanced initial data*, Theor. Comput. Fluid Dyn., 11 (1998), pp. 155–169.

[41] A. J. Majda and P. E. Souganidis, *Existence and uniqueness of weak solutions for precipitation fronts: A novel hyperbolic free boundary problem in several space variables*, Comm. Pure Appl. Math., 63 (2010), pp. 1351–1361.

[42] D. H. Marsico, L. M. Smith, and S. N. Stechmann, *Energy decompositions for moist Boussinesq and anelastic equations with phase changes*, Journal of the Atmospheric Sciences, 76 (2019), pp. 3569–3587.

[43] O. Phillips, *The interaction trapping of internal gravity waves*, Journal of Fluid Mechanics, 34 (1968), pp. 407–416.

[44] M. Remmel, *New models for the rotating shallow water and Boussinesq equations by subsets of mode interactions*, ProQuest LLC, Ann Arbor, MI, 2010. Thesis (Ph.D.)–The University of Wisconsin - Madison.

[45] M. Remmel and L. Smith, *New intermediate models for rotating shallow water and an investigation of the preference for anticyclones*, Journal of Fluid Mechanics, 635 (2009), pp. 321–359.

[46] R. Rogers and M. Yau, *A short course in cloud physics*, Butterworth–Heinemann, Burlington, 1989.

[47] J. Rosemeier, M. Baumgartner, and P. Spichtinger, *Intercomparison of warm-rain bulk microphysics schemes using asymptotics*, Mathematics of Climate and Weather Forecasting, 4 (2018), pp. 104–124.

[48] S. Schochet, *Fast singular limits of hyperbolic PDEs*, Journal of Differential Equations, 114 (1994), pp. 476–512.

[49] ——, *The mathematical theory of low Mach number flows*, ESAIM: Mathematical Modelling and Numerical Analysis, 39 (2005), pp. 441–458.

[50] L. M. Smith and S. N. Stechmann, *Precipitating quasigeostrophic equations and potential vorticity inversion with phase changes*, J. Atmos. Sci., 74 (2017), pp. 3285–3303.

[51] L. M. Smith and F. Waleffe, *Transfer of energy to two-dimensional large scales in forced, rotating three-dimensional turbulence*, Physics of Fluids, 11 (1999), p. https://doi.org/10.1063/1.870022.

[52] ——, *Generation of slow large scales in forced rotating stratified turbulence*, Journal of Fluid Mechanics, 451 (2002), pp. 145–168.

[53] K. Spyksma, P. Bartello, and M. K. Yau, *A Boussinesq moist turbulence model*, J. Turbulence, 7 (2006), pp. 1–24.

[54] S. N. Stechmann, *Multiscale eddy simulation for moist atmospheric convection: Preliminary investigation*, J. Comput. Phys., 271 (2014), pp. 99–117.

[55] C.-N. Tzou and S. N. Stechmann, *Simple second-order finite differences for elliptic PDEs with discontinuous coefficients and interfaces*, Comm. App. Math. and Comp. Sci., 14 (2019), pp. 121–147.

[56] A. N. Wetzel, L. M. Smith, and S. N. Stechmann, *Moisture transport due to baroclinic waves: Linear analysis of precipitating quasi-geostrophic dynamics*, Math. Clim. Weather Forecast., 3 (2017), pp. 28–50.

[57] ——, *Discontinuous fronts as exact solutions to precipitating quasi-geostrophic equations*, SIAM J. Appl. Math., 79 (2019), pp. 1341–1366.

[58] A. N. Wetzel, L. M. Smith, S. N. Stechmann, and J. E. Martin, *Balanced and unbalanced components of moist atmospheric flows with phase changes*, Chin. Ann. Math. Ser. B, 40 (2019), pp. 1005–1038.

[59] A. N. Wetzel, L. M. Smith, S. N. Stechmann, J. E. Martin, and Y. Zhang, *Potential vorticity and balanced and unbalanced moisture*, J. Atmos. Sci., 77 (2020), pp. 1913–1931.

[60] B. A. Wingate, P. Embid, M. Holmes-Cerfon, and M. A. Taylor, *Low Rossby limiting dynamics for stably stratified flow with finite Froude number*, Journal of Fluid Mechanics, 676 (2011), pp. 546–571.

[61] M. C. Zelati, M. Frémond, R. Temam, and J. Tribbia, *The equations of the atmosphere with humidity and saturation: uniqueness and physical bounds*, Physica D: Nonlinear Phenomena, 264 (2013), pp. 49–65.

[62] M. C. Zelati, A. Huang, I. Kukavica, R. Temam, and M. Ziane, *The primitive equations of the atmosphere in presence of vapour saturation*, Nonlinearity, 28 (2015), p. 625.

[63] M. C. Zelati and R. Temam, *The atmospheric equation of water vapor with saturation*, Bollettino dell'Unione Matematica Italiana, 5 (2012), pp. 309–336.

[64] Y. Zhang, L. M. Smith, and S. N. Stechmann, *Effects of clouds and phase changes on fast-wave averaging: A numerical assessment*, submitted, (2020).